AD-A082 108 BATTELLE COLUMBUS LABS OH F/6 19/1
DEVELOPMENT OF A COMPUTERIZED MATHEMATICAL MODEL FOR THE HOT/CO--ETC(U)
SEP 78 G D LAHOTI, T L SUBRAMANIAN, T ALTAN DAAA25-76-C-0427
UNCLASSIFIED ARSCD-CR-78019 NL

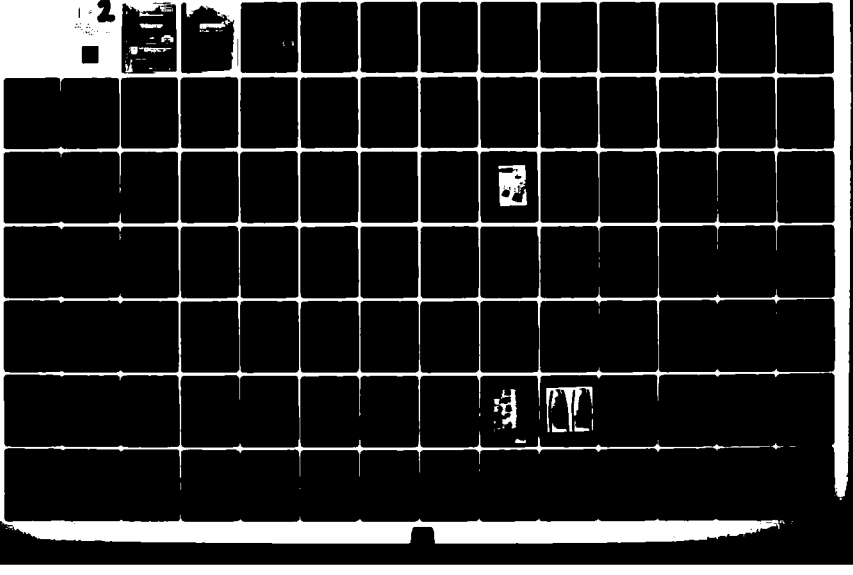

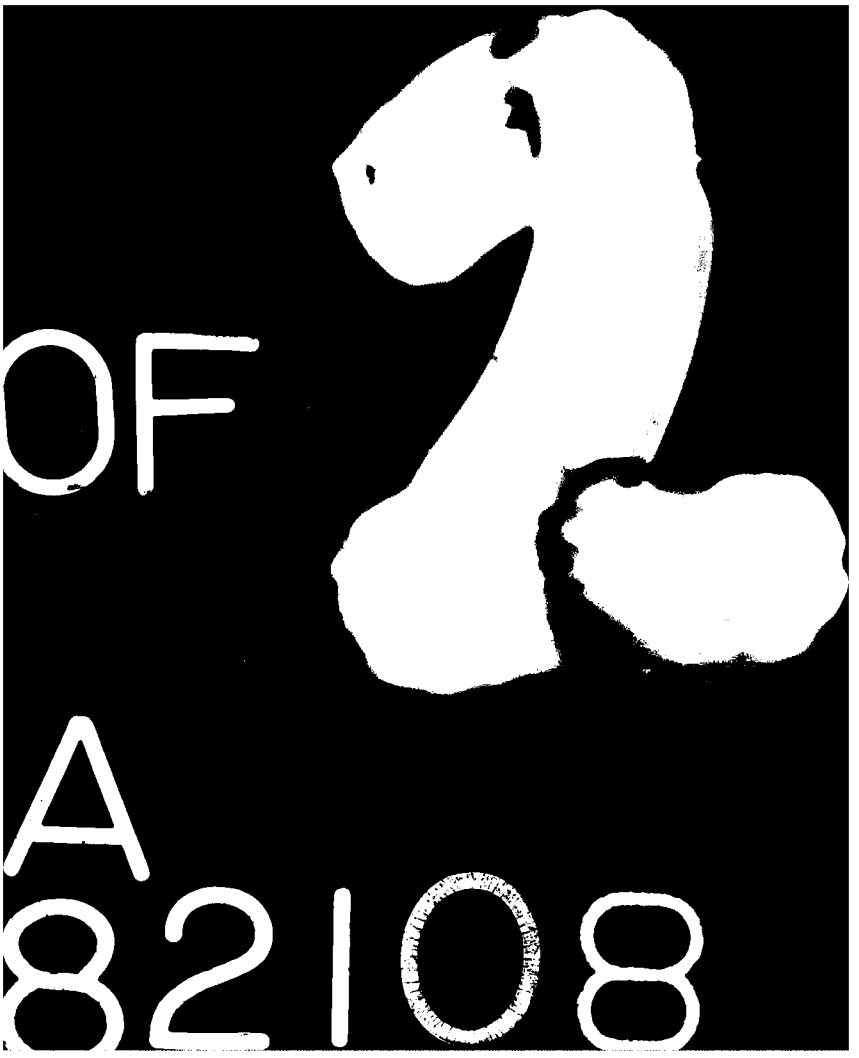
OF
2
A
82108

Unclassified

SECURITY CLASSIFICATION OF THIS PAGE (When Data Entered)

REPORT DOCUMENTATION PAGE

READ INSTRUCTIONS BEFORE COMPLETING FORM

1. REPORT NUMBER: ARSCD-CR-78019	2. GOVT ACCESSION NO.: AD-E400180
3. RECIPIENT'S CATALOG NUMBER:	
4. TITLE (and Subtitle): DEVELOPMENT OF A COMPUTERIZED MATHEMATICAL MODEL FOR THE HOT/COLD NOSING OF SHELLS	5. TYPE OF REPORT & PERIOD COVERED: Final Report, June 21, 1976 to Jan. 20,1978
	6. PERFORMING ORG. REPORT NUMBER:
7. AUTHOR(s): G. D. Lahoti, T. L. Subramanian, and T. Altan	8. CONTRACT OR GRANT NUMBER(s): DAAA25-76-C0427
9. PERFORMING ORGANIZATION NAME AND ADDRESS: Battelle's Columbus Laboratories, 505 King Avenue, Columbus, Ohio 43201	10. PROGRAM ELEMENT, PROJECT, TASK AREA & WORK UNIT NUMBERS: AMCMS Code 4932 05 6716, Project No. 5766716
11. CONTROLLING OFFICE NAME AND ADDRESS: U.S. Army Armament Research and Development Command, Dover, N.J. 07801	12. REPORT DATE: September 1978
	13. NUMBER OF PAGES: 174
14. MONITORING AGENCY NAME & ADDRESS(if different from Controlling Office)	15. SECURITY CLASS. (of this report): Unclassified
	15a. DECLASSIFICATION/DOWNGRADING SCHEDULE:

16. DISTRIBUTION STATEMENT (of this Report)

Approved for public release; distribution unlimited

17. DISTRIBUTION STATEMENT (of the abstract entered in Block 20, if different from Report)

DTIC ELECTE MAR 19 1980 S D B

18. SUPPLEMENTARY NOTES

19. KEY WORDS (Continue on reverse side if necessary and identify by block number)

Nosing, Artillery Shell, Induction Heating, Shell Preform, Load-Stroke Curve, Metal Flow, Local Buckling

20. ABSTRACT (Continue on reverse side if necessary and identify by block number)

The state of the technology in shell nosing and the previous studies on the shell-nosing process are briefly reviewed. A number of computerized mathematical models were developed in order to optimize the process variables, and were integrated into one comprehensive computer program called NOSING. The various capabilities of the computerized models developed under this program include the following:

(a) Designing of preform shape prior to hot nosing. This capability is also available on a programmable HP-67 hand calculator;

DD FORM 1 JAN 73 1473 EDITION OF 1 NOV 65 IS OBSOLETE

Unclassified

SECURITY CLASSIFICATION OF THIS PAGE (When Data Entered)

(b) Prediction of temperature distribution due to induction heating and prior to hot nosing;

(c) Prediction of metal flow during the nosing operation;

(d) Prediction of the load-stroke curve during nosing.

The computer program NOSING is capable of simulating both cold and hot nosing of shells and capable of determining the optimum combination of process parameters.

FOREWORD

This Final Report, prepared for the U.S. Army Armament Research and Development Command, covers the work performed under Contract No. DAAA25-76-C0427, from June 21, 1976, through January 20, 1978. It is published for technical information only and does not necessarily represent the recommendations, conclusions, or approval of the U.S. Army Armament Research and Development Command.

This contract, with Battelle's Columbus Laboratories, Columbus, Ohio, was on the "Development of a Computerized Mathematical Model for the Hot/Cold Nosing of Shells". The technical supervision of this contract was provided by Mr. Fee M. Lee, DRDAR-SCM-E, of U.S. Army Armament Research and Development Command, Dover, New Jersey.

This program was conducted at Battelle in the Metalworking Section, with Mr. T. G. Byrer as Section Manager. Drs. G. D. Lahoti and T. L. Subramanian were the principal investigators of the program and, at Battelle, the work was technically directed by Dr. T. Altan, Research Leader. Other members of Battelle staff were consulted as necessary.

TABLE OF CONTENTS

TABLE OF CONTENTS
(Continued)

LIST OF ILLUSTRATIONS

Figure No.

LIST OF ILLUSTRATIONS
(Continued)

LIST OF TABLES

LIST OF SYMBOLS

α	Meridinal coordinate
α_o	Meridinal coordinate at nose base
α_1	Meridinal coordinate at nose tip
δ	Skin depth
μ	Permeability, coefficient of friction
ν	Poissons ratio
ξ	Distribution of elongation along the nosed position
ρ	Electrical resistivity
$\bar{\sigma}$	Flow stress
σ_c	Circumcumferential stress
σ_m	Meridinal stress
B_1	Distance of center for radius R_1 from nose base
B_2	Distance of center for radius R_2 from nose base
D	Outside diameter of the shell preform
E	Modulus of elasticity
e_{max}	Maximum elongation due to nosing
f	Frequency
h	Wall thickness at angle α
h_o	Wall thickness at nose base
ℓ_1	Length of the nose position
m	Friction shear factor ($0 \leq m \leq 1$)
p	Die pressure
R	Load resistance
R_1	Outer shell ogive radius
R_2	Inner shell ogive radius
r	Outside radius at an angle α
r_i	Inside radius of shell
r_1	Outside radius at nose tip
r_o	Outside shell radius at nose base
X	Axial coordinate
X_c	Inductance

SUMMARY

In this report, the state of the technology in shell nosing and the theoretical and experimental studies on shell-nosing process are briefly reviewed. In order to determine an optimum combination of the process variables, a number of computerized mathematical models for cold and hot nosing of shells were developed. All these models were assembled in one comprehensive computer programm called NOSING.

Various capabilities for computerized modeling of the nosing process, developed in this project, are:

- Preform Design. Based on the consideration of local strains in the deformed shell during nosing, a method for designing of nosing preforms was computerized. This method for preform design is capable of considering elongation due to nosing, and it has also been programmed on HP-67 programmable calculator.
- Temperature Distribution Prior to Nosing. A mathematical model to predict time-dependent temperature distributions due to induction heating of preform prior to hot nosing was developed and computerized. The analysis assumes uniform heat generation along the length of the tube inside the coil and neglects the end effects. Therefore, the predictions are less accurate near the end of the induction coil.
- Prediction of Metal Flow During Nosing. A mathematical model for predicting metal flow in nosing of shells was developed. This model considers preforms with uniform wall thickness. Thus, the model is exactly valid for nosing of shells up to 105-mm size shells, which are normally nosed from preforms with uniform or near-uniform wall thicknesses. For larger shells, where the preform wall thickness is not uniform, this analysis can be applied only approximately.
- Load-Stroke Curve in Nosing. In order to generate the load-stroke curve in the nosing operation, using preforms with non-uniform wall thickness, a computer program to simulate the nosing process was developed. This program simulates the nosing process in a finite number of discrete steps and utilizes Nadai's stress analysis, and considers the flow stress

of the deforming material as a function of the strain, strain rate and temperature. It also checks for local bulging at the nose base, or for Euler's buckling, at each step of simulation.

- Computer Program NOSING. Finally, all the mathematical models described above were integrated in a comprehensive computer program named NOSING. This program is capable of simulating both cold and hot nosing of shells and determining the optimum combination of process parameters.

INTRODUCTION

In all modern methods of shell manufacturing, the cavity is formed to finish shape and the machining is restricted to the outer surface of the shell. The open end of the rough-machined shell is closed in and the ogive is formed. The closing in is accomplished by forcing a contoured die axially over the open end of the shell, while the body of the shell is well supported by a chuck, as shown in Figure 1. In all high-explosive shells, from 75 mm to 240 mm, the fuze thread diameter is the same. Therefore, the open end of the largest shell must be deformed about three times as much as the smaller calibers to produce the same size fuze hole. As a result, 155-mm shells and larger sizes are hot nosed, while the 75-mm to 105-mm shells can be cold nosed.

The present program was aimed at increasing the productivity in nosing of artillery shells. The flow of metal in nosing is very complex and a slight variation in the friction or the temperature conditions may result in misformed shell due to improper metal flow. There is very little quantitative technical information available and, in most shell-manufacturing plants, extensive experience and expensive trial-and-error techniques are necessary in order to design the nosing process. Further, cold or hot nosing of shells is traditionally carried out in hydraulic presses at moderate speeds. Recently, high-speed mechanical presses

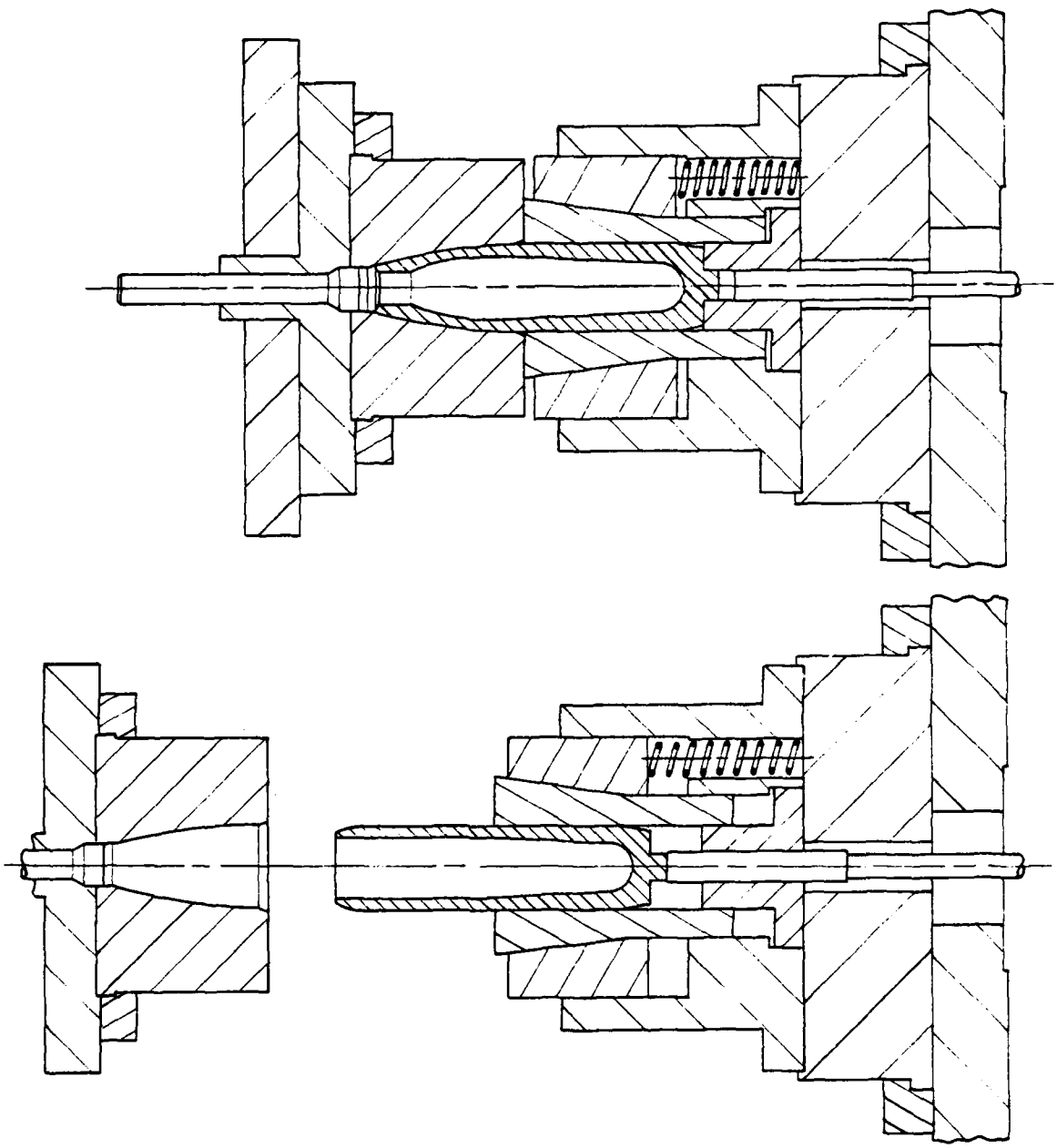

Fig 1 Section Through Tool Assembly of Nosing Press

are being considered for the nosing operation. The process design, as practiced today, leaves much to experience and intuition. In such situations, mathematical modeling of the process capable of predicting, for example, conditions leading to buckling in hot nosing or extent of wall thickening in cold nosing are essential in order to eliminate expensive trial-and-error methods. Thus, an objective and reliable procedure can be developed to select the optimum equipment, tooling, and operating conditions.

OBJECTIVES

The overall objective of the present program was to develop analytical techniques to determine the optimum combination of process variables for defect-free nosing of shells. Both cold and hot-nosing operations were considered.

The specific objectives of the present program were the following:

(a) In hot nosing, determine temperature distribution in the shell wall due to preheating.

(b) Develop a method for predicting the load-stroke curve in both cold and hot nosing under a specified combination of process variables, such as die configuration, wall temperature, lubricant, and speed of operation.

(c) Develop a criterion for predicting buckling due to axial loads in hot and cold nosing.

(d) Determine the effect of ram speed on the forming load, metal flow, and possibility of buckling in both cold and hot nosing.

(e) Using the information developed in the above items (a) through (d), develop a computer program to determine optimum combination of process variables for cold and hot nosing of shells.

PROGRAM HIGHLIGHTS

The present program was conducted over a period of 18 months and the work under it included the following major tasks:

Task 1. Temperature Distribution after Preheat

The coils in the preheaters provide the heat source to the shell during nosing. By modeling the coils as an energy source, the heat conduction equations for the shell were solved. The solution technique provided the temperature distribution in the shell as a function of location and time. Cool-off due to any delays between preheating and actual nosing was also accounted for.

Task 2. Metal Flow and Velocity During Nosing

The distribution and velocity of the metal flow was modeled using one of the methods of plasticity. Temperatures (from Task 1), stroke, strain rate, friction and die geometry were included in the metal-flow calculations.

Task 3. Stress Analysis

A numerical extension of the original Nadai stress analysis in nosing was computerized. The results were an estimate of the axial, radial and circumferential stresses and strains during nosing.

Task 4. Material Failure Analysis

Using the stress analysis (Task 3), a criterion for local plastic buckling or bulging was formulated. This criterion contains the effects of friction, temperature, strain and strain rate.

Task 5. Optimization Computer Program

A computer program utilizing the results of Tasks 1 to 4 was written. Parametric study to determine optimal nosing conditions of selected shells was performed.

BACKGROUND ON SHELL NOSING

The small caliber shells (up to 105 mm) can be cold nosed while larger shells (155 mm and up) are hot nosed. In cold nosing, initially the whole shell is at constant temperature and it has uniform flow stress. However, the deformation work hardens the shell material nonuniformly, and the resistance to further deformation by various parts of the shell is also unequal. The elastic spring back is very small compared to plastic strain and, therefore, the dies are given the shape of rough-finished nose. The slight elastic back spring is removed in the process of finish turning.

During the nosing operation, the shell metal in the die can move either radially inward, or in the direction of tangent to the die profile, or in both the directions. Since metals under plastic state flow in the direction of least resistance, the flow of metal in cold nosing is affected by the characteristics of the lubricant and the speed of the nosing operation. If the lubrication is not sufficient and if the nosing is slow, the lubricant is squeezed out and the friction between shell and die not only keeps the shell from lengthening, but shortens it. Conversely, if the lubrication is adequate and if the nosing is done rapidly, the lubricant is squeezed out to a lesser extent; the friction is reduced and the shell is lengthened. The finish of the external shell surface in rough turning also affects the metal flow in nosing; smoother finish encourages the escape of the lubricant while very rough surface finish results in compression of the ridges left from machining and provides improved lubrication.

In hot nosing, the open end of a forged shell is preheated radially to temperatures between 1500 F to 1900 F by tubular wound induction coils. Then the shell is nosed by forcing it into a suitably shaped die. The flow stress of the

deforming material under these conditions is a function of strain rate and temperature. The temperatures in the shell wall are influenced by (a) preheating conditions, (b) heat generation, due to deformation and friction, and (c) heat transfer to the nosing die. Determination of these temperature distributions along the length of the shell wall is important and necessary in order to predict accurately the axial nosing loads.

Because of the temperature distribution along the axis of the shell, the flow of metal in hot nosing is also complex. In fact, the temperature distribution is rather critical and much experimentation has been done on the heating and on the contour of rough-turned shells. Preheating is done at a certain rapid rate so that the high temperature does not travel back to that part of the shell which should remain comparatively cold; otherwise, buckling of the shell wall occurs, as shown in Figure 2.

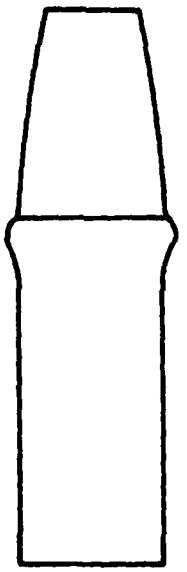

Fig 2 Buckling at the Nose Base in Hot Nosing of Shells

Lubrication plays an important role in hot nosing also. Usually, the lubricant is sprayed on rough-turn shells before preheating for the nosing operation. The lubricant evaporates somewhat unevenly during preheating and a nonuniform lubrication may exist prior to nosing. This causes an uneven or oblique top. Further, lack of adequate lubrication causes the shell to be short and the walls to become thicker, whereas good lubrication results in longer shells with less wall thickening. The influence of die temperature and the speed of nosing further complicates the situation.

The Variables of the Shell-Nosing Process

As discussed earlier, many factors influence the shell-nosing process. In order to optimize the process, the variables which determine the process conditions must be considered individually and collectively, and their contribution to the process must be defined quantitatively. The significant variables of the shell-nosing process are listed in the following:

(A) Projectile Material Variables
- Flow stress and its dependency on strain, strain rate and temperature
- Physical and thermal properties (density, specific heat, thermal conductivity)
- Metallurgical properties

(B) Tooling Variables
- Die configuration
- Die and container materials and their properties

(C) Process Variables
- Projectile forging dimensions
- Depth of penetration in the die
- Projectile forging temperature
- Die temperature
- Speed of operation
- Lubrication and the lubricant properties
- Nosing load and the die pressure

- Limiting load and penetration for buckling
- Variations in the wall thickness and length of the projectile
- Alignment of nosing die and nest

(D) Product Properties

- Concentricity of projectile, free from bulging and buckling
- Dimensional tolerances and surface finish
- Mechanical properties (tensile, fatigue, etc.)
- Metallurgical properties (grain size, phase transformation, etc.)

A Brief Review of Theoretical and Experimental Studies on Shell Nosing

Nadai (Ref.1) conducted an extensive theoretical investigation on the forces required in nosing of shells for the ASME Special Research Committee on Forging of Steel Shells. Although hot nosing was of primary interest, Nadai's developments can be extended to the cold-nosing process too. This work is basically an extension of the theory of curved shells to cover cases in which the metal is in a plastic state of equilibrium. The theory is based upon constant coefficient of friction and ignores variations in the flow stress of the shell material. General equations for both conical and curved shell nose were established for the plastic state and for variable wall thickness. However, investigation with uniform wall thickness was considered. The distribution of the meridianal and circumferential stress and of the nosing pressure were studied for a number of cases. Nadai also attempted to analyze the distortion of the metal elements during the formation of the nose, and develop expressions to predict the original contour of the shell which after nosing furnished a prescribed profile on the nose of the shell. Onat and Prager (Ref.2) extended Nadai's work and included the changes in the shell-wall thickness due to the nosing operation. They investigated the influence of these changes on the stresses in nosing. A linearized theory of nosing of shells has been presented by Singh (Ref.3) who has shown that excellent approximations to the predictions of von Mises' theory can be obtained. However, none of these analyses take into account (a) the dependence of the flow stresses on strain in cold nosing, and on strain rate and temperature in

hot nosing, (b) variation in temperature along the length of the shell nose in hot nosing, and (c) variation of the friction coefficient in the axial direction.

The published literature on nosing of shells also includes a few systematic experimental studies. The model tests by Carlson (Ref.4), conducted for the ASME Special Research Committee on Forging of Steel Shells, show the effects of temperature, lubrication, and speed on the nosing process. Carlson has also presented an analysis of the strain distributions and has indicated a method for predicting the nose profile necessary to produce a desired finish shape. Recently, Cruden and Thomson (Ref.5) conducted an experimental study of the nosing process to establish the limitations of the process and to assess the effects of the various process parameters. Some of the practical aspects of shell nosing, based on surveys of plant practices, are summarized in a report by Veth (Ref.6), et al. However, the recommendations of these studies are largely qualitative in nature and cannot be used reliably for process optimization without an extensive investigation of similar nature.

PREFORM DESIGN FOR NOSING OF SHELLS

During the nosing operation, the shell metal inside the die can move either radially inward, or in the direction of the tangent to the die profile, or in both directions. Certain shell specifications require uniform wall thickness after nosing, such as in the case of 175 mm, M437 shell; whereas, in the case of other shells, such as 155 mm M107, the required wall thickness after nosing is defined by two ogive radii, as shown in Figure 3. Thus, in order to obtain the desired shape after the nosing operation, the design of the rough-turned shell or the preform prior to nosing is very important. This problem is one which costs the shell-forging industry thousands of dollars, since there is no easy and unique way to predict what the original profile should be, and several die try-outs are necessary to establish the nosing process.

It has been observed that certain sizes and shapes of shells elongate considerably during nosing, while in others there is practically no axial elongation. For those shells which do not elongate, the problem is easier since it can be assumed that each element of the shell wall moves radially only. However, when the shell elongates considerably, the metal flow becomes complex. For shells with uniform wall thickness after nosing, Nadai (Ref.1) has outlined an approach for designing

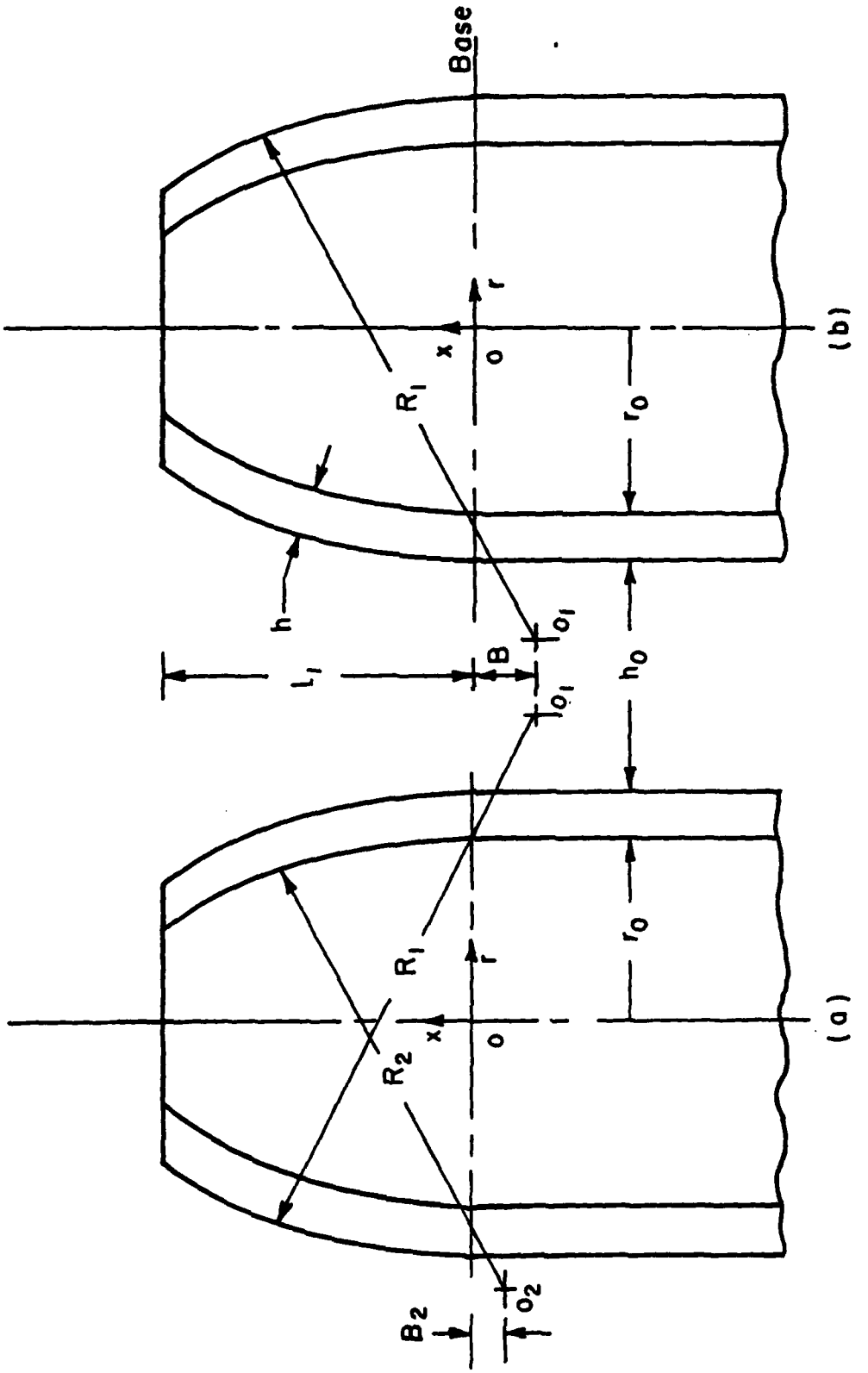

Fig 3 Configurations of As-Nosed Shells

preforms, based on the strains in the shell nose. In the following, Nadai's approach, extended by Carlson (Ref.4), is used.

Calculation of As-Nosed Configuration

Although as-nosed configurations can be easily drawn, often numerical values of the inside and outside radii at a given axial location is needed for comparing measured values with the theoretical values. As mentioned earlier, the nosed portion of the shell is described in two different ways: (a) by two radii R_1 and R_2, as shown in Figure 3(a), and (b) by a radius R_1 and wall thickness h, as shown in Figure 3(b). For the configuration given by Figure 3(a), the inner radius r_i and the outside radius r at an axial distance x is given by:

$$r_i = (r_o - h_o) - R_2(\cos\alpha_i - \cos\alpha_2) \quad ,$$

$$r = r_o - R_1 (\cos\alpha_o - \cos\alpha_1) \quad , \tag{1}$$

where $\alpha_o = \sin^{-1} (B_1/R_1)$

$$\alpha_i = \sin^{-1} (B_2/R_2)$$

$$\alpha_1 = \sin^{-1} \left(\frac{B_1 + x}{R_1} \right) \quad .$$

$$\alpha_2 = \sin^{-1} \left(\frac{B_2 + x}{R_2} \right) \quad .$$

For the configuration described by Figure 3(b), the outer radius is still obtained as described above. However, the inner surface is described by (x_i, r_i), the coordinates of inner surface as below:

$$x_i = (R_1 - h) \sin\alpha_1 - B_1 \tag{2}$$

$$r_i = (r_o - h_o) - (R_1 - h)(\cos\alpha_o - \cos\alpha_1) \quad .$$

The above calculations, to determine the geometry of the nosed shell, have been programmed on a programmable hand calculator (HP-67). This program, called NOSE, can be stored on a magnetic strip for easy reloading in the calculator. For given geometrical inputs, such as R_1, B_1, ℓ_1, and h or R_1, B_1, R_2, B_2, and ℓ_1, NOSE calculates the coordinates of the inner and outer surfaces of the nosed portion by incrementing the axial coordinate by 1 inch. The program NOSE and instructions for its use are included in Appendix A.

In order to illustrate the use of the program NOSE, calculations were made for 155 mm M107 shell. For this purpose, the dimensions were selected from engineering drawing as given in Table 1. The calculated results, as displayed on HP-67 calculator, are given in Table 2.

Table 1 Dimensions for 155 mm M107 Shell

Outside radius at nose base, r_o	= 3.10 inch
Radius of ogive, R_1	= 65.50 inch
Length of the nose portion, ℓ_1	= 11.00 inch
Uniform wall thickness, h	= 0.65 inch
Distance of ogive center from nose base, B_1	= 5.25 inch

Calculation of Preform Shape

Figure 4 shows the generalized configuration of the as-nosed shell, This configuration will be used in the following design procedure, since it is used in defining large caliber shells where preform design is crucial. A possible preform shape is also shown in the same figure with broken lines. The outside surface of the preform is straight and is parallel to the axis. The inside surface is made of straight-line segments. The length of the preform is shorter than the finish shape by an amount e_{max}, the estimated elongation of the shell during nosing.

Table 2 As-Nosed Profile of 155 mm M107 Shell

Outside Surface		Inside Surface	
Axial Distance x, inch	Outer Radius r, inch	Axial Distance x_i, inch	Inner Radius r_i, inch
0.000	3.100	0.000	2.450
1.000	3.012	0.938	2.363
2.000	2.908	1.928	2.260
3.000	2.789	2.918	2.142
4.000	2.654	3.908	2.009
5.000	2.504	4.898	1.860
6.000	2.337	5.888	1.695
7.000	2.155	6.878	1.514
8.000	1.960	7.869	1.318
9.000	1.742	8.859	1.105
10.000	1.511	9.849	0.877
11.000	1.263	10.839	0.631

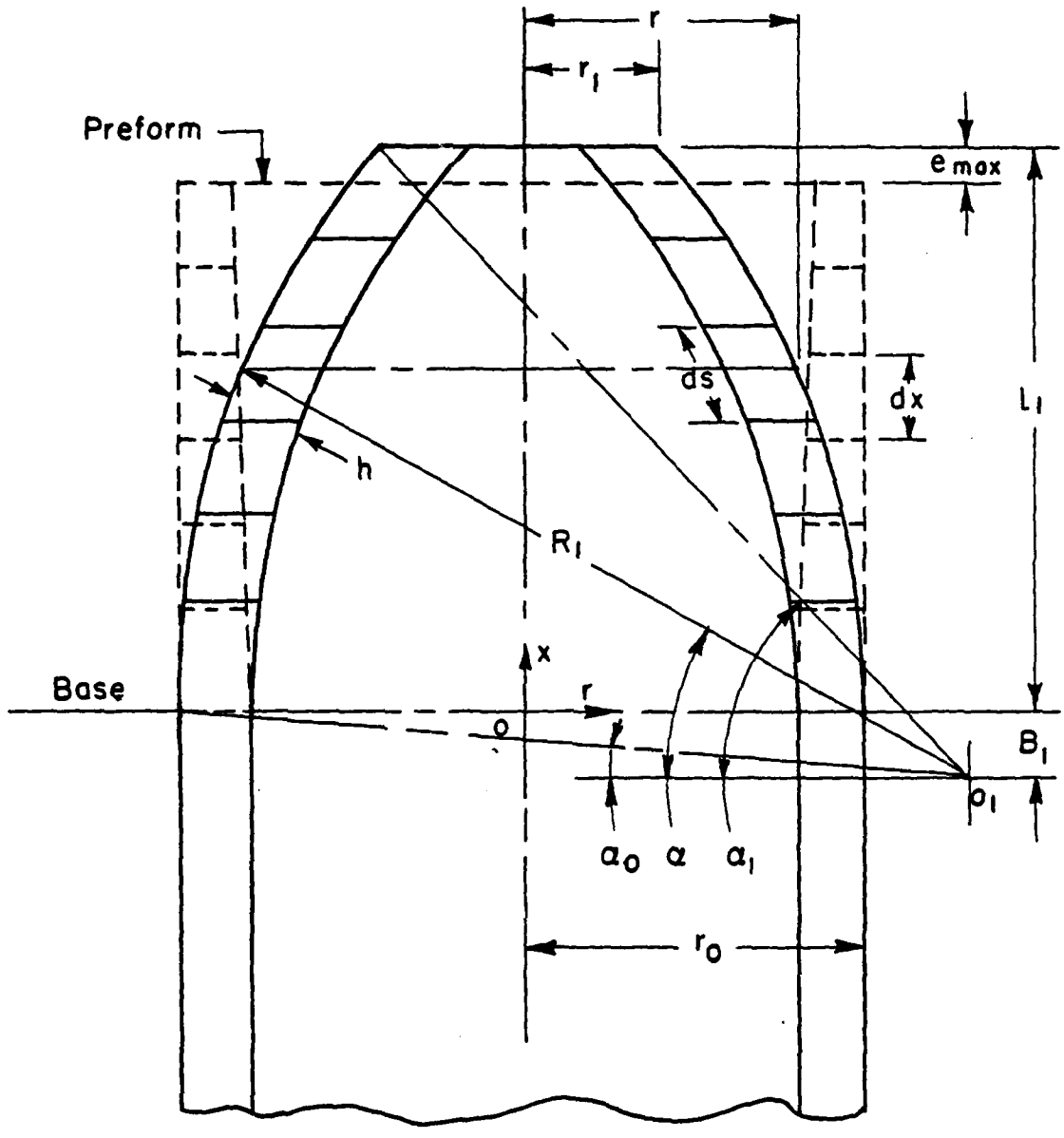

Fig 4 Configuration of Preform and As-Nosed Shape

If the shell does not elongate due to nosing, the preform wall thickness h_o at a distance x from the nose base is given as below:

$$h_o = r_o \frac{rh}{\cos(\alpha - \alpha_o)} \quad . \qquad (3)$$

If the shell elongates considerably, an element originally at x goes to $x + \xi$ after nosing, where ξ is the axial displacement of the element. The preform thickness in such a case is given by:

$$h_o = r_o \frac{rh}{\cos(\alpha - \alpha_o)} \left(1 + \frac{d\xi}{dx}\right) \quad . \qquad (4)$$

The detailed derivations of the Equations (3) and (4) and a procedure for estimating ξ from the maximum elongation, e_{max}, are summarized in Appendix A.

The design of preform represents a very important step in nosing operation and it will be very useful to a shop engineer to have the design procedure on a programmable hand calculator. Therefore, the above procedure for preform design was also programmed on an HP-67. This program, called PREFORM, can be stored on a magnetic strip for easy reloading. For given dimensions of the shell nose and estimated elongation e_{max}, beginning at the nose base, PREFORM calculates preform wall thickness in increments of 1 inch. At the end of preform calculation, if the user inputs estimated values of the coefficient of friction and the flow stress of the shell material, the program also calculates estimated nosing load. It should be apparent, however, that the method used for designing the preform from the known final shape gives only approximate answers. For example, the preform wall thickness at the tip cannot be determined using this approach, and it must be extrapolated. The program PREFORM and instructions for its use are also included in Appendix A.

In order to illustrate the use of the program NOSE, calculations were made for obtaining the preform shape for 155 mm M107 shell. For this purpose, the dimensions given in Table 1 were used, together with an estimated value of elongation e_{max} = 0.500 inch. The coefficient of friction at die-workpiece interface and the flow stress for shell material were taken as 0.10 and 35,000 psi, respectively. Table 3 shows the preform wall thicknesses at various axial locations from the nose base, and the estimated nosing load. Similar tables can be generated for other shells.

TEMPERATURE DISTRIBUTION DUE TO PREHEATING PRIOR TO NOSING

Nosing of large shells (155 mm and above) is invariably done at hot-working temperatures. Hence, prior to nosing, the end portion of the tube to be formed is heated. Heating a portion of the tube causes a temperature distribution along its length prior to deformation. If the heating is slow and gradual, the unheated portion of the tube gains heat by conduction. Consequently, during nosing, the tube tends to buckle under axial load, as shown in Figure 2. Excess metal not only accumulates outside the tube, as seen in Figure 2, but also forms a ring on the inside near the entrance of the nosing die. Therefore, it is imperative that heating is done at a predetermined rapid rate to reduce the heat transfer by conduction.

Because of its numerous advantages, induction heating is the most preferred heating technique for the nosing operation. The major advantages of the induction heating are:

(a) Uniform temperature distribution all around the shell
(b) Precise control of the final temperature
(c) Rapid heating rate, which reduces the effects of scale formation and heat conduction.

There are many publications on Applied Mathematics and on Induction Heating, describing procedures to estimate the heat generated in induction heating (Ref.7-14). To avoid lengthy derivations, all these procedures provide equations valid for solid billets only. Alternatively, special-purpose graphs, the so-called 'P-Q' curves, are recommended by others for use in the estimation

Table 3 Preform Shape Prior to Nosing of 155 mm M107 Shell

Without Elongation ($e_{max} = 0$)		With Elongation ($e_{max} = 0.5$ inch)	
Axial Distance from Nose Base, inch	Preform Wall Thickness, inch	Axial Distance from Nose Base, inch	Preform Wall Thickness, inch
0.0	0.650	0.0	0.650
1.0	0.632	1.0	0.632
2.0	0.610	2.0	0.610
3.0	0.585	3.0	0.585
4.0	0.558	4.0	0.558
5.0	0.527	5.0	0.527
6.0	0.492	6.0	0.492
7.0	0.455	7.0	0.455
8.0	0.413	8.0	0.414
9.0	0.369	9.0	0.371
10.0	0.321	10.0	0.354
11.0	0.269	10.5	0.346*
Estimated Nosing Load, P = 484,355 lbs		Estimated Nosing Load, P = 484,355 lbs	

* Estimated by extrapolation.

of heat generated in tubular charges (Ref.13-17). However, the existing P-Q curves are valid only for non-magnetic materials and additional curves need to be generated for magnetic materials.

A brief look at the references cited above will indicate that most of the analyses on induction heating have been conducted in a period when use of computers for scientific analyses was fairly unknown. Therefore, simplified procedures by approximate methods were necessary to avoid time-consuming calculations. Furthermore, most of these analyses were aimed at the design of induction coils for specific applications (Ref.15-17). Hence, the given equations are good only to estimate the total heat generated in a given time interval.

In recent years, some companies specializing in induction heating have improved existing analytical procedures and developed computer programs for advanced analysis (Ref.18-20). By use of these computer programs, temperature distributions in slab, cylindrical, and tubular charges made up of magnetic and non-magnetic materials can be estimated under a variety of heating conditions. However, neither the analytical procedure nor the computer programs are readily available for public use. In addition, heating of tubes prior to nosing poses another problem. In this operation, only a part of the tube is heated. During the heating and the subsequent transfer of the tube to the nosing press, heat is conducted to the unheated portion of the tube. Thus, the heat transfer causes a temperature gradient along the axis of the tube. The nature of this temperature gradient is very critical to avoid the buckling of the tube during nosing. The existing general equations (Ref.21-22) are, therefore, not applicable to partially heated tubes. Hence, in order to estimate the temperature distribution in a partially heated tube, special-purpose equations were derived. The derivation procedure and the derived equations are given in Appendix B.

Heat Transfer During Induction Heating

During induction heating of a tube end, a major portion of the heat generated remains in the charge, i.e., the tube; a part of the heat flows into the unheated cold section of the tube by conduction; an additional fraction of the heat generated is lost to the environment by convection and radiation. In order to predict the local temperatures, it is necessary to consider the heat

equalization due to heat transfer. Because of the complexity of the phenomenon, it is appropriate to use the finite-difference method for solving the heat transfer equations. During a small time interval, Δt, it is assumed that the heat generation takes place instantaneously at the beginning of the interval Δt. Using these calculated values of temperature as temperatures before Δt, the heat flow is analyzed and the temperature field, which exists after the heat loss by conduction, convection, and radiation during the same interval Δt, is determined. The repetition of these two steps simulates numerically the heat generation and transfer simultaneously and gives the temperature distribution as a function of time. The difference equations used in the finite-difference heat transfer analysis, under different boundary conditions of the shell-nosing operation, are also given in Appendix B.

Heat Transfer after Induction Heating

After the heating of the tube, temperature equalization takes place during the interval between heating and the actual forming operation. During this period, no heat is generated, but heat is conducted to the cooler portion of the tubes and is convected and radiated to the atmosphere. Temperature fields which exist during and after this cooling period are generated using the same procedure and the equations used before, but excluding the heat generation aspect.

Prediction of Temperature Fields in Inductively Heated Tubular Components

In order to effectively apply these principles of heat generation and transfer to practical problems, the entire procedure is computerized. The set of computer programs performing this analysis is called INHEAT. Figure 5 shows the functional flow chart of INHEAT. As seen in Figure 5, a complete simulation of the induction heating and subsequent temperature equalization is undertaken to determine the non-steady state temperature distributions in tubes at various time intervals. This process analysis is applicable to both magnetic and non-magnetic materials.

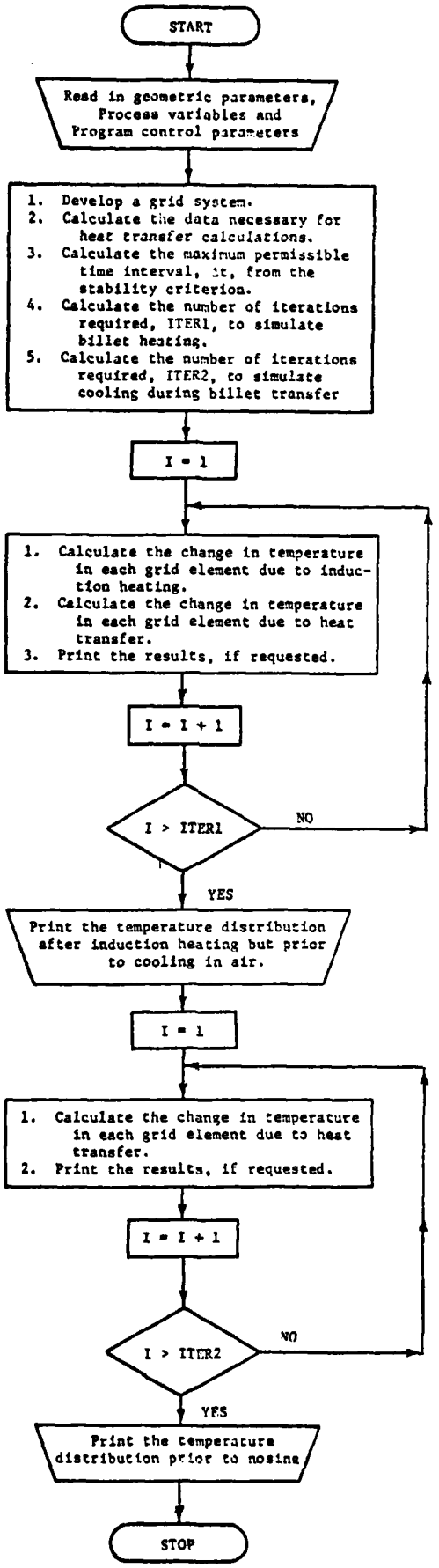

Fig 5 Functional Flow Chart of the Computer Program INHEAT

For the purpose of heat transfer analysis by finite-difference method, a portion of the vertical cross section of the tube is considered as to be divided into a number of trapezoidal grid elements, as seen in Figure 6. The maximum value of Δt for the proposed grid pattern is determined using the stability criterion, given in Appendix B. For simulation, it is assumed that the temperature rise due to induction heating takes place instantaneously during the time interval Δt, followed by heat transfer during the same time interval.

At the beginning, the temperature in each grid point is set to the same value as the preheat temperature of the tube, or the room temperature if the tube is not preheated. Temperature rise due to induction heating during a time interval Δt is calculated from the process variables and added to each grid within the heating zone of the tube. Using these calculated values of temperature, the heat flow is analyzed and the temperature field which exists after heat transfer in the time interval Δt is determined. By repeating the sequence of heat generation and heat transfer, the non-steady state temperature fields in the tube at various time intervals are determined.

During this analysis, all the temperature dependent material properties, such as heat capacity, thermal conductivity, electrical resistivity and magnetic permeability are estimated separately for each grid in the system using its instantaneous temperature.

Following induction heating, temperature equalization takes place during the transfer of the billet to the press. Thus, the temperature distribution prior to nosing is the one after temperature equalization. Hence, to obtain the temperature distribution prior to nosing, the same heat transfer analysis, excluding the heat generation aspect, is performed for the duration of billet transfer. After the simulation, temperature distributions at the end of the induction heating and prior to nosing are printed in a tabular form as shown in Figure B-2 of Appendix B, attached to this report. Intermediate results, if desired, may also be obtained by assigning appropriate values to program control parameters, as described in Appendix B.

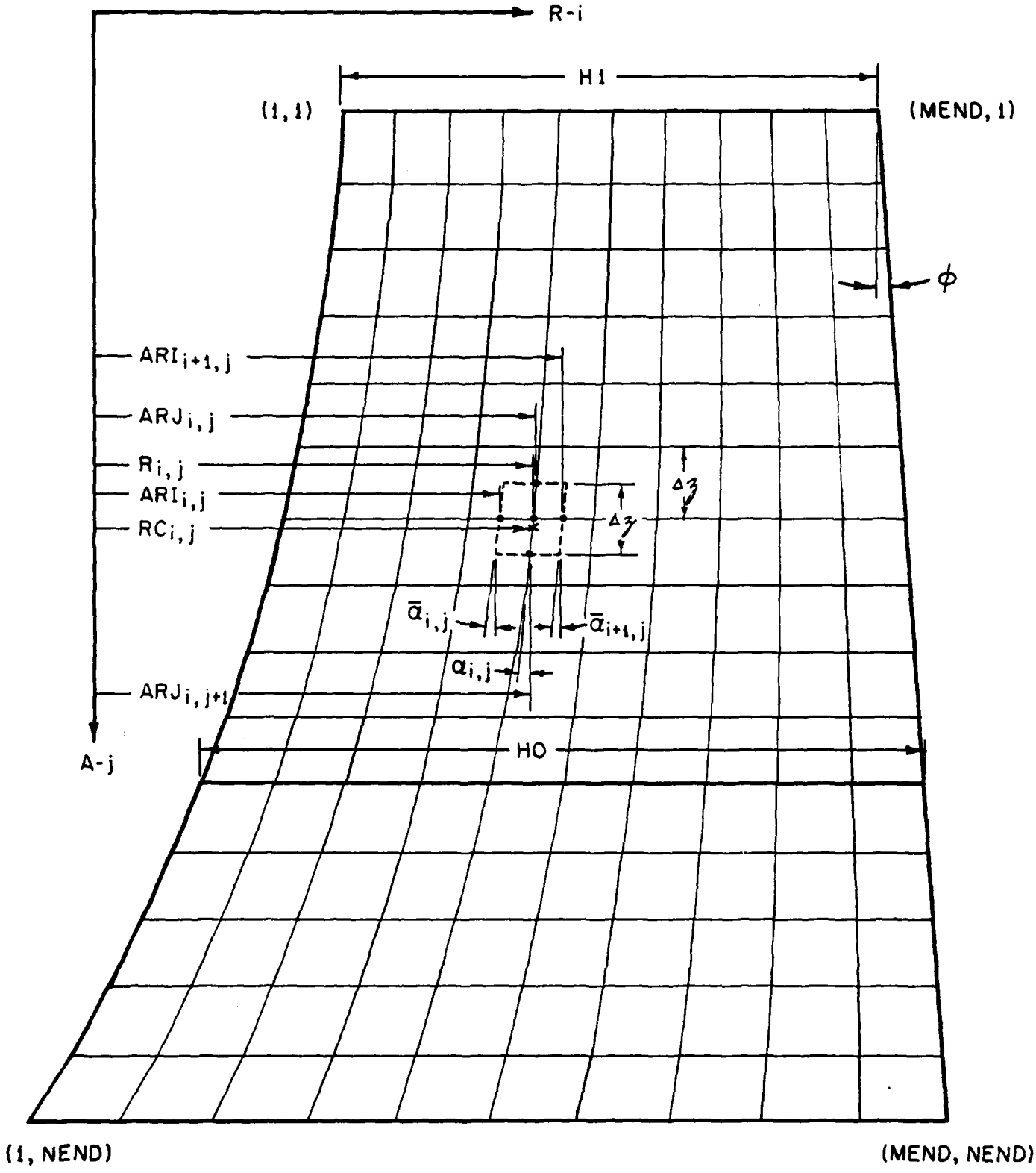

Fig 6 Trapezoidal Elements in the Grid System for Heat Transfer Analysis

Experimental Evaluation

To assess the applicability and the accuracy of the computer programs INHEAT, the following special-purpose experiments were conducted. As illustrated in Figure 7, four thermocouples were welded on the outer surfaces of each of two 2-inch OD, 1.5-inch ID and 8-inch long tubes. One of the tubes was made of stainless steel type 304. This tube was totally annealed (15 minutes at 1050 C and rapidly cooled in air blast) prior to induction heating to eliminate the effect of cold work on its magnetic permeability. The other tube was made of AISI 1045 medium carbon steel. An induction coil, with 14 turns over a length of four inches, was specially made using 0.25-inch OD copper tube. For insulation, the entire length of the tube was wrapped with fiberglass sheets. To eliminate the excessive heating of the induction coil during induction heating, water was continuously circulated through the tube using a separate pump.

Figure 8 illustrates the experimental set up with one of the steel tubes in position in the induction coil. The terminals of the thermocouples are connected to two, two-channel Honeywell Electronic 19 recorders. The power to the induction coil was supplied by an Ajax Magnathermic Corporation's induction machine, Model 23HT. This machine is equipped with a motor generator set. The output voltage of the generator can be adjusted between 0 and 800 volts; consequently, the output current and the output power will vary between 0 and 125 amps and 0 and 100 KVA, respectively. To improve the power factor, the generator output circuit is equipped with an adjustable capacitor set. The output circuit is also equipped with an adjustable transformer to match the load voltage of the coil to the generator output voltage. The output frequency of the generator is fixed at 10 KHz. The equivalent heating circuit used in this equipment is schematically represented in Figure 9.

Prior to the actual experiment, several preliminary tests were run (a) to improve the power factor of the generator output by adjusting the capacitor in the circuit, and (b) to match the load voltage to the output voltage of the generator by varying the transformer ratio. During the individual heating of both steel tubes, output from all the four thermocouples were recorded on Honeywell recorders. The current in the induction coil circuit

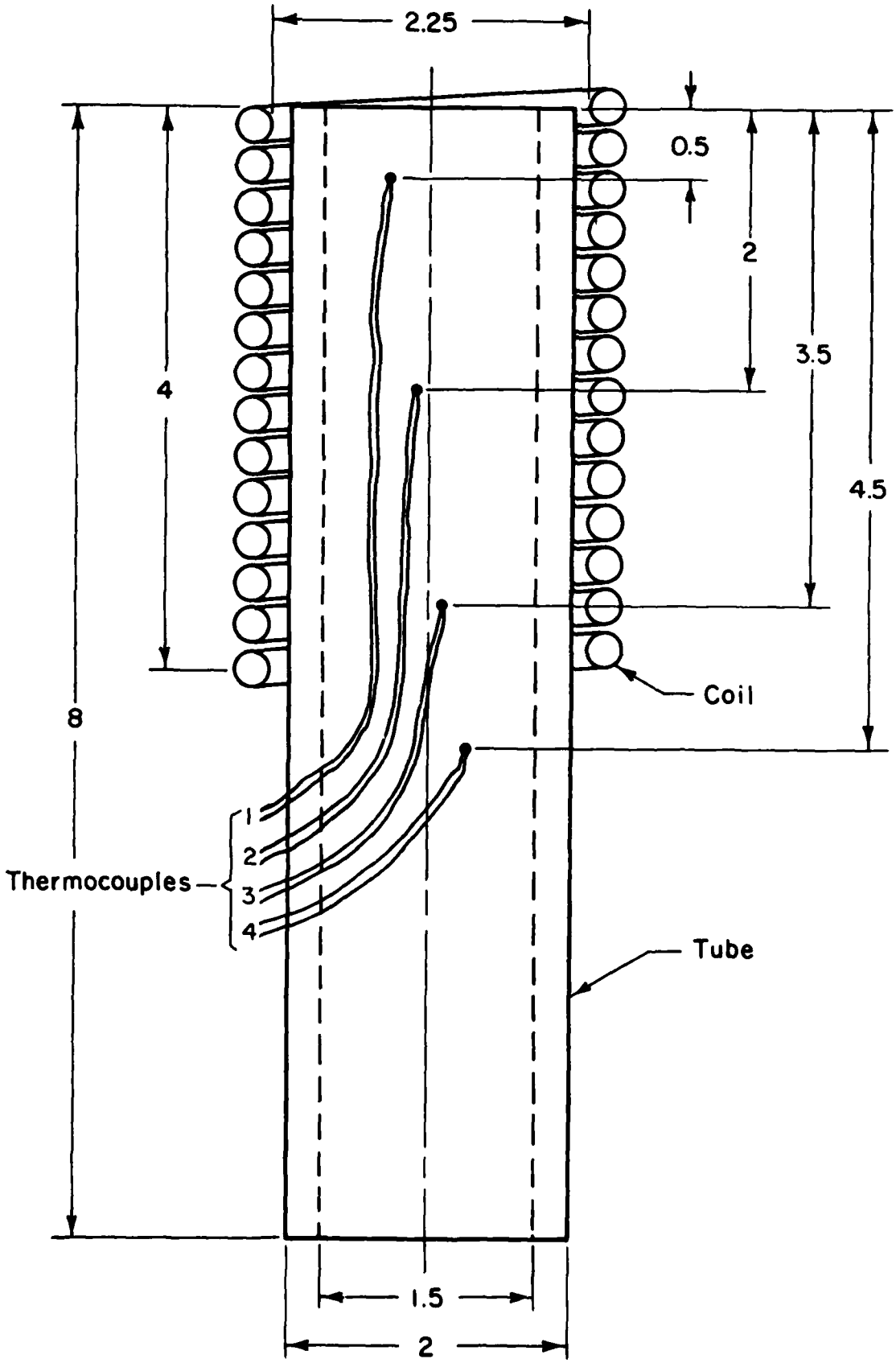

Fig 7 Schematic Representation of the Induction Heating Set Up

Fig 8 Experimental Set Up for Induction Heating of Tubes

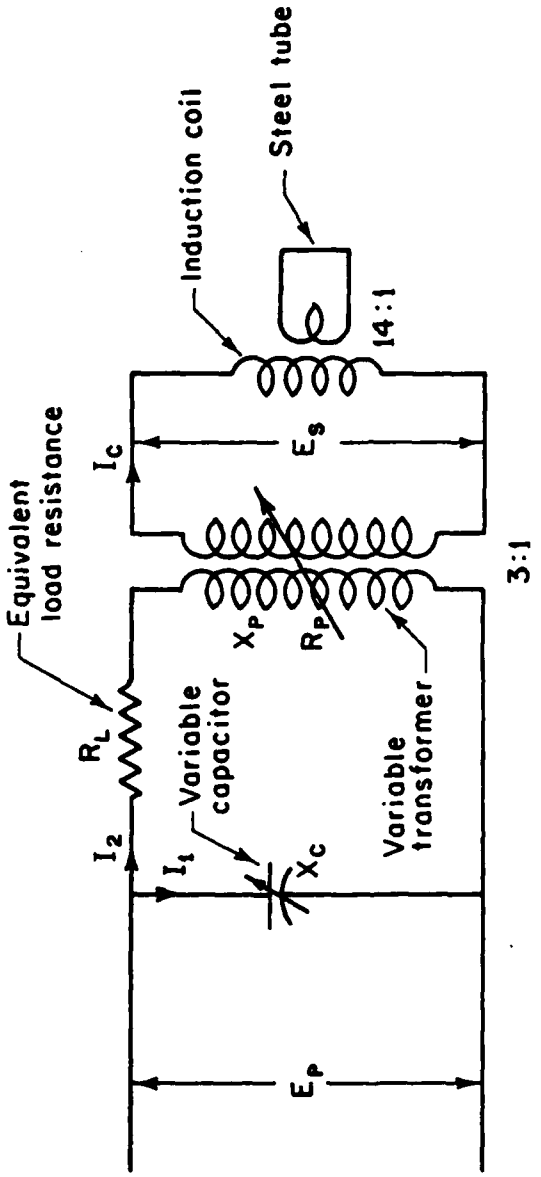

Fig 9 Schematic of the Equivalent Heating Circuit

could not be measured due to the non-availability of suitable meter to measure 1000 amps at 10 KHz. However, the voltage across the coil was measured using a Hewlett-Packard RMS voltmeter capable of functioning between 50 Hz and 3 MHz. The output voltage of the generator was adjusted such that the tubes will be heated from room temperature to about 1000 C in about 20 seconds.

Computer-Aided Estimation of Temperatures for Experimental Conditions

Since the current in the induction coil circuit could not be measured directly, it was estimated by the following procedure:

From the skin depth of the tube, the load resistance was calculated using the formula:

$$R = \frac{\rho \pi D}{\delta \ell_c} , \qquad (5)$$

where ρ is the electrical resistivity of the material

D is the outer diameter of the tube

ℓ_c is the length of the induction coil

and δ is the skin depth and is given by $\frac{1}{2\pi} \frac{\rho}{\mu f}$.

Using the transformer ratios, the equivalent load resistance R_L in the primary, Figure 9, was estimated from R, given by Equation (5). The inductance X_c was calculated from the capacitor in the primary circuit. Since the circuit was tuned up, it was assumed that the inductance of the adjustable transformer primary, X_p in Figure 9, is equal to X_c and its resistance R_p is negligible. From the known primary input voltage E_p and the resistance R_L and inductance X_p, the current in the primary I_2 was obtained applying Ohm's law. The current in the secondary, I_c, is the product of the primary current I_2, and the transformer ratio.

Also, since the secondary voltage was measured separately, the secondary current I_c was estimated independently following the procedure described in References 15 and 16. Both the estimated currents were close within acceptable engineering accuracy.

Using this estimated current value in INHEAT, temperatures at various points in the tube were estimated. The formula given in Appendix B to estimate the temperature rise due to induction heating is for ideal heating condition. Because the practical conditions differ considerably from the ideal situation, an efficiency factor was introduced in Equation (B-11a) of Appendix B in estimating the temperatures. This efficiency factor, which depends upon (a) the coil design, (b) cross-sectional geometry of the copper tube forming the coil, (c) air gap between the coil and the tube heated, and (d) physical properties of the material being heated, was estimated as 50 percent in the present tests. In a practical condition, the efficiency factor can be estimated by running a preliminary trial, measuring the temperature at a specific point on the tube and comparing the results with the estimated temperature.

Comparison of Predictions with Experimental Results

For comparison with the actually measured temperatures, the estimated temperatures at different locations of the thermocouples were plotted along with the measured temperatures. Figure 10 shows the temperature distributions in type 304 stainless steel. Estimated temperatures in thermocouples 1, 2 and 3 (refer to Figure 7 for the locations of the thermocouples) are very close to each other at all times. Measured temperatures in thermocouples 1 and 2 are similarly distributed as the estimated temperatures, except for a slow response during the early stages of heating. This slow response is attributed to the inertia effect of the mechanical type recorder used in this experiment. With the use of optical or some other quick response recorders, this discrepancy could be eliminated.

The measured temperature in thermocouple 3 is very much lower than the estimated temperature. In the estimation procedure, temperature rise due to induction heating is assumed to be uniform over the entire length of the induction coil. However, when the length of the induction coil is shorter than the workpiece, heat generated closer to the end of the induction coil is less than predicted, due to end effects. Due to this well-known phenomenon, a provision has already been incorporated in the computer programs to account for the variations in heat generation along the axis of the coil; but due to the lack of any reliable data, this particular feature could not be used in the present analysis. As a result,

the estimated temperature distribution at the location of thermocouple 3 is much higher than the measured distribution. In order to determine the true distribution of heat generation along the axis of the coil, it is necessary to run more trials with a number of thermocouples along the entire length being heated. A similar trend of deviations exhibited by thermocouple 4 (refer to Figure 10) is purely a consequence of the difference between the measured and estimated temperature distributions from thermocouple 3.

Figure 11 shows the temperature distributions in AISI 1045 steel. Similar to the results in Figure 10, the retarded response of the measured temperatures may be attributed to the inertia effect of the mechanical recording device. Unlike in the stainless steel, the measured temperature distribution from thermocouple 1 is very much lower than the estimated distribution. Although the above discrepancy may be attributed to various factors associated with the assumptions of the mathematical model and with the conditions of the experiments. However, the main factor responsible for poor correlation between the predicted and the experimental results near the lower end of the coil, Figure 12, is the well-known "end effect". In the mathematical modeling of the problem, this end effect was assumed to be negligible for the sake of simplicity and a one-dimensional analysis was developed. A rigorous two-dimensional analytical approach, considering the end effect, may be very complicated and may or may not significantly improve the end results. Hence, it is believed that a combined analytical-empirical approach may be easier and more suitable for the present application.

Because of the end effects, the amount of heat generated per unit volume near the lower end of the coil is smaller than that around the mid length of the coil. Thus, the generation of induction heat, due to a uniformly spaced coil, is not uniform along the length of the coil and will be as shown in Figure 12. This pattern of heat generation may depend upon several factors, such as (a) size of the tube, (b) magnetic properties of the material heated, (c) the frequency of the heating current, (d) heating rate, and more importantly, (e) the coil design. Neither analytical nor empirical results considering the end effects are available in any reviewed technical publications. Hence, it is necessary to conduct experiments with 105 mm, 155 mm, 175 mm and 8-inch diameter shell preforms to generate the heat generation profiles. At this time, it is expected that in a given installation (i.e., for a particular coil design), the size of the tube on the heat generation pattern will have the maximum effect on heat generation and the

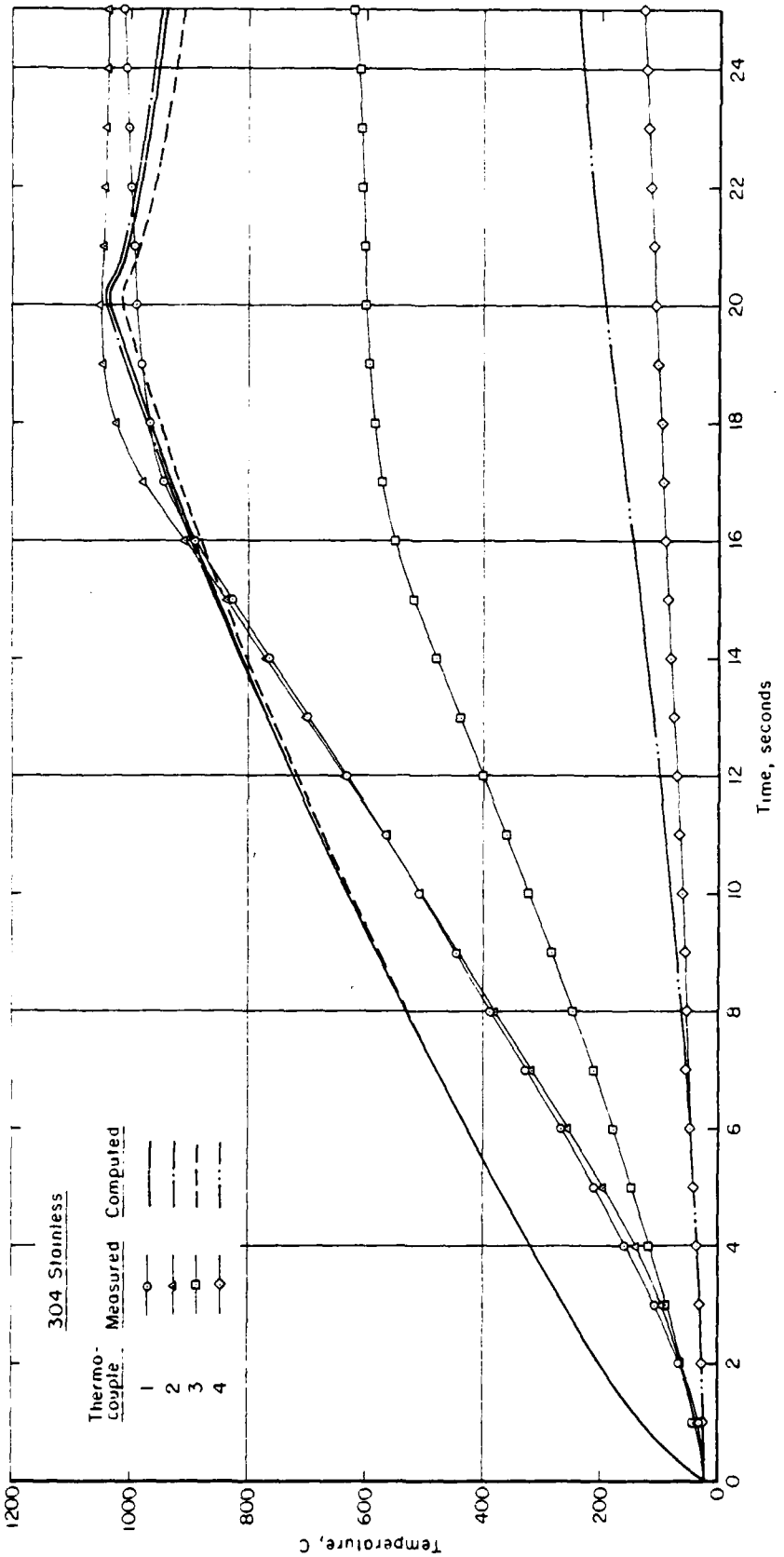

Fig 10 Measured and Computed Temperature Distributions in Stainless Steel Tube

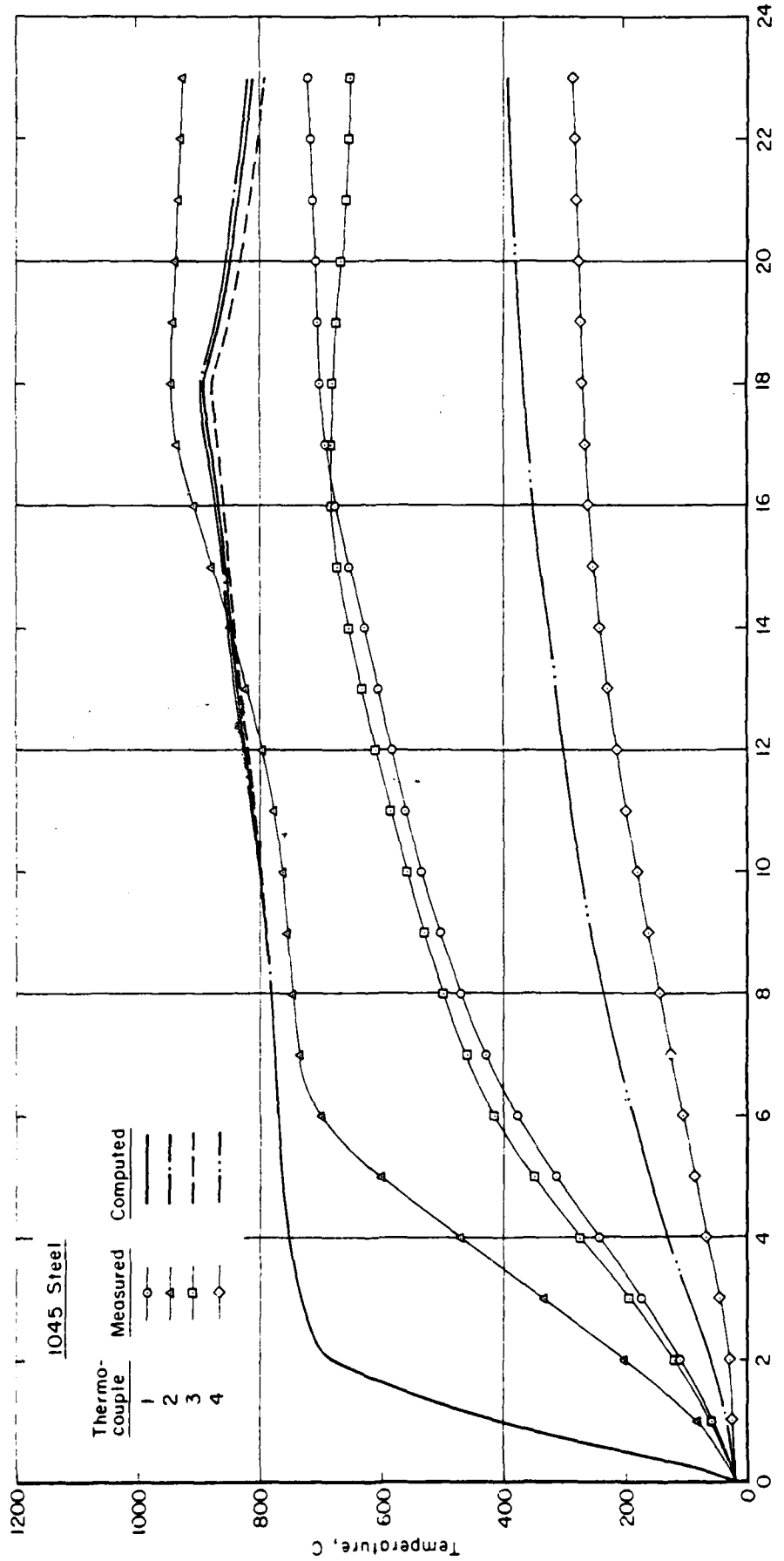

Fig 11 Measured and Computed Temperature Distributions in 1045 Steel Tube

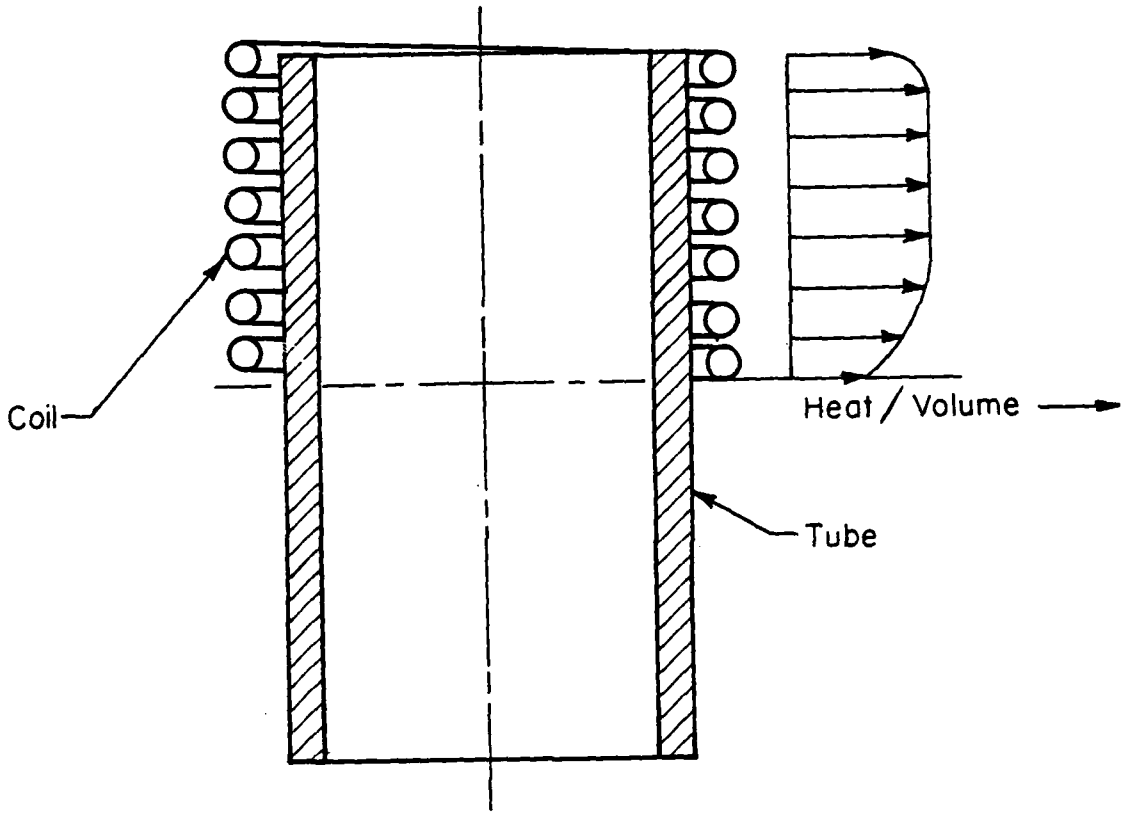

Fig 12 Heat Generation in Partially Heated Tube by Induction Heating

other process variables, listed above, will have negligible effects. By conducting a planned set of experiments, the least important variables, influencing heat generation in the shell wall, can be identified and eliminated from the list. Also, the heat generation patterns under various conditions of the effective variables can be established. Once these profiles are determined, the computer program INDHET can use these heat generation patterns as inputs and predict the results more accurately than the predictions now.

ANALYSIS AND PREDICTION OF METAL FLOW IN NOSING

In nosing of shells, the shape of the outer surface of the shell follows the die profile while the inner surface is not supported, as shown in Figure 13. Thus, during the nosing operation, the part of the tube or shell within the die zone can move either radially inward, or in the direction of the tangent to the die profile, or in both directions, simultaneously. Under plastic state, metals flow in the direction of least resistance; therefore, the metal flow in cold nosing is affected by the frictional restraint at the die-workpiece interface and by the work-hardening characteristics of the material being deformed. In hot nosing, the metal flow depends upon the friction, the temperature of the workpiece and the speed of the die. In general, wall thickening increases with increasing friction, and in fact, under severe friction conditions, the nosed tube or shell may shrink in length instead of elongating.

Under this program, a mathematical model for predicting metal flow in nosing of shells was developed. This model considers preform with uniform wall thickness and utilizes Hill's general method of analysis for metalworking processes (Ref. 23-24). Thus, the model is exactly valid for nosing of shells up to 105-mm size, which are usually nosed from preforms with uniform walls. For larger shells, where the preform wall thickness is not uniform, this analysis can be applied only approximately.

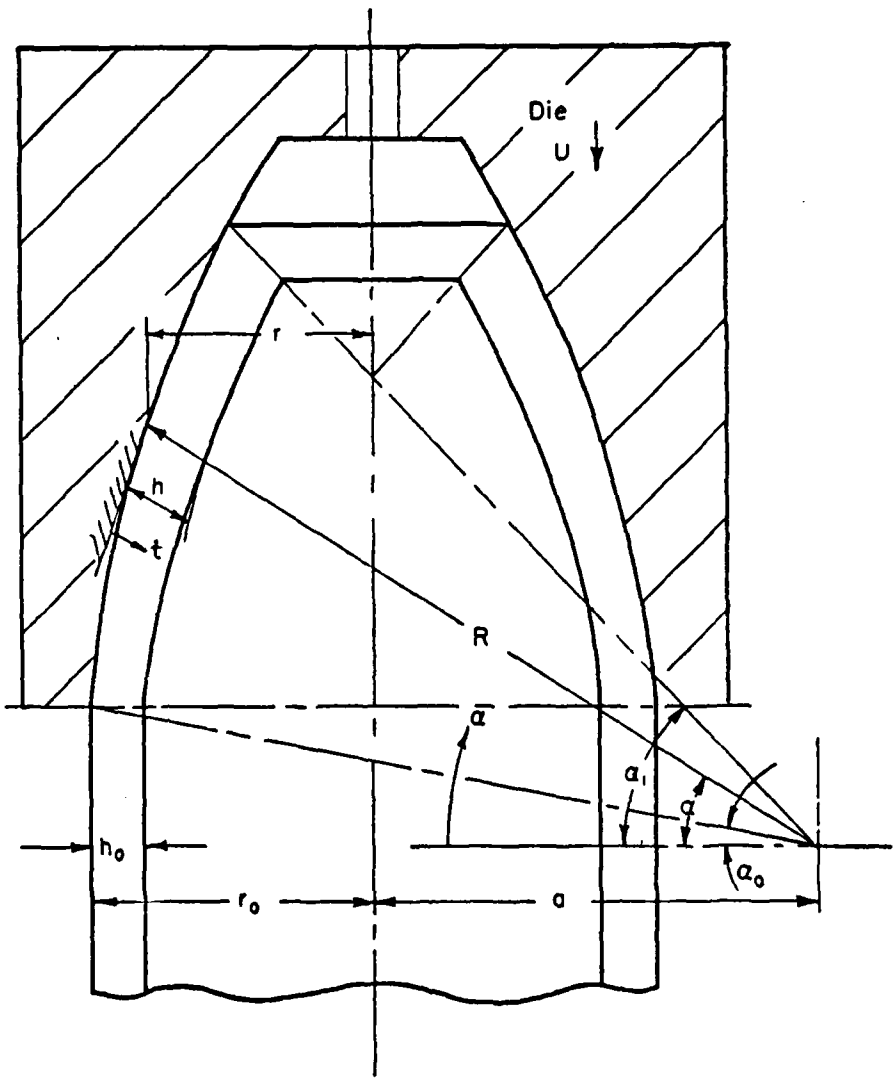

Fig 13 Configuration of Shell During Nosing

Analysis

The first step in using Hill's method consists of choosing a class of kinematically-admissible velocity fields (with $h(\alpha)$, the unknown thickness function in a (see Figure 13) from which the best approximation will eventually be selected. The associated stress distribution is determined using the flow rule and the yield criterion, which will generally not satisfy all the statical requirements. Therefore, a second kinematically-admissible velocity field, called the orthogonalizing field, and which can be similar to the first velocity field, is selected and the converse to the virtual work-rate principle is applied. This results into a system of equilibrium equations and boundary conditions, suited to the particular approximating velocity field and uniquely determining its best member. The details of Hill's method and the analysis of metal flow in nosing of shells using this method are included in Appendix C.

As given by Equation (C-15) in Appendix C, the thickness function, $h(\alpha)$, of shell wall is defined by a second order ordinary differential equation. Using the boundary conditions given by Equation (C-16) in Appendix C, Equation (C-15) can be easily solved using a numerical technique. However, since the boundary conditions are available at each end of the interval, some type of interative method is required for numerical integration of Equation (C-15). For this purpose, initially two guesses of $h'(\alpha_o)$ are made and the Equation (C-15) is solved by a fifth order Runge-Kutta Method. Normally, these solutions will not satisfy the second of the boundary conditions, Equation (C-16). Therefore, a third guess value of $h'(\alpha_o)$ is determined using the first two solutions by linear extrapolation such that the projected error in $h'(\alpha_1)$ is zero, and the entire integration procedure is repeated. This last step is repeated with last two solutions until the error in $h'(\alpha_1)$ is within specified error bounds. Further, the Equation (C-15) is singular when $\alpha_o = 0$, since $r'(\alpha = \alpha_o = 0) = 0$. In this particular case, a solution can be obtained by taking α_o as a small positive quantity instead of zero. The error caused by this approximation is relatively small.

Based on the above analysis, a computer program, named NOSFLW, was developed to predict metal flow during nosing of shells. The program NOSFLW is coded in FORTRAN IV and requires approximately $25{,}000_8$ words of memory space in a

CDC CYBER 70 computer. A typical run requires approximately 7.0 system seconds, including 5.5 seconds on the central processor. All the input data to the computer program NOSFLW are transferred through READ statements. These include variables defining the geometries of the preform and nosed shell, the friction shear factor at the die-workpiece interface, the velocity of the die, the flow stress of the workpiece material and two guess values of the slope of the inner profile at the base of the nose. As output, the computer program prints the coordinates of the inner and outer profiles of the nose, the elongation due to nosing, the maximum thickening of the wall and the estimated nosing load. The computer printout also gives the velocity field in the deformation zone, i.e., the velocities, the strains and strain rates as functions of locations along the nosed portion. A functional flow chart of the computer program NOSFLW is given in Figure 14.

Parametric Study

In order to illustrate the application of the analysis and the associated computer program, predictions were made for cold nosing of 105-mm M1 shell from a tubular preform with uniform wall thickness. For this purpose, the values of the input variables to the computer program NOSFLW were selected from the engineering drawings (after including the finish machining allowances) as given in Table 4.

Table 4 Dimensions for 105-mm M1 Shell

Outside diameter at the nose base	= 108 mm
Radius of curvature of the nose ogive	= 650 mm
Initial wall thickness of the preform	= 12 mm
Axial length of the nosed portion	= 150 mm
Distance of the ogive center from nose base	= 25 mm

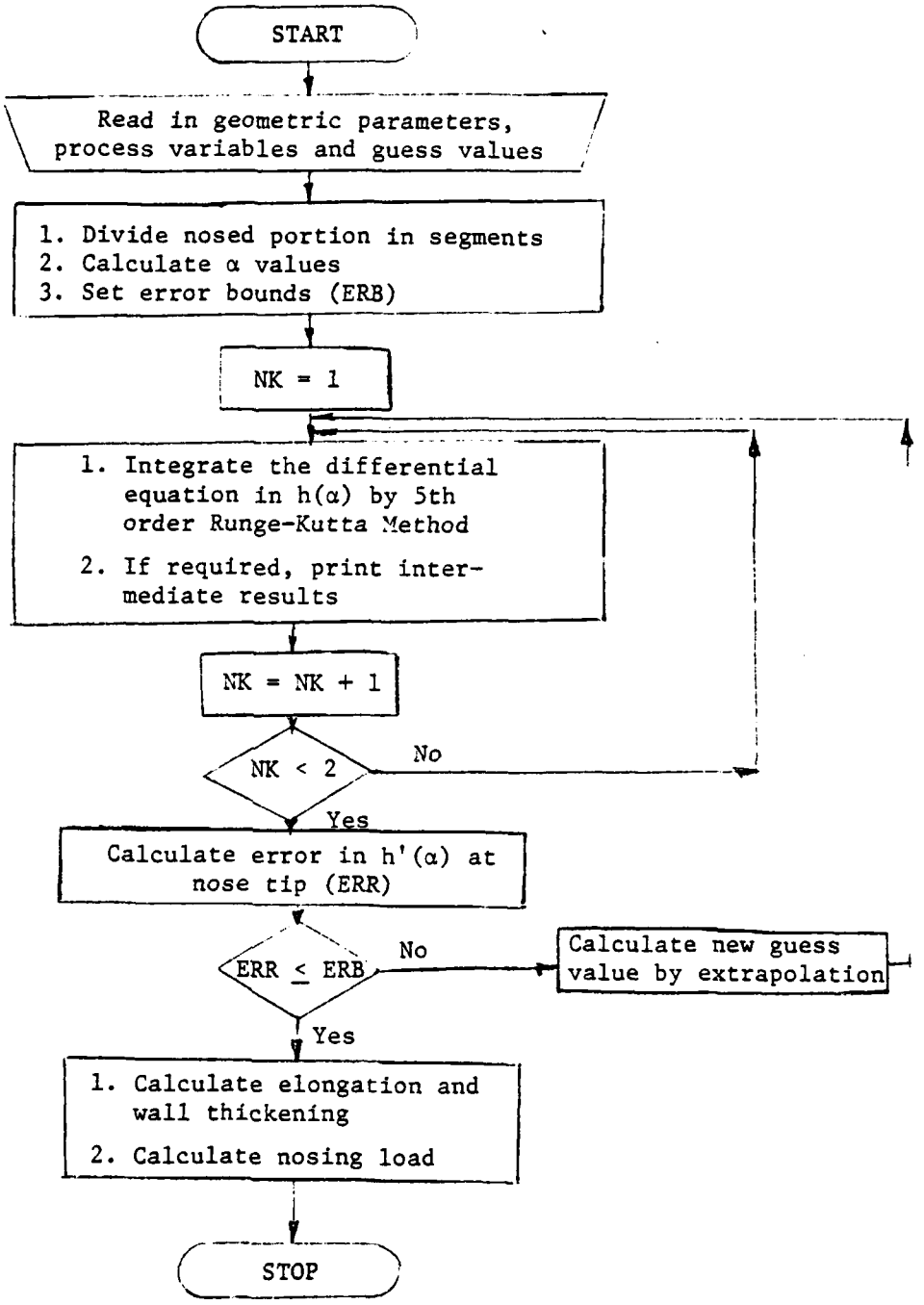

Fig 14 Functional Flow Chart of the Computer Program NOSFLW

The friction shear factor at the die-workpiece interface was estimated to be 0.05. The computer program predicts a maximum wall thickening of 68.34 percent and an elongation of 1.7 percent after nosing is completed. The actual preform geometry and the predicted shell geometry after nosing is shown in Figure 15. Although no experimental data were available for comparison, the nosed shape in Figure 15 is in reasonably good agreement with the desired shape after nosing for 105-mm M1 shell.

As stated earlier, depending upon the frictional restraint at the tool-workpiece interface, the shell length may increase or decrease as it penetrates in the nosing die. As seen in Figure 16, at low values of the friction shear factor, the shell elongates due to nosing, whereas, at high values of friction, the shell elongates in the initial stages of nosing and then starts to shrink in length as penetration into the die is increased. This predicted trend is in agreement with experimental observations reported in the literature (Ref.6).

During nosing, the shell-wall thickness invariably increases with increasing penetration in the die and with increasing frictional restraint at the die-workpiece interface. Figure 17 illustrates this trend as predicted by the present analysis and the associated computer programs.

As a by-product, the present analysis also predicts the load required during nosing of shells. Figure 18 shows predicted values of the nosing load normalized with respect to area of cross section and the flow stress at the nose base for various values of the friction shear factor selected in the present study. The trend is in agreement with experimental observations (Ref.4). This analysis is also capable of predicting the limiting conditions of the process. As seen in Figure 18, a complete nosing operation will not be possible with a friction shear factor larger than 0.07 due to local yielding at the nose base. For this reason, good lubrication is essential in nosing of shells, apart from obtaining a desired geometry after nosing.

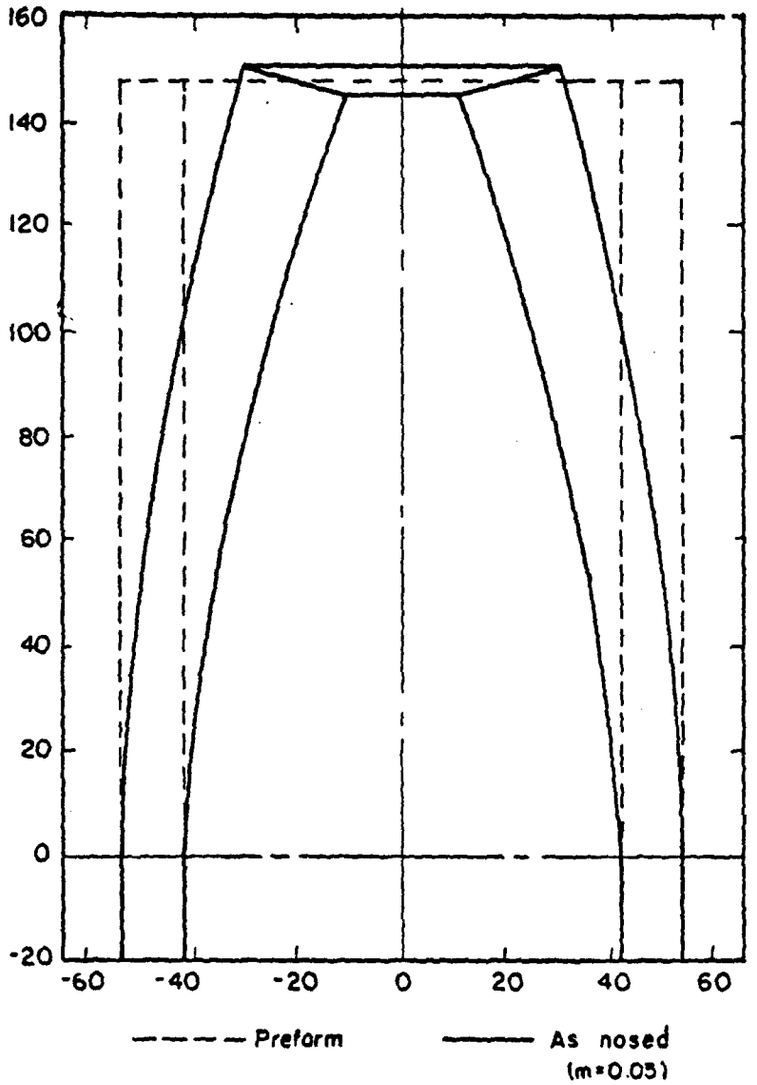

Fig 15 Preform Shape and As-Nosed Shape Predicted by the Computer Program NOSFLW for 105 mm M1 Shell

(All Dimensions in mm)

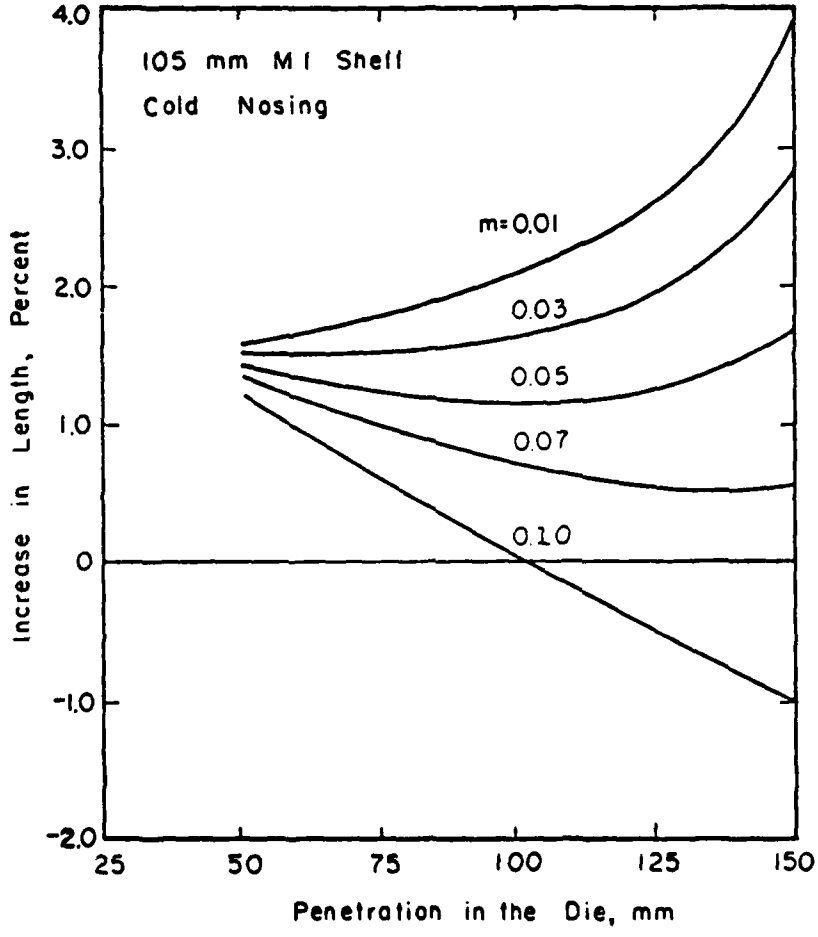

Fig 16 Elongation in Shell Length Due to Nosing at Various Friction Values

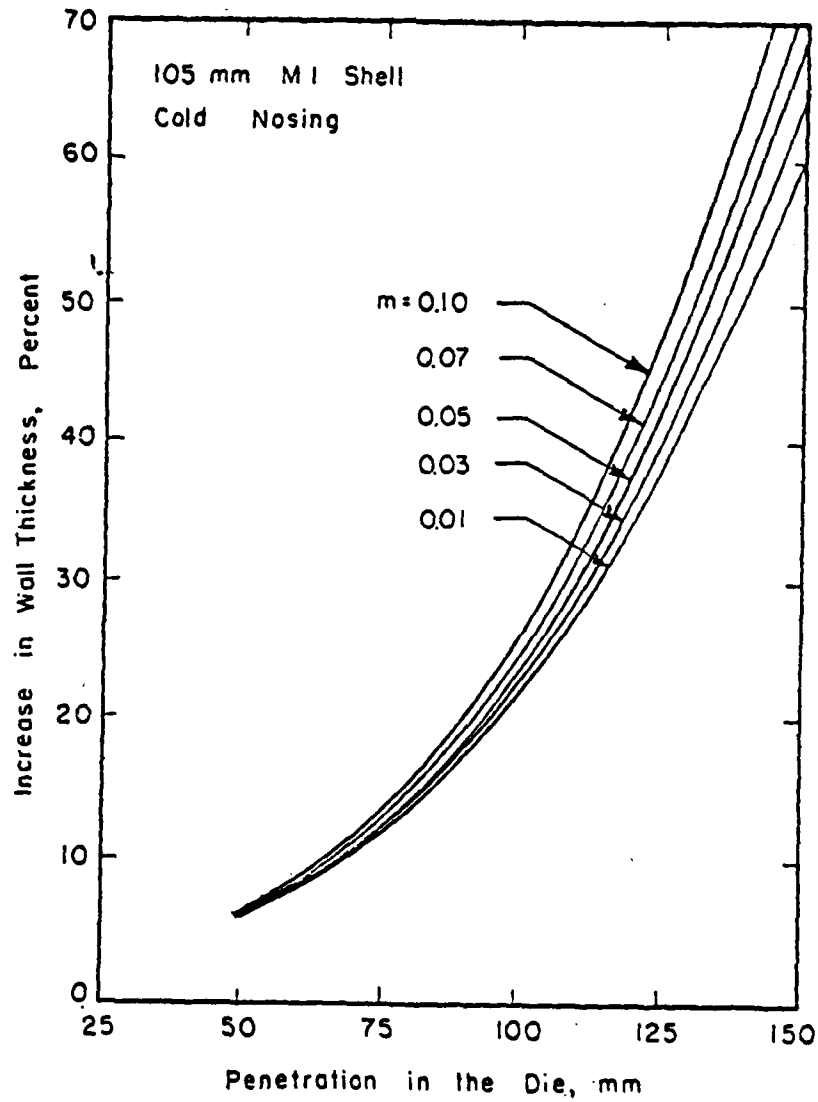

Fig 17 Increase in Wall Thickness Due to Nosing at Various Friction Values

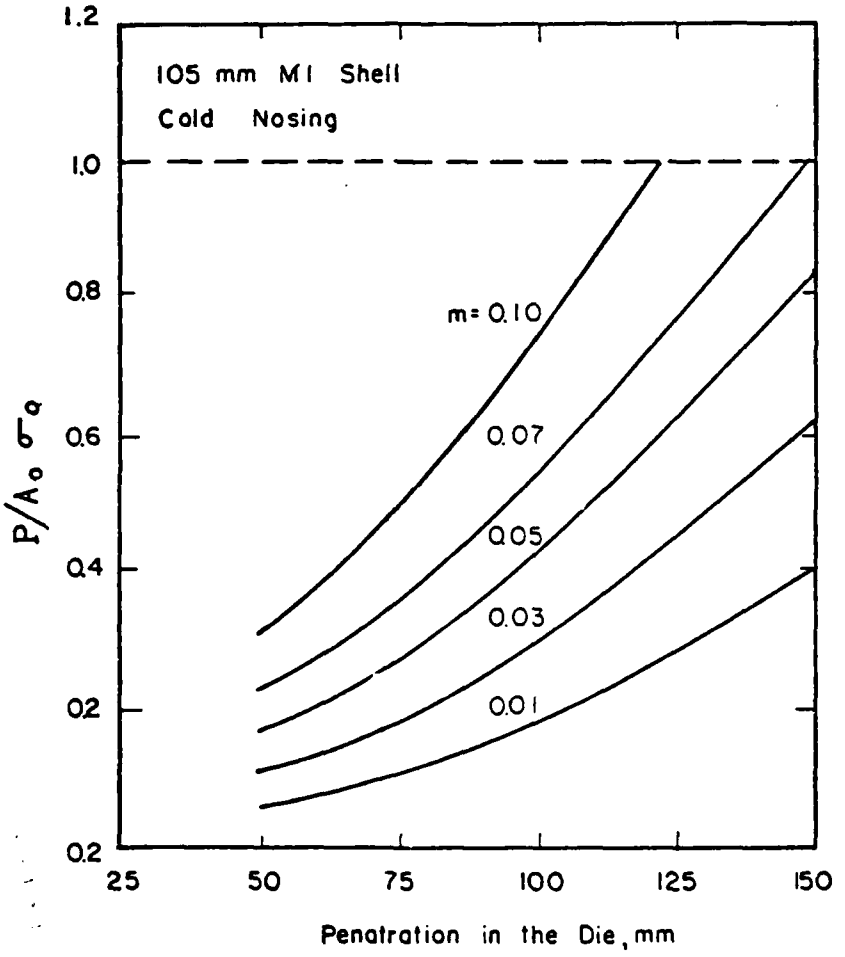

Fig 18 Normalized Load During Nosing at Various Values of Friction Shear Factor (P = Nosing Load, A_o and σ_o are the area of cross section and the flow stress at the nose base)

ANALYSIS OF STRESSES AND MATERIAL FAILURE IN NOSING OF SHELLS

Nadai (Ref.1) analyzed the stresses in nosing of shells. The analysis assumed that the tube material is perfectly plastic and that the wall thickness does not change appreciably during the nosing process. Onat and Prager (Ref.2) extended Nadai's work and included the changes in the shell-wall thickness. However, both analyses assume a preform of uniform wall thickness and calculate the state of stresses at the end of the nosing operation. Therefore, in order to generate a load-stroke curve and treat preforms with nonuniform wall thickness, a step-by-step approach of stress analysis is described in the following. In addition, the following analysis is valid for real materials since it considers the flow stress of the deforming material as a function of strain, strain rate and temperature.

A schematic diagram of nosing of shells is shown in Figure 19. The length of the preform is divided into a number of segments. For nonuniform-walled preforms, if the number of segments is sufficiently large, the variation in thickness along the length of the segment can be ignored, and the average thickness of the segment can be taken as its uniform thickness. Using this simplification, Onat and Prager's analysis can be applied to each element. If the preform has uniform wall thickness, this simplication is not necessary. However, for the sake of generality, the analysis was developed for nosing with nonuniform-walled preforms.

The nosing operation can be simulated by moving the die over one segment of the preform at a time. Thus, when a segment is inside the die, it is deformed plastically and takes a new average thickness given by (3), if the shell does not elongate, or by Equation (4), if elongation due to nosing is considered. During the next step, this segment is pushed further inside the die and a new element of the preform is deformed for the first time. At each step, the stresses and the thickness of each element are calculated. Thus, the nosing process is simulated in a finite number of discrete steps.

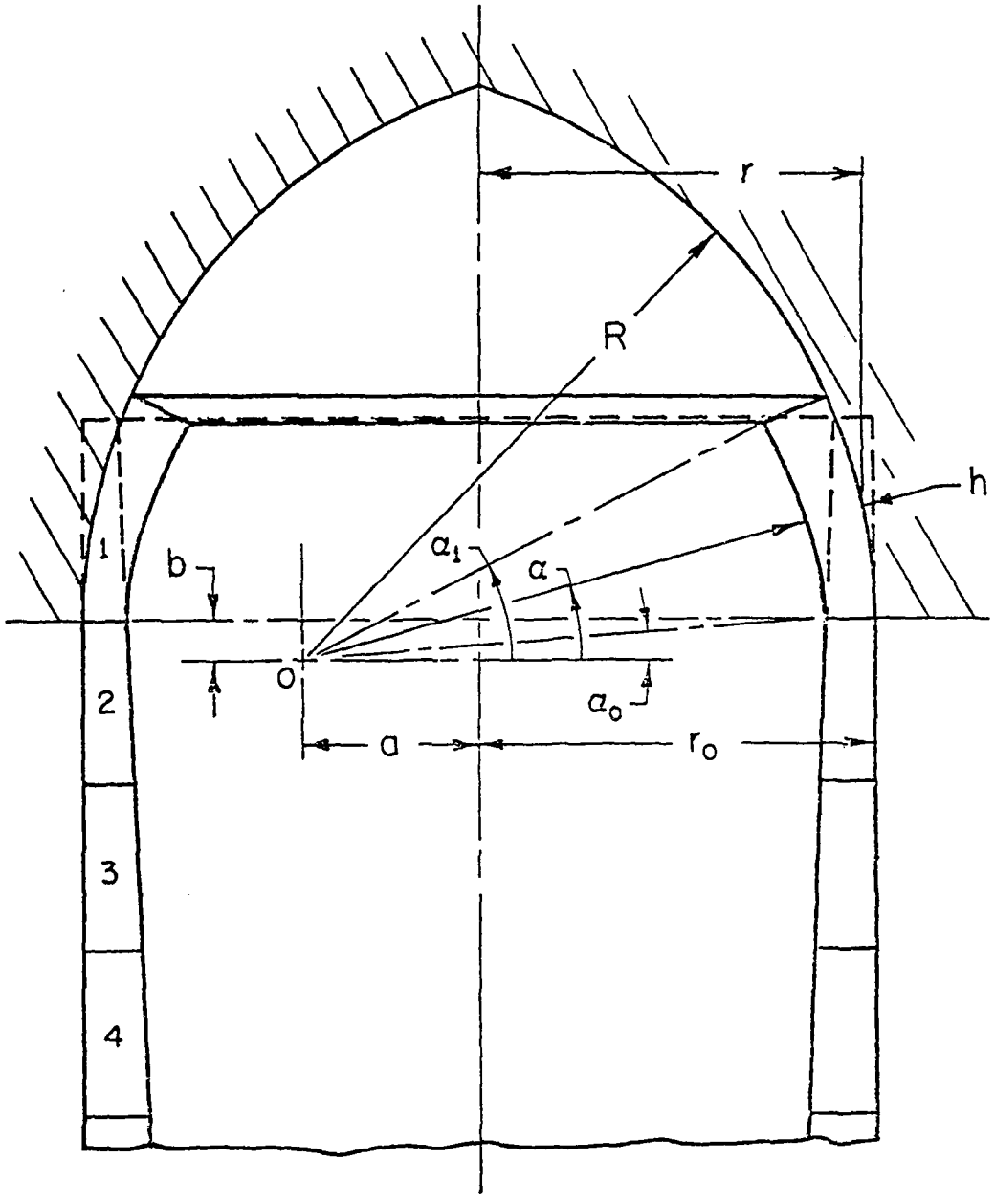

Fig 19 Schematic Diagram of Nosing of Shells

Analysis of Stresses

Let us consider the analysis of stresses for element (1), Figure 19. The analysis of stresses for the subsequent elements will be the same, except for the boundary conditions which are to be determined from the known stress distribution of the preceding element. The surface traction exerted by the die on the nose is the normal pressure, p, and the friction shear stress, $f = \mu p$, where μ is the coefficient of friction. The meridianal stress and the circumferential stress produced by these surface tractions in the thin-walled nose far exceed p and f in absolute value. Therefore, the state of stress in the nose wall can be treated as plane with the circumferential stress σ_c and the meridianal stress σ_m as the principal stresses. Since these principal stresses are compressive, and since σ_c can be expected to exceed σ_m in absolute value, according to Tresca's yield criterion,

$$\sigma_c = -\bar{\sigma} \quad , \tag{6}$$

where $\bar{\sigma}$ is the material flow stress, and it is a function of the strain, strain rate and temperature. Equilibrium of forces in the meridianal and the circumferential directions, together with Equation (9), yield the following:

$$\frac{d\sigma_m}{d\alpha} + \mu\,\sigma_m = \bar{\sigma}\,\frac{\sin\alpha + \mu\cos\alpha}{\cos\alpha - a/R} \quad . \tag{7}$$

Integration above equation gives the distribution of the meridianal stress σ_m as below:

$$\sigma_m = \sigma' e^{\mu(\alpha_1 - \alpha)} - \bar{\sigma} e^{\mu(\alpha_1 - \alpha)} \int_{\alpha}^{\alpha_1} \frac{\sin\alpha + \mu\cos\alpha}{\cos\alpha - a/R} e^{\mu(\alpha - \alpha_1)}\, d\alpha \quad , \tag{8}$$

where σ' is the meridianal stress at $\alpha = \alpha_1$, the tip of the element under consideration. For element (1), $\sigma_m = 0$ at $\alpha = \alpha_1$. With this boundary condition, the meridianal stress σ_m can be found as a function of α for element (1). For the subsequent elements, the boundary condition at the leading end of the element is given from the known value of σ_m from the analysis of stresses in the preceding

element. Thus, because the value of σ_m at the boundary of elements (1) and (2) is known from the analysis of stresses in element (1), Equation (8) can be solved to determine stresses in element (2). Similar procedure is applied to subsequent elements. A detailed derivation of this stress analysis is given in Appendix D.

In the calculations, the flow stress of each element considered as a function of the strain, strain rate, and temperature. The strain in an element is the cumulative strain. The strain rate is calculated from a simple velocity field given in Appendix C. The temperature of an element will depend upon the heat generated due to plastic deformation and friction, and the heat conduction to the colder dies. The expressions for the strain, strain rate and the temperature of an element inside the die are also included in Appendix D.

Material Failure

In practical nosing operations, material failure sometimes occur and it has been reported from various shell-forging plants (Ref.6). In hot nosing, the critical load is a function of the temperature distribution along the nose of the shell as well as the wall thickness to diameter ratio. Thus, if the temperature distribution is not correct, local bulging at the base of the nose can occur due to improper metal flow. This local swelling of the wall thickness can also occur in the curved portion of the nose. To avoid this type of material failure, the condition to be satisfied is that the meridian stress σ_m at the base of the nose should not reach the yield stress in pure compression at the nose base. Thus, to avoid local bulging in hot nosing,

$$\sigma_m < \bar{\sigma} \quad \text{at} \quad \alpha = \alpha_o \quad . \tag{9}$$

In cold nosing, unless the shell is properly designed, it may buckle under the forces necessary for nosing. In most cases, the shell wall is so thick that the proportional limit of the material will be reached before the equilibrium of the shell becomes unstable, and the local buckling will occur. The elastic buckling of cylindrical shells is treated by Timoshenko. The critical stress necessary to cause elastic buckling is given by the following formula:

$$\sigma_{cr} = \frac{E\,h}{r_o \sqrt{3(1-\nu^2)}} \quad , \tag{13}$$

where E = modulus of elasticity

h = thickness of shell

r_o = outside radius of shell

ν = poisson's ratio.

This formula is valid when the critical stress is below the proportional limit of the material. Thus, at each step of simulation, both local bulging and elastic buckling is investigated.

Computer Simulation

In order to facilitate the application of the stress and the material failure analyses, a computer program, called NOSTRS, was developed to simulate the nosing process. This computer program is capable of treating both cold and hot nosing of shells. A function flow chart of the computer program NOSTRS is given in Figure 20. The computer program NOSTRS is coded in FORTRAN IV and requires approximately $35{,}000_8$ words of memory space in a CDC CYBER-70 computer. A typical run requires approximately 16 seconds, including 9.7 seconds on the central processor. All the input data to the computer program NOSTRS are transferred through READ statements. These include variables defining the geometry of the nosed shell, the friction coefficient at the die-workpiece interface, the die velocity, the type of preform (uniform or nonuniform walled), the temperature distribution in the preform, and the physical and thermal properties of materials.

The computer program begins with the calculation of the as-nosed shape from the input dimensions of the nose portion. If the shell under consideration requires a preform with nonuniform wall, the next step is to design the preform shape and divide its length in a specified number of segments. The actual simulation begins after this step. The die is moved on the topmost segment with the specified velocity. This causes the element to deform plastically. At this stage, the new average thickness of the element is calculated. Next, the average strains and strain rate and the adiabatic heating in the element are calculated. After considering heat transfer approximately, the new average temperature of the element is estimated. At these calculated values of the strain, strain rate and temperature, the flow stress is determined by interpolation or extrapolation,

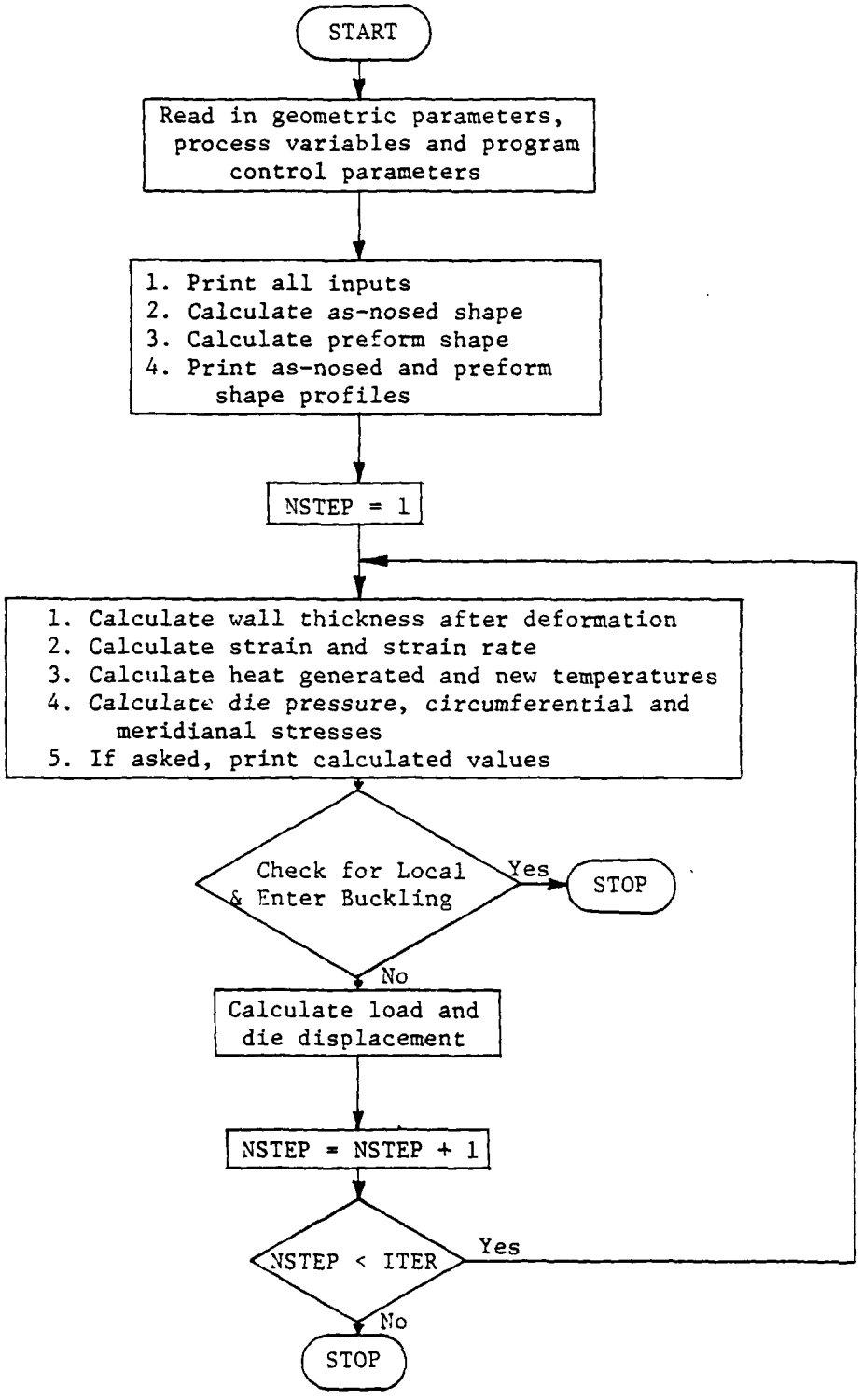

Fig 20 Functional Flow Chart of the Program NOSTRS

from a table. Once the material flow stress is obtained, the stress distribution in the element is determined from the stress analysis. The meridianal stress at the current nose base is used to check for local bulging and also to check for Euler's buckling. In addition, the load applied by the nosing dies is estimated. If no material failure is predicted, the die is moved to cover the next segment of the preform and all the above steps of simulation are repeated until (a) nosing is completed, or (b) material failure is predicted. In either case, appropriate messages are printed and the simulation is stopped.

Parametric Study

In order to illustrate the application of the stress and material failure analysis and the associated computer program, predictions were made for cold nosing of 105-mm M1 shell, and hot nosing of 155 mm M107 shell. The dimensions of the as-nosed shape for 155-mm M107 and 105-mm M1 shell are taken as given in Tables 1 and 4, respectively.

The flow stress data for AISI 1045 steel under cold and hot-working conditions were taken from the literature (Ref.25). For cold nosing of 105-mm M1 shell, the preform was considered to have uniform walls, since the wall thickness is not uniform after nosing. The computer simulation was carried out for various values of the coefficient of friction in the practical range with phosphate and soap lubrication. The load-stroke curves for this shell, shown in Figure 21, reflect work-hardening of the shell material as it penetrates the die. It may be of interest to note that the computer simulation also predicts considerable warming of the shell (150 C) due to nosing.

Since 155-mm M107 shell has uniform wall after nosing, a preform shape for this shell was designed, as given in Table 3. The preforms for nosing of this shell are normally preheated by induction heating. In the present study, an experimentally measured temperature profile, ranging from 350 C at the nose base to 900 C at the nose tip (prior to nosing) was used. The computer simulation was carried out for various values of the coefficient of friction in the practical range with graphite and water lubrication. The load-stroke curves for this shell are given in Figure 22. The flow stress of the material was taken as a function of local strain, strain rate and temperature, which was estimated after adiabatic heating and conduction to the die. As the shell penetrated the die, cooling was greater than the heating due to plastic deformation, and at the end of the simulation, nose tip was considerably cooler than in the beginning of the

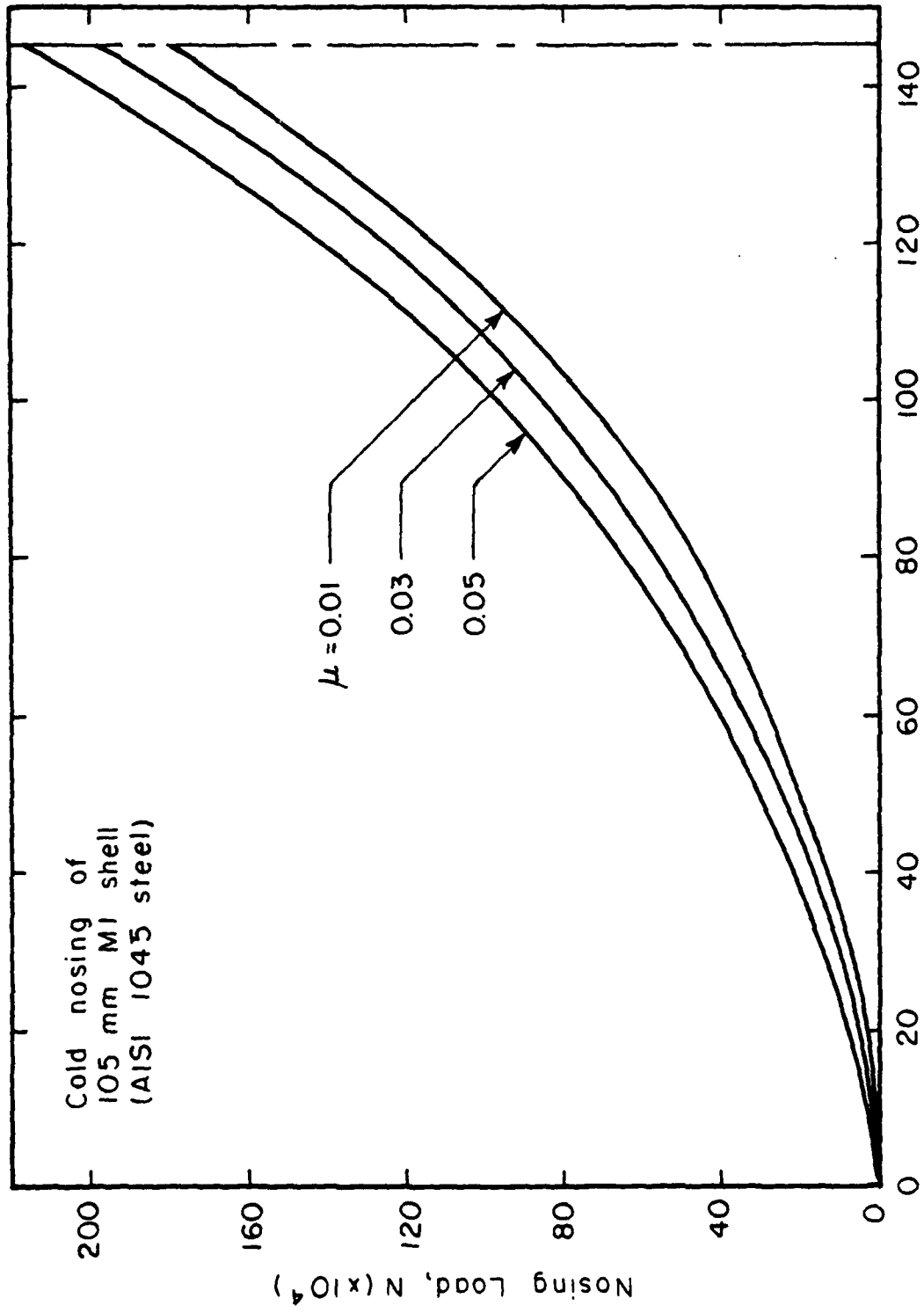

Fig 21 Load-Stroke Diagram for Cold Nosing of 105-mm M1 Shell at Various Values of Friction Coefficients

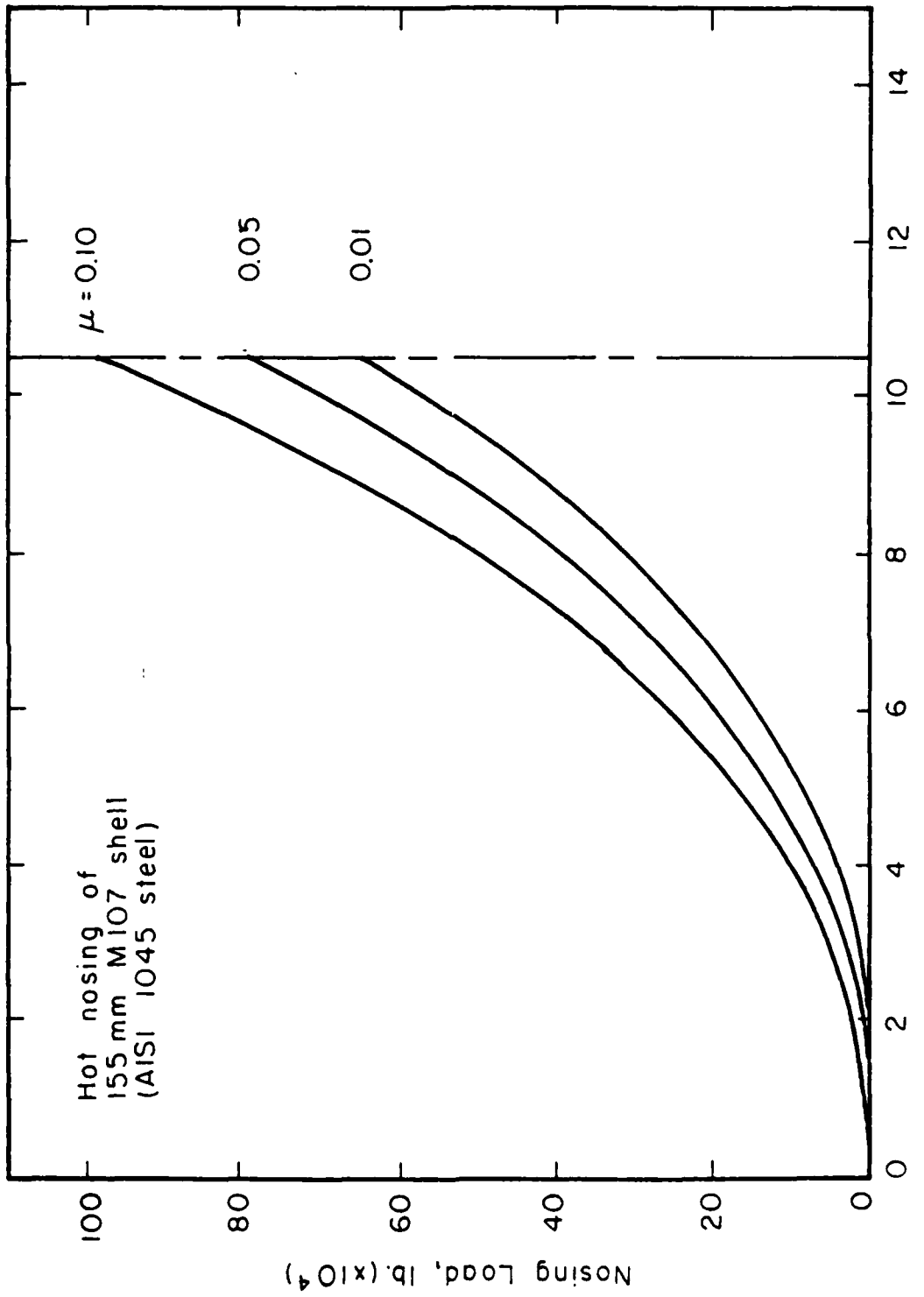

Fig 22 Load-Stroke Diagram for Hot Nosing of 155-mm M107 Shell at Various Values of Friction Coefficients

simulation. This prediction is in agreement with observation in actual hot nosing of 155-mm M107 shell. If the friction at the interface was increased local bulging was predicted. This has also been observed in practical nosing operations.

DEVELOPMENT OF AN OPTIMIZATION COMPUTER PROGRAM

A comprehensive computer program, named NOSING, was developed based on the analyses of nosing operation under previous four sections. Basically, the computer program NOSING is an integrated form of the computer programs INHEAT, NOSFLW and NOSTRS, and it is capable of determining the optimum process variables, both in cold and hot nosing of shells. For a given shell, this program predicts:

(a) As-nosed and preform shape
(b) The temperature profile in the preform due to induction heating prior to nosing
(c) The metal flow during the nosing operation
(d) The load-stroke curve for the nosing operation considering the flow stress of the shell material as a function of strain, strain rate and temperature
(e) The possibility of local buckling or Euler's buckling during nosing.

In addition, the program also predicts whether the nosing can be accomplished in single or multiple hits. A functional flow chart of the computer program NOSING is shown in Figure 23. As seen in the flow chart, the program is provided with options to bypass intermediate steps, if the necessary information is read-in instead of being calculated.

The computer program NOSING can be used in both batch and interactive modes and requires approximately $41{,}000_8$ words of memory space. The input to the program is made through NAMELIST IDATA, and the input variable can be read-in either in SI units or the conventional (inch-lb-C) units, depending upon the user's option. The output from the program is printed in units in which the input is read-in. To illustrate this feature and to describe the output from the computer program NOSING, two typical brief outputs are given in Figures 24 and 25. The output for cold nosing of 105-mm M1 shell is in SI units, as shown in Figure 24, whereas the output for hot nosing of 155-mm M107 shell is in the conventional

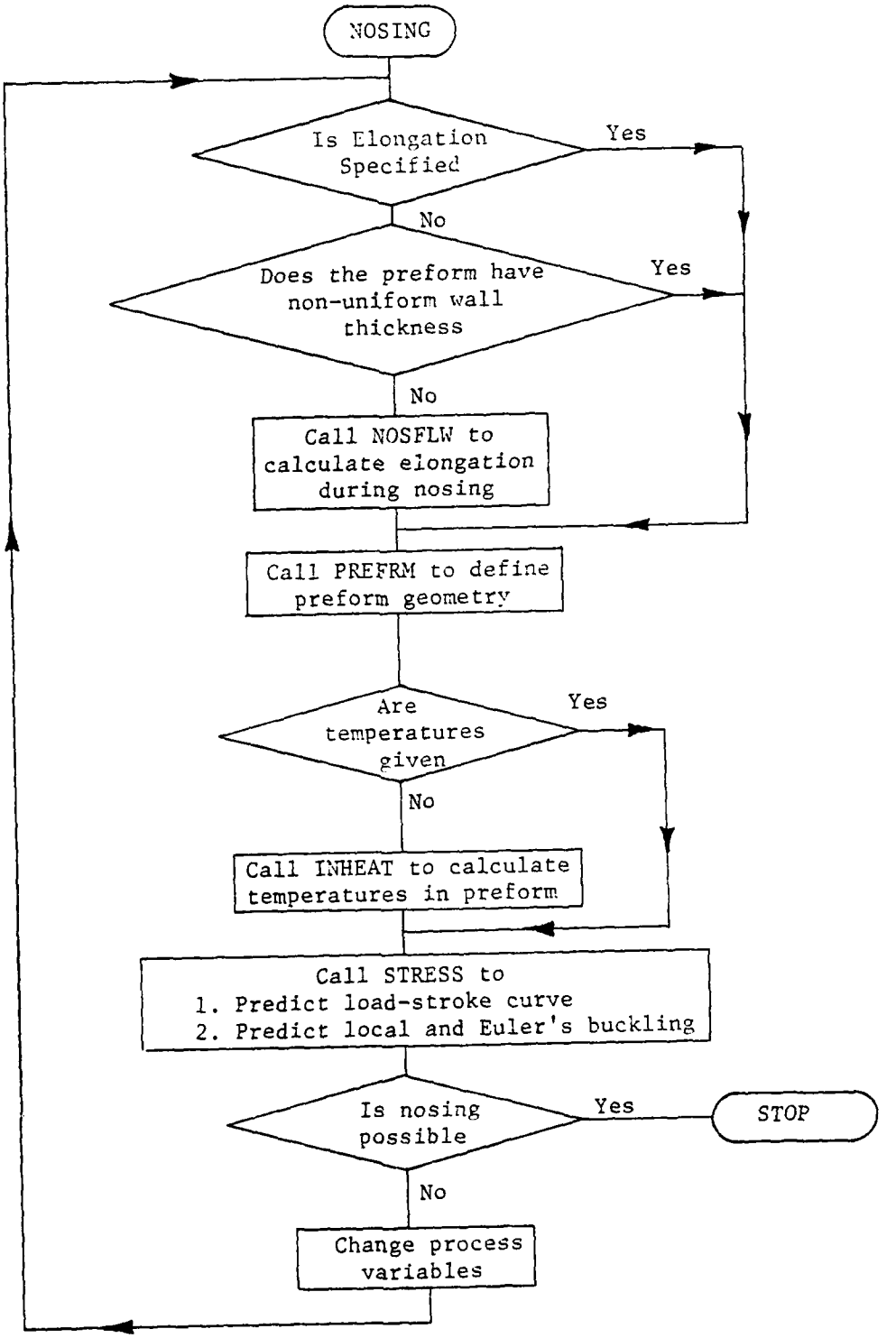

Fig 23 Functional Flow Chart of the Optimization Computer Program NOSING

THE FOLLOWING RESULTS ARE FOR NOSING OF 105 MM SHELLS

THE PREFORM HAS UNIFORM WALLS OF THICKNESS HO

INPUT TO THE PROGRAM NOSING

OUTSIDE DIAMETER OF THE ROUGH-TURNED SHELL,MM	=	105.000
INSIDE DIAMETER OF THE ROUGH-TURNED SHELL,MM	=	84.000
WALL THICKNESS AT THE NOSE BASE,MM	=	12.000
RADIUS OF CURVATURE R1 OF OUTSIDE NOSE PROFILE,MM	=	650.000
AXIAL DISTANCE OF CENTER OF R1 FROM NOSE BASE,MM	=	-25.000
AXIAL LENGTH OF THE NOSED PORTION AFTER NOSING,MM	=	150.000
AXIAL VELOCITY OF THE NOSING DIE,MM/SEC	=	25.000
OUTSIDE DIAMETER OF THE NOSING DIE,MM	=	250.000
FRICTION SHEAR FACTOR AT DIE-WORKPIECE INTERFACE	=	.010
COEFFICIENT OF FRICTION	=	.050
NUMBER OF AXIAL SEGMENTS FOR ST-FOS ANALYSIS AND TEMPERATURE ESTIMATION	=	10

GUESS FOR SLOPE AT NOSE BASE(H#) = 20.000

GUESS FOR SLOPE AT NOSE BASE(H#) = 21.000

Fig 24 A Typical Output From the Computer Program NOSING in SI Units (Cold Nosing of 105 mm M1 Shell)

RESULTS FROM THE CONVERGED SOLUTION

ALFA	WALL THICKNESS	OUTER SURFACE AXIAL DISTANCE	OUTER SURFACE RADIUS	INNER SURFACE AXIAL DISTANCE	INNER SURFACE RADIUS
DEG	MM	MM	MM	MM	MM
2.204	12.000	0.000	54.000	0.000	42.000
3.546	12.494	15.199	53.237	14.426	40.767
4.887	13.007	30.375	52.115	29.267	39.158
6.229	13.547	45.521	50.644	44.051	37.177
7.570	14.124	60.629	48.816	58.768	34.815
8.911	14.748	75.689	46.635	73.405	32.065
10.253	15.433	90.694	44.102	87.948	28.915
11.594	16.196	105.636	41.218	102.381	25.353
12.936	17.060	120.507	37.985	116.688	21.358
14.277	18.059	135.297	34.405	130.844	16.904
15.618	19.240	150.000	30.480	144.820	11.951

ESTIMATED UNIT PRESSURE (P/(A*SIGMA)) = .405E+00

ELONGATION OF SHELL DUE TO NOSING, PERCENT= 4.0111

MAXIMUM THICKENING OF SHELL WALL, PERCENT= 60.3299

VELOCITY, STRAIN, AND STRAIN RATE DISTRIBUTION

ALFA	AXIAL DISTANCE	OUTER RADIUS	MERIDIONAL VELOCITY	NORMAL VELOCITY	STRAIN	STRAIN RATE
DEG	MM	MM	MM/S	MM/S	MM/MM	1/S
2.204	0.000	54.000	25.000	519.401	0.000	.052
3.546	15.199	53.237	24.356	522.377	.041	.054
4.887	30.375	52.115	23.898	536.259	.082	.059
6.229	45.521	50.644	23.612	561.782	.125	.068
7.570	60.629	48.816	23.496	600.612	.171	.083
8.911	75.689	46.635	23.554	655.864	.222	.098
10.253	90.694	44.102	23.802	732.532	.279	.114
11.594	105.636	41.218	24.267	836.704	.343	.140
12.936	120.507	37.985	24.995	987.764	.417	.173
14.277	135.297	34.405	26.073	1202.765	.501	.214
15.618	150.000	30.480	27.629	1525.930	.600	.267

Fig 24 (Continued)

SUMMARY OF RESULTS

NOSING OF THIS SHELL IS POSSIBLE IN 1 HIT

SEG. NO.	SIGM(I),MN/SQ.M	SIGT(I),MN/SQ.M	SIGC(I),MN/SQ.M	WALL THICKNESS,MM	TEMPERATURE,C
1	0.	-.6031E+03	-.8976E+03	.2126E+02	.1545E+03
2	-.1315E+03	-.4326E+03	-.8975E+03	.1879E+02	.1259E+03
3	-.2363E+03	-.3536E+03	-.8673E+03	.1701E+02	.1001E+03
4	-.3210E+03	-.2981E+03	-.8377E+03	.1567E+02	.7970E+02
5	-.3899E+03	-.2573E+03	-.8069E+03	.1465E+02	.6340E+02
6	-.4460E+03	-.2261E+03	-.7743E+03	.1386E+02	.5046E+02
7	-.4915E+03	-.2015E+03	-.7404E+03	.1325E+02	.4031E+02
8	-.5281E+03	-.1813E+03	-.7025E+03	.1276E+02	.3254E+02
9	-.5569E+03	-.1537E+03	-.6593E+03	.1243E+02	.2631E+02
10	-.5796E+03	-.1514E+03	-.6255E+03	.1217E+02	.2276E+02
11	-.5977E+03	-.1491E+03	-.6255E+03	.1200E+02	.2000E+02

Fig 24 (Continued)

AS-NOSED PROFILE OF THE SHELL

AXIAL DISTANCE MM	INNER RADIUS MM	AXIAL DISTANCE MM	OUTER RADIUS MM
146.769	13.914	150.000	30.480
132.046	22.641	135.000	34.491
117.323	26.395	120.000	38.101
102.600	29.582	105.000	41.348
87.877	32.407	90.000	44.227
73.154	34.877	75.000	46.743
58.431	36.993	60.000	48.899
43.708	38.762	45.000	50.701
28.985	40.184	30.000	52.150
14.262	41.263	15.000	53.249
0.000	42.000	0.000	54.000

SEG. NO.	DIE DISPL.,MM	NOSING FORCE,N
1	.1442E+02	-.6339E+05
2	.2884E+02	-.1430E+06
3	.4326E+02	-.2453E+06
4	.5769E+02	-.3761E+06
5	.7211E+02	-.5396E+06
6	.8653E+02	-.7424E+06
7	.1010E+03	-.9920E+06
8	.1154E+03	-.1300E+07
9	.1298E+03	-.1682E+07
10	.1442E+03	-.2163E+07

Fig 24 (Continued)

THE FOLLOWING RESULTS ARE FOR NOSING OF 155 MM SHELLS

THE PREFORM HAS NON-UNIFORM WALLS PRIOR TO NOSING

INPUT TO THE PROGRAM NOSING

OUTSIDE DIAMETER OF THE ROUGH-TURNED SHELL,INCH	=	6.210
INSIDE DIAMETER OF THE ROUGH-TURNED SHELL,INCH	=	4.900
WALL THICKNESS AT THE NOSE BASE,INCH	=	.650
RADIUS OF CURVATURE R1 OF OUTSIDE NOSE PROFILE,IN=		65.500
AXIAL DISTANCE OF CENTER OF R1 FROM NOSE BASE,IN.=		-5.250
AXIAL LENGTH OF THE NOSED PORTION AFTER NOSING,IN=		11.000
AXIAL VELOCITY OF THE NOSING DIE,INCH/SEC	=	1.000
OUTSIDE DIAMETER OF THE NOSING DIE,INCH	=	12.000
FRICTION SHEAR FACTOR AT DIE-WORKPIECE INTERFACE	=	.010
COEFFICIENT OF FRICTION	=	.050
NUMBER OF AXIAL SEGMENTS FOR STRESS ANALYSIS AND TEMPERATURE ESTIMATION	=	10
ESTIMATED ELONGATION DUE TO NOSING INCH	=	.500
LENGTH OF THE INDUCTION COIL INCH	=	3.000
RMS CURRENT IN THE INDUCTION COIL AMP	=	400.000
NUMBER OF TURNS IN THE COIL	=	4.
SUPPLY FREQUENCY CYCLES/SECOND	=	10000.
BILLET TEMPERATURE PRIOR TO HEATING C	=	20.0
AMBIENT TEMPERATURE C	=	20.0
HEATING TIME SECONDS	=	20.000
COOLING TIME SECONDS	=	5.000
COIL EFFICIENCY PERCENT	=	50.0
NUMBER OF RADIAL DIVISIONS FOR TEMP. ESTIMATION	=	4

Fig 25 A Typical Output From the Computer Program NOSING in Conventional Units (Hot Nosing of 155 mm M107 Shell)

AS-NOSED PROFILE OF THE SHELL

AXIAL DISTANCE INCH	INNER RADIUS INCH	AXIAL DISTANCE INCH	OUTER RADIUS INCH
10.339	.631	11.000	1.263
9.750	.900	9.900	1.535
8.661	1.149	8.800	1.736
7.571	1.378	7.700	2.018
6.482	1.589	6.600	2.230
5.393	1.779	5.500	2.423
4.304	1.951	4.400	2.596
3.215	2.104	3.300	2.750
2.126	2.238	2.200	2.886
1.037	2.353	1.100	3.002
0.000	2.451	0.000	3.100

PREFORM FOR 155 MM SHELL

SEGMENT NO.	AXIAL DISTANCE INCH	WALL THICKNESS INCH	TEMPERATURE C
1	10.500	.288	900.000
2	9.450	.333	875.000
3	8.400	.378	775.000
4	7.350	.426	700.000
5	6.300	.470	675.000
6	5.250	.510	650.000
7	4.200	.546	600.000
8	3.150	.577	575.000
9	2.100	.605	525.000
10	1.050	.630	450.000
11	0.000	.650	375.000

Fig 25 (Continued)

VALUE OF DELT AS CALCULATED BY HEATCB = .11403
NUMBER ITERATIONS REQUIRED = 176

TEMPERATURE DISTRIBUTION AFTER INDUCTION HEATING AND PRIOR TO COOLING

	1	2	3	4	5
1	686.67	699.74	715.35	734.16	742.09
2	679.30	691.30	710.35	732.60	745.76
3	660.34	674.67	697.31	725.70	746.18
4	639.63	656.06	682.97	717.91	746.91
5	620.29	638.50	668.28	710.46	747.66
6	604.50	622.96	656.42	703.20	748.28
7	590.67	607.93	644.03	696.09	748.77
8	574.10	594.17	631.96	689.41	749.16
9	560.23	580.55	621.22	683.56	749.57
10	548.30	567.02	611.16	677.65	749.77
11	538.25	554.90	576.10	657.49	746.39
12	130.23	132.24	135.33	136.30	139.30
13	35.15	35.36	35.53	35.62	35.57
14	21.50	21.52	21.53	21.53	21.52
15	20.12	20.12	20.12	20.12	20.12
16	20.01	20.01	20.01	20.01	20.01

DELT = .11403 NUMBER OF ITERATIONS REQUIRED FOR COOLING = 44

TEMPERATURE DISTRIBUTION PRIOR TO MOLING:

	1	2	3	4	5
1	675.02	681.15	687.23	691.32	675.24
2	681.36	687.79	690.55	689.16	682.25
3	671.06	673.49	673.74	687.23	676.15
4	656.31	666.35	674.59	676.50	669.50
5	641.31	654.74	665.57	670.44	664.02
6	627.64	642.01	656.85	665.14	659.54
7	614.60	630.50	648.53	660.29	655.57
8	603.73	620.23	640.59	655.59	652.03
9	595.31	610.39	633.10	651.25	648.89
10	587.15	599.71	624.22	645.67	644.73
11	536.36	553.30	551.62	609.07	611.19
12	158.79	160.62	162.57	163.76	163.22
13	43.63	43.86	44.00	44.03	43.89
14	22.63	22.86	22.97	22.97	22.86
15	20.29	20.29	20.29	20.29	20.29
16	20.02	20.02	20.02	20.02	20.02

Fig 25 (Continued)

SUMMARY OF RESULTS

NOSING OF THIS SHELL IS POSSIBLE AN 1 HIT

SEC. NO.	SIGA(I),KSI	SIGT(I),KSI	SIGC(I),KSI	WALL THICKNESS,INCH	TEMPERATURE,C
1	0.	-.2492E+02	-.4595E+02	.7066E+00	.3129E+03
2	-.1081E+02	-.1700E+02	-.4612E+02	.6731E+00	.7936E+03
3	-.1934E+02	-.1431E+02	-.4605E+02	.6566E+00	.7219E+03
4	-.2746E+02	-.1570E+02	-.5368E+02	.6546E+00	.6650E+03
5	-.3437E+02	-.1610E+02	-.5943E+02	.6534E+00	.6449E+03
6	-.4135E+02	-.1516E+02	-.5960E+02	.6523E+00	.6257E+03
7	-.4670E+02	-.1412E+02	-.5834E+02	.6515E+00	.5869E+03
8	-.5228E+02	-.1916E+02	-.5344E+02	.6505E+00	.5656E+03
9	-.5453E+02	-.2035E+02	-.5190E+02	.6504E+00	.5209E+03
10	-.6570E+02	-.2251E+02	-.1049E+03	.6501E+00	.4477E+03
11	-.7030E+02	-.1965E+02	-.9072E+02	.6500E+00	.3750E+03

Fig 25 (Continued)

SEG. NO.	DIF DISPL.,IN	MOSING FORCE,LB
1	.1050E+01	-.6113E+04
2	.2100E+01	-.1767E+05
3	.3150E+01	-.3213E+05
4	.4200E+01	-.5429E+05
5	.5250E+01	-.1437E+06
6	.6300E+01	-.2910E+06
7	.7350E+01	-.3215E+06
8	.8400E+01	-.4470E+06
9	.9450E+01	-.6024E+06
10	.1050E+02	-.7983E+06

Fig 25 (Continued)

units, as shown in Figure 25. If a user desires more detailed output, such as a printout at every stage of simulation, one can do by simply specifying an option for higher order of output. A detailed description of the computer program NOSING, including its various subroutines and subprogram, and a list of important variables is given in Appendix E. The instructions for preparing input to the program are also included in Appendix E. By changing the input variables selectively, the output from the computer program can be used in determining an optimum combination of process variables.

EXPERIMENTAL EVALUATION

In order to evaluate the accuracy and capability of the computerized mathematical models for predicting metal flow and stresses during nosing of shells, laboratory experiments were conducted. These cold nosing experiments were nearly equivalent to nosing of 105 mm M1 shells.

Experimental Details

Nine-inch long specimens were cut from cold-drawn mild steel (AISI 1018) seamless tubing with 4-1/4-inch OD and 7/16-inch thick wall. The specimens were annealed and shot blasted to remove scale. The remainder of the scale, developed during annealing, was removed by machining the inner and the outer surfaces of the tubular specimens. The sharp corners on the specimens were also removed by chamfering both ends. All the specimens were marked and the dimensions (outside diameter, wall thickness and length) were measured and recorded. The cleaned specimens were then pickled, phosphated and coated with commercial soap lubricant at a cold forging plant (Metal Forge, Columbus, Ohio).

The nosing die was machined from a 10-inch diameter x 11-inch long piece of annealed H-12 tool steel. The shape of the die cavity was machined to correspond to the nosed portion of a 105 mm M1 shell. The die was so designed that it can be bolted down to the base plate of Battelle's 700-ton HPM hydraulic press. The inner surface of the die was cleaned and polished with emery paper. The die block was then heat treated and tempered to R_c 52-54. The scale developed

during heat treating on the inner surface of the die block was cleaned by a wire brush, and then the inner surface was polished once again with emery paper.

The nosing experiments were conducted on Battelle's 700-ton HPM hydraulic press. This press was instrumented for recording the load and the ram displacement individually on a visicorder (light-beam oscillograph). The tool assembly for conducting the nosing experiments is shown in Figure 26. The nosing die was kept stationary and the workpiece was pushed in, as shown in Figure 26. At the end of the nosing operation, the nosed piece was taken out of the die with the aid of the ejector.

The inner surface of the die was coated with MoS_2 spray prior to nosing. The specimens were pushed to various depths into the die. The ram speed was also increased from very slow (manual) to 80 inches/minute. The nosing load and the ram displacement were recorded. Several of the specimens showed slight buckling at the nose base near the end of the stroke. In fact, it was noticed that by increasing the die penetration by 1/8-inch beyond the critical depth of penetration, local buckling at the nose base was initiated. However, since the shells elongate due to nosing, the accurate nose profile could be obtained successfully by depending on the elongation in length. At the end of nosing, the specimens were inspected and the diameter at the nose tip and the final length of the specimen were measured. The test results are summarized in Table 5. Figure 27 shows a lubricated specimen prior to nosing and several specimens after nosing. Specimen Number 2 and 7 were cut along a diametral plane and the cross sections were marked with lines at 1-inch apart along the axis, as shown in Figure 28. The outside diameter and thickness of the nosed specimens along these lines were then measured.

Results and Discussion

The flow stress of annealed mild steel (AISI 1018) was determined earlier at Battelle by conducting uniform compression tests. As shown in Figure 29, the actual true stress vs. true strain curve ($\bar{\sigma}$-$\bar{\varepsilon}$) was approximated by the expression:

$$\bar{\sigma} = 37.0\ (1 + 50\ \bar{\varepsilon})^{0.264} \quad , \tag{14}$$

where $\bar{\sigma}$ is the flow stress at an effective strain $\bar{\varepsilon}$. The relationship given by Equation(14) was used in the computer program NOSING to calculate metal flow and forces for the conditions of laboratory nosing experiments.

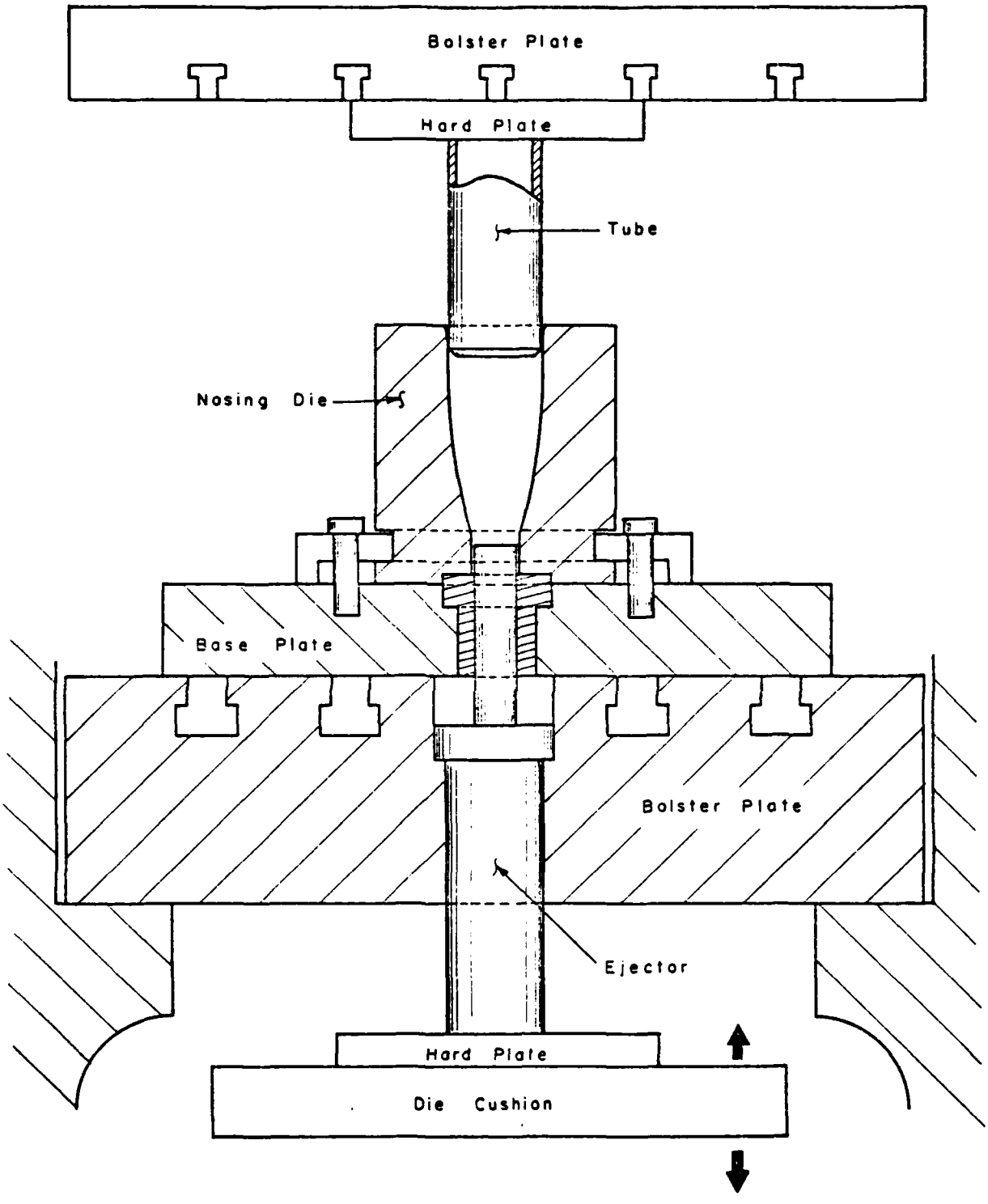

Fig 26 Tool Assembly for Cold Nosing Experiments

Table 5 Summary of Cold Nosing Experiments

Specimen No.	Ram Speed, in/min.	Initial Dimensions, Inch			Final Dimensions, Inch		Maximum Ram Displacement inch	Maximum Nosing Load, Ton	Buckling at Nose Base
		Outside Diameter	Wall Thickness	Length	Diameter at Nose Tip	Length			
1	Manual	4.125	0.415	9.000	2.362	8.877	4.8	225	Yes
2	6.0	4.125	0.427	9.002	2.665	9.228	4.0	125	None
3	"	4.126	0.428	9.000	2.563	9.185	4.6	150	Yes
4	"	4.125	0.427	9.000	2.675	9.088	4.4	165	Yes
5	"	4.125	0.416	8.998	2.675	9.213	4.0	125	None
6	20.0	4.125	0.427	9.000	2.540	9.236	4.2	145	Slight
7	"	4.124	0.391	9.000	3.165	9.210	2.75	60	None
8	"	4.125	0.427	9.000	2.524	9.233	4.3	150	Slight
9	"	4.125	0.419	9.000	2.500	9.190	4.4	160	Yes
10	"	4.125	0.421	9.000	2.459	9.236	4.25	155	Slight
11	"	4.125	0.412	9.000	2.464	9.217	3.9	160	None
12	"	4.125	0.412	8.483	2.540	8.718	4.2	140	None

Fig 27 A Lubricated Specimen Prior to Nosing (White) and Several Specimens After Cold Nosing Equivalent to 105 mm M1 Shell

Specimen No. 2 Specimen No. 7

Fig 28 Cross Section of Specimens 2 and 7 After Nosing

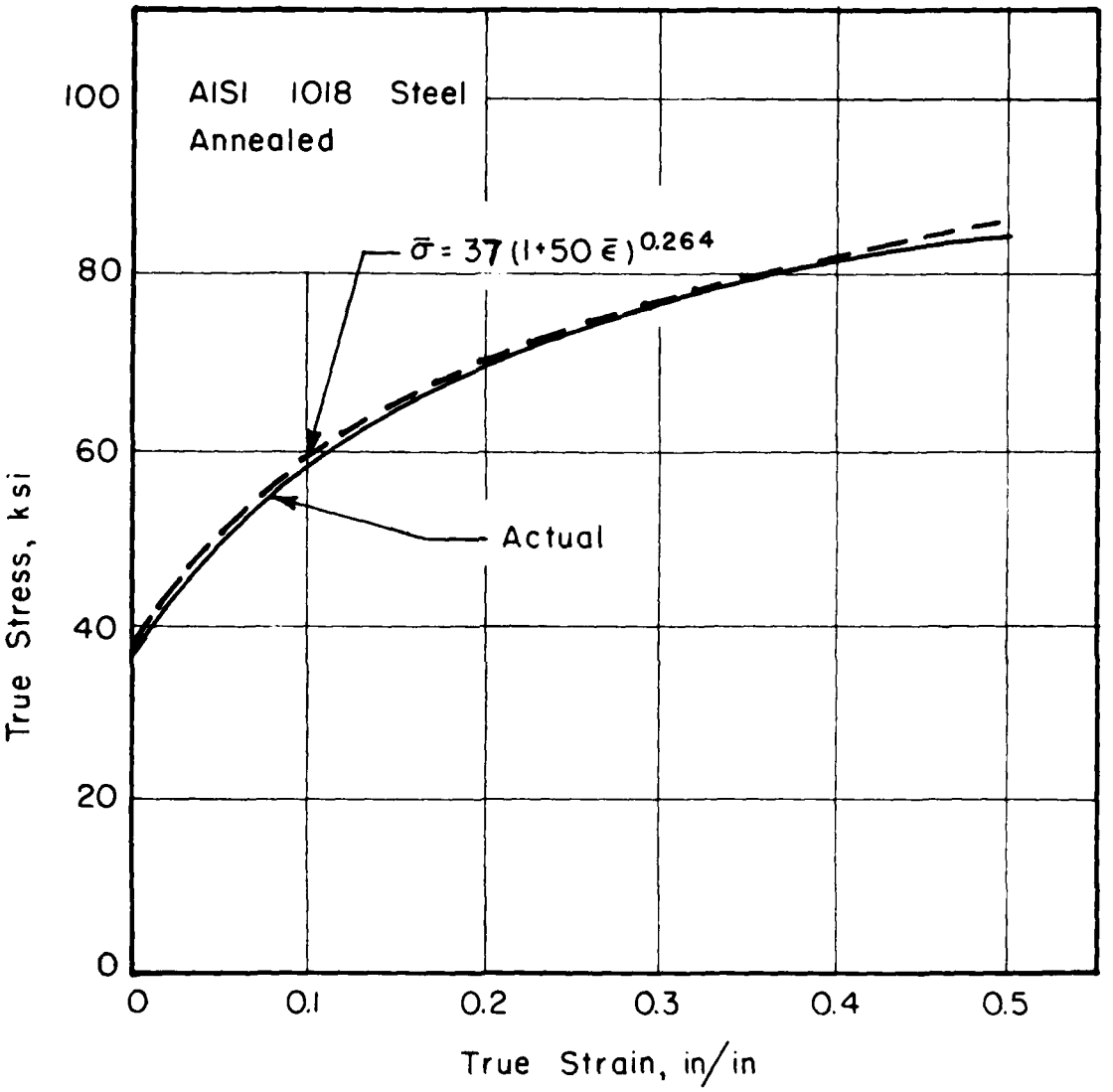

Fig 29 True Stress - True Strain Curve
for Annealed Mild Steel (AISI 1018)

The metal flow model utilizes a constant friction factor m ($0 \leq m \leq 1$), where the friction shear stress τ at the die-workpiece interface is given by $m\,\bar{\sigma}/\sqrt{3}$. Since the value of the friction factor at the die workpiece interface in nosing experiments were not known, predictions were made for several values of friction factors. As seen in Figure 30, experimentally obtained elongation in length fits well with the predicted values for m = 0.05. Therefore, for the specimen number 2, the predictions of metal flow were made using this value of friction factor. As seen in Figure 31, the predicted change in wall thickness and length of the shell are in good agreement with the measured values.

The stress analysis, developed by Nadai (Ref.1), utilizes a constant coefficient of friction μ. Therefore, the load-stroke curves for nosing of 105 mm M1 shell were generated at various values of the coefficient of friction using the computer program NOSING. As seen in Figure 32, the experimentally measured curves agree well with theoretically predicted curve for $\mu = 0.1$. It is of interest to note that $\mu = 0.1$ is typically used in cold forging analysis of steel specimens with phosphate coating and soap lubrication. Further, using $\mu = 0.1$, the computer program NOSING predicted local buckling near the very end of the stroke. Slight local buckling was also observed in several specimens. Thus, the computer program NOSING is capable of predicting the load-stroke curve in cold nosing with good accuracy and it is also capable of predicting local buckling due to nosing. Similar evaluations of the computer program NOSING for hot nosing conditions should be conducted in the future.

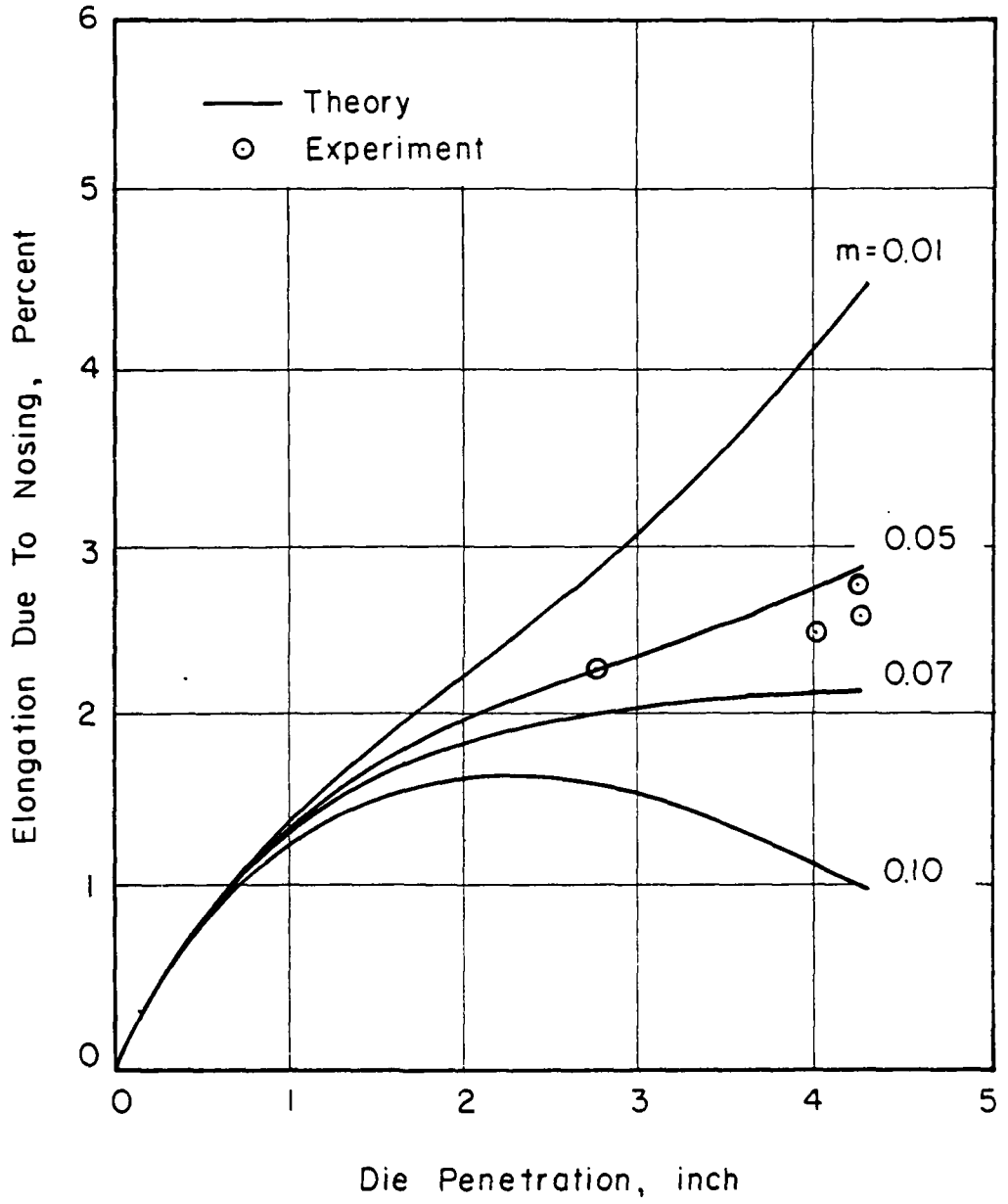

Fig 30 Theoretically Predicted and Experimentally Measured Values of Elongation in Cold Nosing Equivalent to That of 105 mm M1 Shell

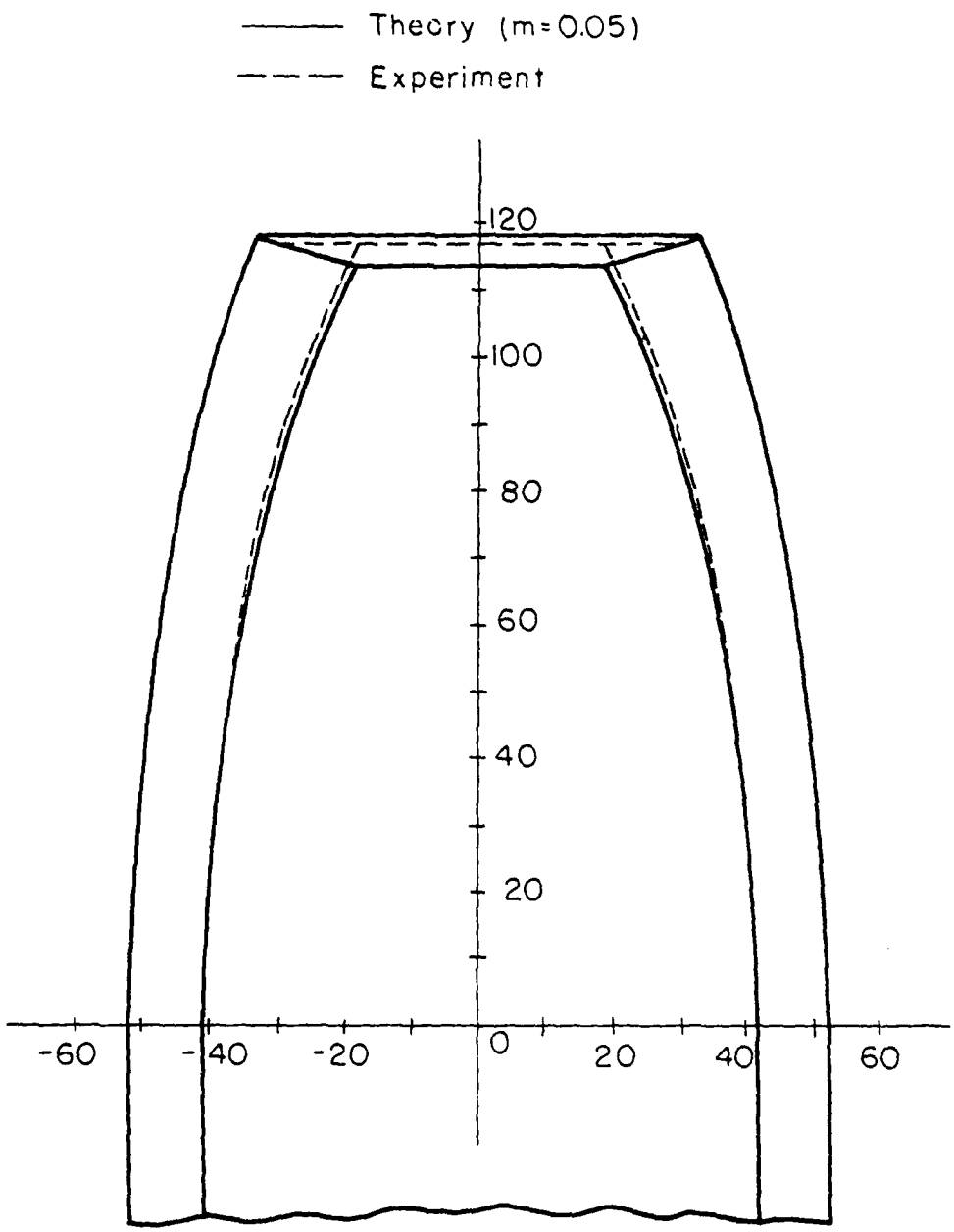

Fig 31 Theoretically Predicted and Experimentally Measured Nose Profiles (All Dimensions are in Millimeters)

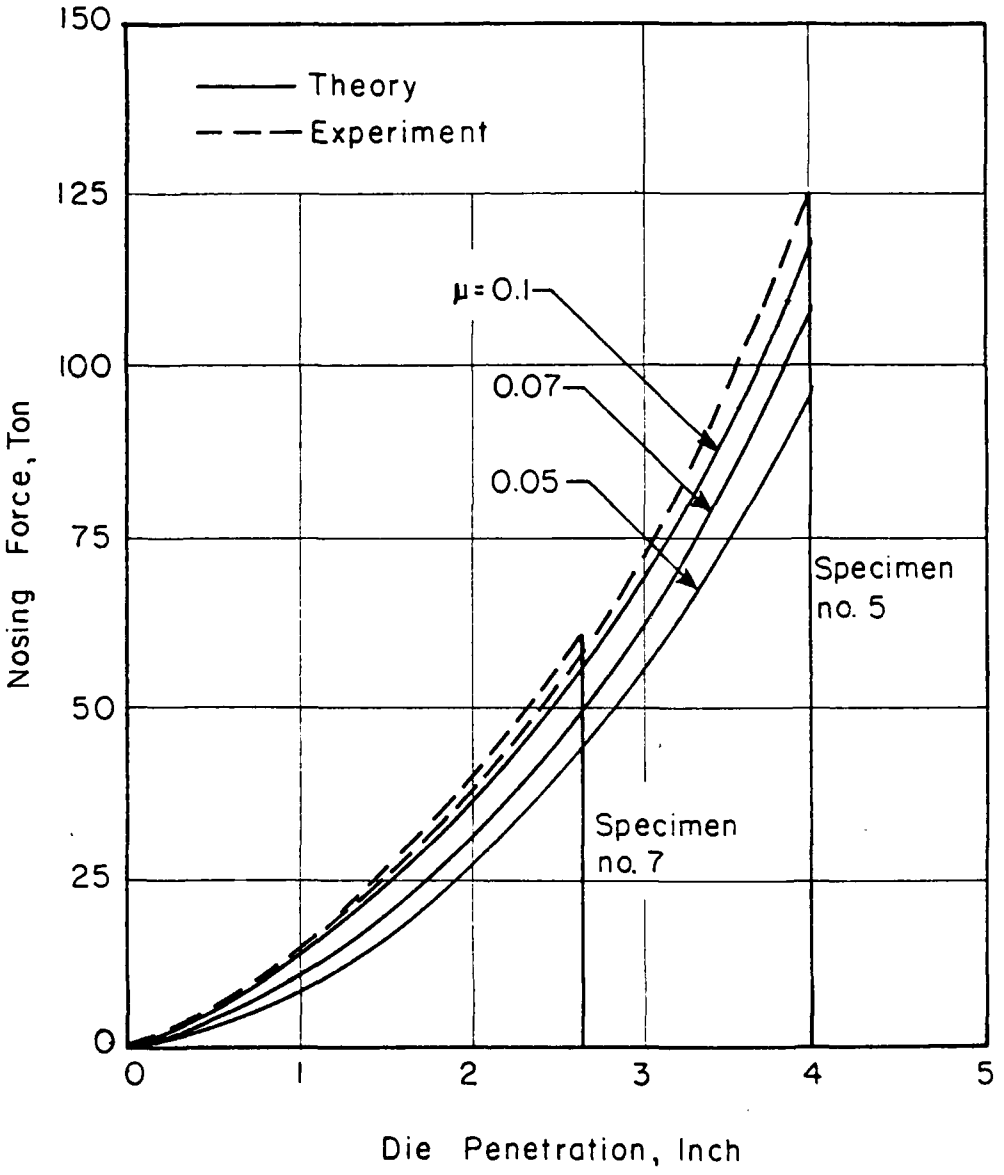

Fig 32 Theoretically Predicted and Experimentally Measured Load-Stroke Curves for Cold Nosing Equivalent to that of 103 mm M1 Shell

REFERENCES

1 Nadai, A., "Plastic State of Stress in Curved Shells: The Forces Required for Forging of the Nose of High-Explosive Shells", Forging of Steel Shells, presented at the annual meeting of the ASME, N.Y., November 29 through December 3, 1943.

2 Onat, E. T., and Prager, W., "Nosing of Shells", Technical Report DA798/15, pp 1-8, Providence, R. I., Brown University, 1954.

3 Singh, M., "A Linearized Theory of Nosing of Shells", Trans. ASME, J. Appl. Mech., 1964, Vol. 31, pp 535-539.

4 Carlson, R. K., "An Experimental Investigation of the Nosing of Shells", Forging of Steel Shells, presented at the annual meeting of the ASME, N. Y., November 29 through December 3, 1943.

5 Cruden, A. K., and Thompson, J. F., "The End Closer of Backward Extruded Cans", *NEL Report No.* 511, National Engineering Lab., Glasgow, 1972.

6 Veth, R. D., Boulger, F. W., Hull, H. E., Goble, P. H., and Shaw, H. L., "An Engineering Survey and Analysis Pertaining to Methods of Manufacturing Artillery Shell", Final Report to Frankford Arsenal, Contract No. DA33-019-507-ORD-8, May, 1959.

7 Pipes, L. A., "Applied Mathematics for Engineers and Physicists", McGraw-Hill, 1958.

8 Reddick, H. W., and Miller, F. H., "Advanced Mathematics for Engineers", John Wiley, 1955.

9 Warren, A. G., "Mathematics Applied to Electrical Engineering", Chapman and Hall, 1958.

10 McLachlan, N. W., "Bessel Functions for Engineers", Oxford Press, 1955.

11 Stansel, N. R., "Induction Heating", McGraw-Hill, 1949.

12 Simpson, P. G., "Induction Heating", McGraw-Hill, 1960.

13 Rodigin, N. M., "Induction Heating of Steel Articles with Normal-Frequency Currents", State Scientific Technical Publishing House of Literature on Ferrous and Nonferrous Metallurgy, Moscow, 1950 (in Russian).

14 Tudbury, C. A., "Basics of Induction Heating", Forging Industries Associations, Cleveland, Ohio, 1960.

15 Vaughan, J. T., and Williamson, J. W., "Design of Induction-Heating Coils for Cylindrical Non-Magnetic Loads", AIEE Transactions, Vol. 64, August, 1945, pp 587-92.

16 Vaughan, J. T., and Williamson, J. W., "Design of Induction-Heating Coils for Cylindrical Magnetic Loads", AIEE Transactions, Vol. 65, 1946, pp 887-92.

17 Baker, R. M., "Design and Calculation of Induction Heating Coils", AIEE Transactions, Vol. 76, Part II, March 1957, pp 31-40.

18 Baker, R. M., "Induction Heating of Moving Magnetic Strip", AIEE Transactions, Vol. 64, 1945, pp 184-189.

19 Kothmann, R. E., "Induction Heating of a Ferromagnetic Cylinder through the Curie Temperature", Research Report 68-1D8-IHEAT-R1, Westinghouse Research Laboratories, Pittsburgh, Pennsylvania, April, 1968.

20 Personal Communication with Dr. R. E. Kothman, Westinghouse Research Laboratories, Pittsburgh, Pennsylvania.

21 Kolodii, B. I., "Temperature Distribution and Thermal Stresses in an Inductively-Heated Hollow Cylinder", Prikladnaya Mekhanika, Vol. 5, No. 10, 1969, pp 35-41.

22 Podstrigach, Ya. S., Goryacheva, Z. I., Kolodii, B. I., Plyatsko, G. V., and Komarov, A. N., "Temperature Fields and Thermal Stresses Produced by Unsteady Induction Heating of Hollow Cylinders", Fiziko-Khimicheskaya Mekhanika Materialov, Vol. 6, No. 2, 1970, pp 113-115.

23 Hill, R., "A General Method of Analysis for Metalworking Processes", J. Mech. Phys. Solids, Vol. 11, 1963, p 305.

24 Lahoti, G. D., and Kobayashi, S., "On Hill's General Method of Analysis for Metalworking Processes", Int. J. Mech. Sci., Vol. 16, 1974, pp 521-540.

25 Altan, T., and Boulger, F. W., "Flow Stress of Metals and Its Application in Metal Forming Analysis", Trans. ASME, J. Engrg. Industry, November 1973, pp 1009-1019.

APPENDIX A

HP-67 PROGRAMS FOR AS-NOSED AND PREFORM SHAPE CALCULATION

APPENDIX A

HP-67 PROGRAMS FOR AS-NOSED AND PREFORM SHAPE CALCULATION

Two programs, one for calculation of as-nosed shape and another for designing of preform shape prior to nosing, were developed on an HP-67 programmable hand calculator. These programs can be stored on magnetic strips and can be reloaded easily.

The first program calculates the inner and the outer profile of as-nosed shape from the nose dimensions. The program is capable of treating the following two cases:

(a) When the nose profile of a shell is described by the outside ogive radius (R_1) and the uniform wall thickness (h_o). In such a case, it calculates outside and inside radii of the nosed portion at axial distances from the nose base in increment of 1 inch. First the axial distance is flashed, then the outside and the inside radii of the nosed shape are flashed on the calculator display.

(b) When the nose profile of a shell is described by the outside ogive radius (R_1) and the inside ogive radius (R_2). In such a case, the outside surface is calculated as before. The inside surface is defined by another set of axial distances and corresponding inside radius. First, outside surface coordinates (axial distance and outside radius) and then the inside surface coordinates (axial distance and inside radius) are flashed on the calculator display.

The listing of this program, the user's instructions, and the program description are given at the end of this Appendix.

The second program in this Appendix calculates the preform shape in order to obtain a certain shape after nosing. The calculations start at the base of the nose and the preform wall thickness is calculated at axial distances in increment of 1 inch. The axial distance from the base of the nose is flashed first on the display of the calculator for five seconds, and then the preform wall thickness at that location is calculated and also flashed for five seconds.

At the end of the preform design calculations, if the coefficient of friction (μ) and the average flow stress ($\bar{\sigma}$) are stored in registers 5 and 6, respectively, and the R/S key of the calculator is punched, the program also calculates an estimated nosing load.

The list of this program, the user's instructions, and the program description are also given at the end of this Appendix.

Preform Design

Let us consider an element of length dx at a distance x of the preform, which becomes a segment of length ds after nosing. If the shell does not elongate due to nosing, the constancy of volume of the element yields (Figure A-1):

$$2\pi\, r_o h_o\, dx = 2\pi\, r\, h\, ds \quad , \tag{A-1}$$

where h_o and h are the initial and final wall thicknesses, and the radius r is given by:

$$r = r_o - R_1\,(\cos\alpha_o - \cos\alpha) \quad .$$

Since $ds/d\alpha = \cos(\alpha - \alpha_o)$, from Equation (A-1), we have:

$$h_o = \frac{rh}{r_o \cos\alpha(\alpha-\alpha_o)} \quad . \tag{A-2}$$

If the shell elongates considerably, an element originally at x goes to $x + \xi$ after the nosing, where ξ is the axial displacement of the element. Therefore, r, h, and ds must be measured at $(x + \xi)$ when r_o and h_o are still measured at x. Since

$$ds = d(x + \xi)\, \cos(\alpha - \alpha_o) \quad ,$$

where $(\alpha - \alpha_o)$ is the slope of the nose profile at $(x + \xi)$, we have:

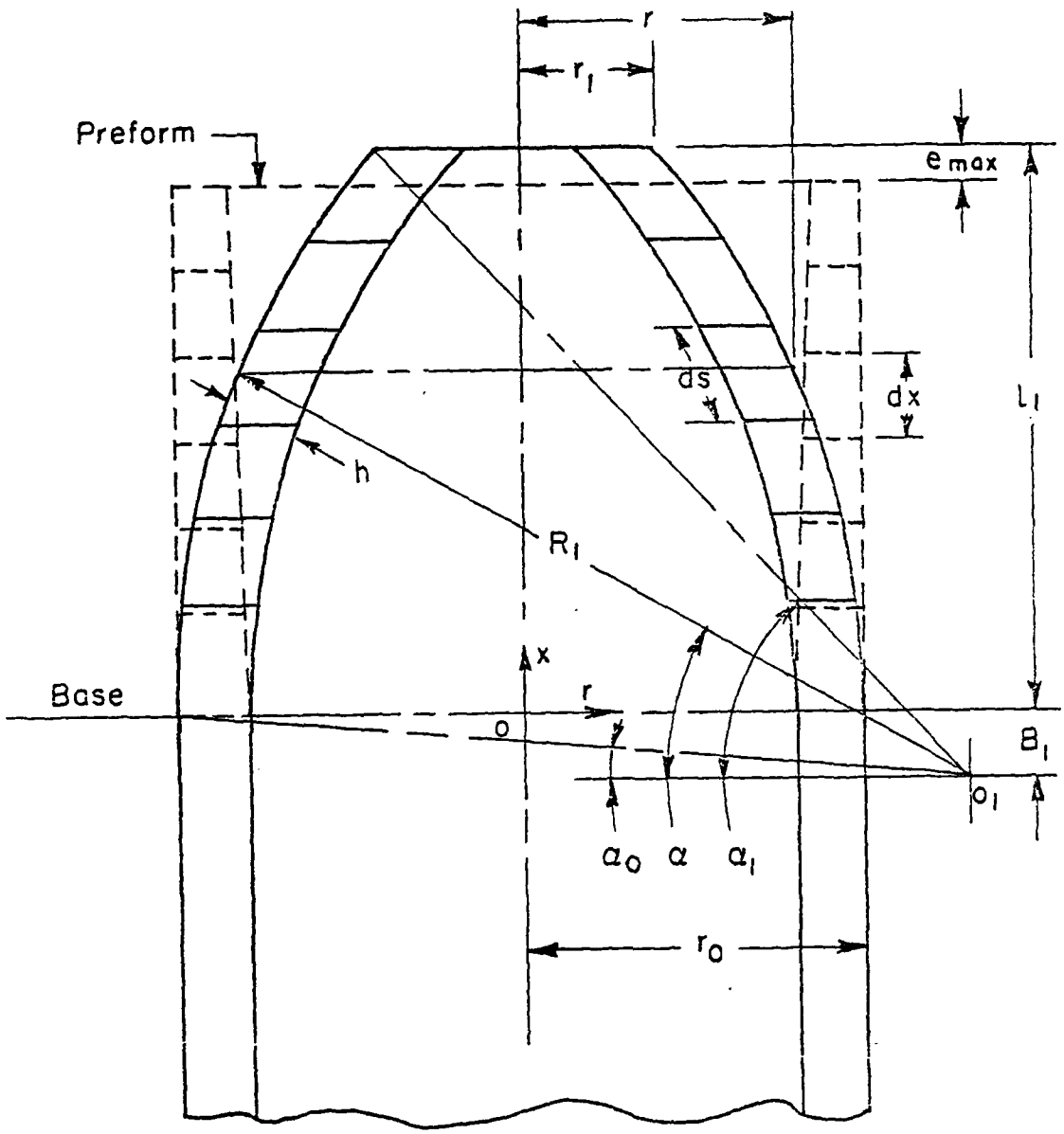

Fig A-1 Configuration of Preform and As-Nosed Shape

$$h_o = r_o \frac{hr}{\cos(\alpha - \alpha_o)} \left(1 + \frac{d\xi}{dx} \right) \quad . \tag{A-3}$$

If we assume that ξ varies as a power function of x given as:

$$\xi = e_{max} \left(\frac{x}{\ell_1}\right)^n \quad ,$$

where e_{max} is the maximum extension occurring at the tip of the nose, then we have:

$$h_o = r_o \frac{hr}{\cos(\alpha - \alpha_o)} \left[1 + \frac{n\, e_{max}}{\ell_1^n} x^{n-1}\right] \tag{A-4}$$

The constants n and e_{max} in the above expression must be estimated from experience. At least one of them can be estimated rather closely as follows:

Since at the tip of the shell, the state of pure compression exists in the circumferential direction, both the axial and the radial strains are equal to half of the circumferential strain, ε_c. The maximum circumferential strain at the tip of the nose is given from reduction in diameter and twice as much as the axial strain as below:

$$-\varepsilon_c = \frac{r_1 - r_o}{r_o} = \frac{2}{\cos(\alpha_1 - \alpha_o)} \left(1 + \frac{d\xi}{dx} \right)_{x=\ell_1} - 1$$

$$= \frac{2}{\cos(\alpha_1 - \alpha_o)} \left(1 + \frac{n\, e_{max}}{\ell_1} \right)$$

Therefore, $$n = \frac{\ell_1}{e_{max}} \left(1 - \frac{\varepsilon_c}{2} \right) \cos(\alpha_1 - \alpha_o) - 1 \quad . \tag{A-5}$$

Thus, if e_{max} is known, h_o is given by Equations (A-4) and (A-5).

User Instructions

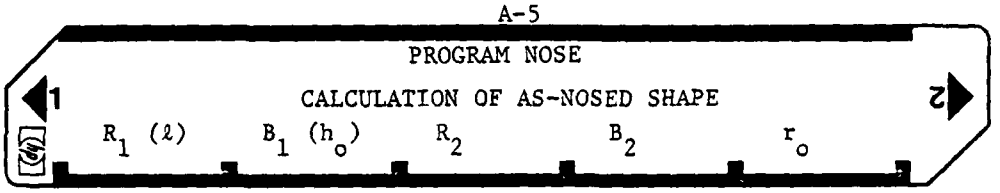

STEP	INSTRUCTIONS	INPUT DATA/UNITS	KEYS	OUTPUT DATA/UNITS
1	Load Side 1 & Side 2 of Card			
2	Input the known values			
	• Radius of outside ogive curvature	R_1 (in)	A	
	• Distance of center of R_1 from			
	Nose base (see Figure 1)	B_1 (in)	B	
	• Radius of inside ogive curvature	R_2 (in)	C	
	• Distance of center of R_2 from			
	nose base (see Figure 2)	B_2 (in)	D	
	• Outside radius at nose base	r_o (in)	E	
	• Length of nosed portion	ℓ (in)	f a	
	• Wall thickness at nose base			
	or uniform wall thickness in nose	h_o (in)	f b	
3	Calculate outside radius and			
	inside radius at various			
	axial locations along the nose		f c	
	Note: If R_2 and B_2 not available, insert			
	zeros for them. Then program calculates			
	inner and outer surface separately			
	Output Form: If $R_2 \neq 0$, $B_2 \neq 0$			
	x r r_i			
	0 --- ---			
	1 --- ---			
	2 --- ---			
	etc			
	Output Form: If $R_2 = 0$, $B_2 = 0$			
	x r x_i r_i			
	0 --- 0. ---			
	1 --- --- ---			
	2 --- --- ---			
	3 --- --- ---			
	etc			

STEP	KEY ENTRY	KEY CODE	COMMENTS
001	f LBL A		
	STO 1		
	h RTN		
	f LBL B		
	STO 2		
	h RTN		
	f LBL C		
	STO 3		
	h RTN		
010	f LBL D		
	STO 4		
	h RTN		
	f LBL E		
	STO 5		
	h RTN		
	g LBLf a		
	STO 6		
	h RTN		
	g LBLf b		
020	STO 7		
	h RTN		
	g LBLf c		
	RCL 2		
	RCL 1		
	÷		B_1/R_1
	g SIN^{-1}		α_o
	STO 8		
	RCL 6		
	h RCI		
030	g x>y		
	GTO f e		
	DSP 4		
	f -x-		
	RCL 2		
	+		
	RCL 1		
	÷		
	g SIN^{-1}		
	f COS		
040	CHS		
	RCL 8		
	f COS		
	+		
	RCL 1		
	x		
	CHS		
	RCL 5		
	+		
	f -x-		
050	STO 0		
	RCL 3		
	f x = 0		
	GTO f d		
	RCL 4		
	RCL 3		
	÷		B_2/R_2

STEP	KEY ENTRY	KEY CODE	COMMENTS
	I SIN^{-1}		
	STO 9		
	h RCI		
060	RCL 4		
	+		
	RCL 3		
	÷		
	g SIN^{-1}		
	f cos		
	CHS		
	RCL 9		
	f cos		
	+		
070	RCL 3		
	X		
	CHS		
	RCL 5		
	+		
	RCL 7		
	-		
	f -x-		
	f ISZ		
	GTO f c		
080	g LBLf d		
	h RCI		
	RCL 2		
	+		
	RCL 1		
	÷		
	g SIN^{-1}		
	STO 9		
	f SIN		
	RCL 7		
090	x		
	CH S		
	h RCI		
	+		
	f -x-		
	RCL 8		
	f COS		
	RCL 9		
	f COS		
	-		
100	RCL 1		
	RCL 7		
	-		
	x		
	CHS		
	RCL 5		
	+		
	RCL 7		
	-		
	f -x-		
110	f ISZ		
	GTO f c		
	GTO f e		

REGISTERS

0	1	2	3	4	5	6	7	8	9
r	R_1	B_1	R_2	B_2	r_o	ℓ	h_o	α_o	x_i (α)
S0	S1	S2	S3	S4	S5	S6	S7	S8	S9

A	B	C	D	E	I

Program Listing

STEP	KEY ENTRY	KEY CODE	COMMENTS
	g LBLf e		
	h RTN		
120			
130			
140			
150			
160			

STEP	KEY ENTRY	KEY CODE	COMMENTS
170			
180			
190			
200			
210			
220			

LABELS

A	B	C	D	E
a	b	c	d	e
)	1	2	3	4
5	6	7	8	9

FLAGS

0
1
2
3

SET STATUS

FLAGS			TRIG	DISP	
	ON	OFF			
0	☐	☐	DEG ☐	FIX ☐	
1	☐	☐	GRAD ☐	SCI ☐	
2	☐	☐	RAD ☐	ENG ☐	
3	☐	☐		n ____	

Program Description

Program Title CALCULATION OF NOSED SHAPES

Name Goverdhan D. Lahoti **Date** Aug 1, 1977

Address Battelle's Columbus Labs, 505 King Avenue

City Columbus State Ohio Zip Code 43201

Program Description, Equations, Variables, etc.

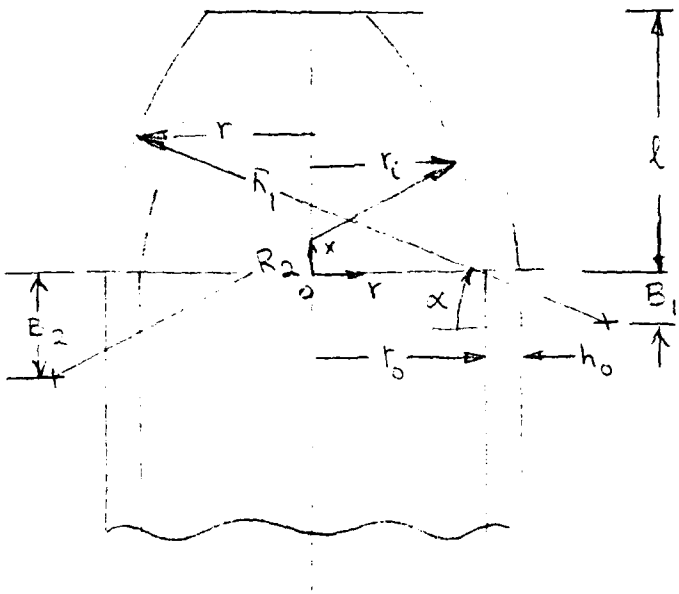

$$r = r_o - R_1 (\cos\alpha_o - \cos\alpha_1)$$

$$r_i = (r_o - h_o) - R_2 (\cos\alpha_i - \cos\alpha_2)$$

$$\alpha_o = \sin^{-1} (B_1/R_1)$$

$$\alpha_i = \sin^{-1} (B_2/R_2)$$

$$\alpha_1 = \sin^{-1} \left(\frac{B_1 + x}{R_1} \right)$$

$$\alpha_2 = \sin^{-1} \left(\frac{B_2 + x}{R_2} \right)$$

Fig A-2

Operating Limits and Warnings When R_1, B_1, R_2, and B_2 are specified, the program computes x, r and r_i, in that order. When R_2 and B_2 are specified 0, (when not available), the program computes x, r and x, r_i pairs for outer and inner profile.

User Instructions

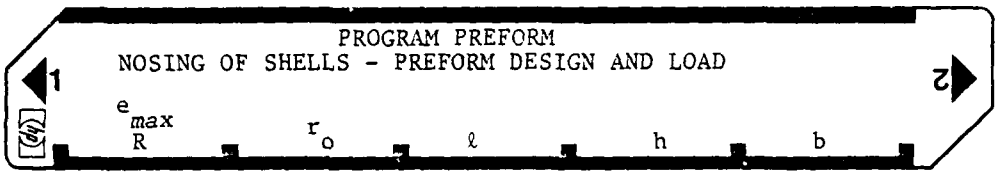

STEP	INSTRUCTIONS	INPUT DATA/UNITS	KEYS		OUTPUT DATA/UNITS
1	Load side 1 and 2 of card				
2	Input the known values				
	Radius of ogive curvature	R(inch)	A		R
	Outside radius of shell	r_o(inch)	B		r_o
	Length of nosed portion	ℓ(inch)	C		ℓ
	Uniform wall thickness in nosed portion	h(inch)	D		h
	Distance of center of ogive arc from the base of the nose (see Figure 1)	b(inch)	E		b
	Estimated elongation due to nosing	e_{max}(inch)	f	a	e_{max}
3	Calculate initial wall thicknesses at various distances from the base of the nose (increment of 1 inch)		f	b	x/h_o(inch)
4	After design of preform, calculation stops. Input values for load calculation				
	Coefficient of friction	μ	STO	5	μ
	Average flow stress of material	$\bar{\sigma}$(psi)	STO	6	$\bar{\sigma}$(psi)
5	Calculate nosing load		R/S		P(lb)

STEP	KEY ENTRY	KEY CODE	COMMENTS
001	f LBL A	31 25 11	
	STO 1	33 01	Input R
	h RTN	35 22	
	f LBL B	31 25 12	
	STO 2	33 02	Input r_o
	h RTN	35 22	
	f LBL C	31 25 13	
	STO 3	33 03	Input ℓ
	h RTN	35 22	
010	f LBL D	31 25 14	
	STO 4	33 04	Input h
	h RTN	35 22	
	f LBL E	31 25 15	
	STO 5	33 05	Input b
	h RTN	35 22	
	g LBLf a	32 25 11	
	STO 6	33 06	Input e_{max}
	h RTN	35 22	
	g LBLf b	32 25 12	
020	RCL 5	34 05	
	RCL 1	34 01	
	÷	81	b/R
	g SIN^{-1}	32 62	α_o
	STO 7	33 07	
	RCL 3	34 03	
	RCL 5	34 05	
	+	61	
	RCL 1	34 01	
	÷	81	(b+ℓ)/R
030	g SIN^{-1}	32 62	α_1
	STO 8	33 08	
	RCL 6	34 06	
	f x≥0	31 81	
	GTO f d	22 31 14	
	g LBLf C	32 25 13	
	RCL 3	34 03	
	h RCI	35 34	
	g x>y	32 81	
	GTO f e	22 31 15	
040	DSP 4	23 04	
	f -x-	31 84	
	RCL 5	34 05	
	+	61	
	RCL 1	34 01	
	÷	81	(b+x)/R
	g SIN^{-1}	32 62	α
	STO 0	33 00	
	f COS	31 63	
	CHS	42	
050	RCL 7	34 07	
	f COS	31 63	cos α_o
	+	61	
	RCL 1	34 01	
	X	71	
	CHS	42	
	RCL 2	34 02	

STEP	KEY ENTRY	KEY CODE	COMMENTS
	+	61	
	RCL 4	34 04	
	X	71	
060	RCL 2	34 02	
	÷	81	
	RCL 0	34 00	
	RCL 7	34 07	
	-	51	
	f COS	31 63	
	÷	81	h_o
	DSP 4	23 04	
	f -x-	31 84	
	f ISZ	31 34	
070	GTO f c	22 31 13	
	GTO f e	22 31 15	
	g LBLf d	32 25 14	
	RCL 3	34 03	
	RCL 6	34 06	
	-	51	
	h RCI	35 34	
	g x>y	32 81	
	GTO f e	22 31 15	
	DSP 4	23 04	
080	f -x-	31 84	
	RCL 8	34 08	
	f COS	31 63	cos α_1
	RCL 7	34 07	
	f COS	31 63	cos α_o
	-	51	
	RCL 1	34 01	
	X	71	
	RCL 2	34 02	
	÷	81	
090	2	02	
	÷	81	
	CHS	42	
	1	01	
	+	61	
	RCL 8	34 08	
	RCL 7	34 07	
	-	51	(α_1 - α_o)
	f COS	31 63	
	X	71	
100	RCL 3	34 03	
	X	71	
	RCL 6	34 06	
	÷	81	
	1	01	
	-	51	n
	STO 9	33 09	
	h RCI	35 34	
	RCL 3	34 03	
	÷	81	x/ℓ
110	RCL 9	34 09	
	h y^x	35 63	
	RCL 6	34 06	

REGISTERS

0	1	2	3	4	5	6	7	8	9
α(β)	R	r_o	ℓ	h	b(u)	e_{max}($\bar{\sigma}$)	α_o	α_1	n
S0	S1	S2	S3	S4	S5	S6	S7	S8	S9

A	B	C	D	E	I

AD-A082 108 BATTELLE COLUMBUS LABS OH F/G 19/1
DEVELOPMENT OF A COMPUTERIZED MATHEMATICAL MODEL FOR THE HOT/CO--ETC(U)
SEP 78 G D LAHOTI, T L SUBRAMANIAN, T ALTAN DAAA25-76-C-0427
UNCLASSIFIED ARSCD-CR-78019 NL

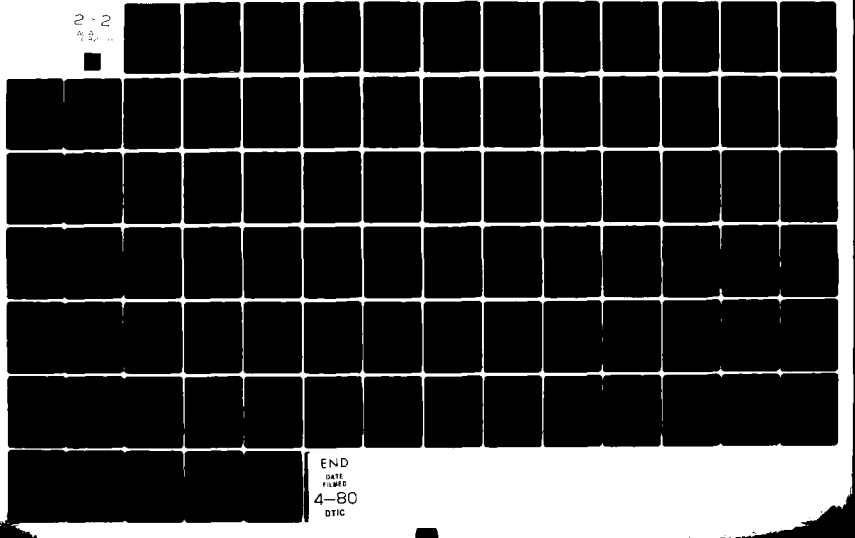

END
DATE FILMED
4-80
DTIC

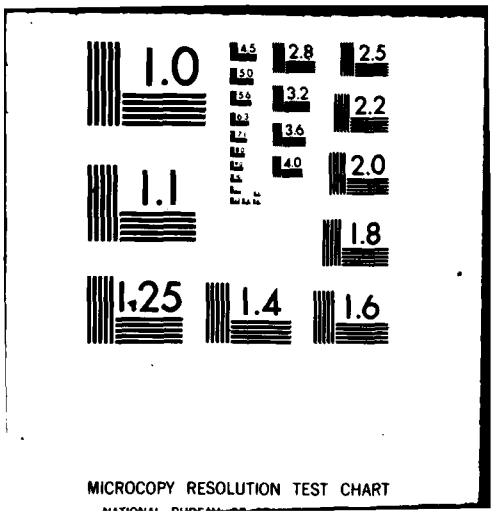
1.0
1.1
1.25
1.4
1.6
1.8
2.0
2.2
2.5
2.8
3.2
3.6
4.0
4.5
5.0
MICROCOPY RESOLUTION TEST CHART

Program Listing

STEP	KEY ENTRY	KEY CODE	COMMENTS
	X	71	e
	h RCI	35 34	
	+	61	x
	RCL 5	34 05	
	+	61	
	RCL 1	34 01	
	÷	81	(x+b)/R
120	g SIN^{-1}	32 62	α
	STO 0	33 00	
	f SIN	31 62	
	RCL 1	34 01	
	X	71	
	RCL 5	34 05	
	-	51	
	h ABS	35 64	
	RCL 9	34 09	
	1	01	
130	-	51	
	h y^x	35 63	x^{n-1}
	RCL 6	34 06	
	X	71	
	RCL 9	34 09	
	X	71	
	RCL 3	34 03	
	RCL 9	34 09	
	h y^x	35 63	
	÷	81	
140	1	01	
	+	61	
	STO 9	33 09	
	RCL 0	34 00	
	f COS	31 63	cos α
	RCL 7	34 07	
	f COS	31 63	cos α_o
	-	51	
	RCL 1	34 01	
	X	71	
150	RCL 2	34 02	
	+	61	
	RCL 0	34 00	
	RCL 7	34 07	
	-	51	
	f COS	31 63	cos $(\alpha - \alpha_o)$
	÷	81	
	RCL 4	34 04	
	X	71	
	RCL 2	34 02	
160	÷	81	
	RCL 9	34 09	
	X	71	h_o
	DSP 4	23 04	
	f -x-	31 84	
	f ISZ	31 34	
	GTO f d	22 31 14	
	g LBLf e	32 25 15	
	R/S	84	
	RCL 5	34 05	

STEP	KEY ENTRY	KEY CODE	COMMENTS
170	g TAN^{-1}	32 64	β
	STO 0	33 00	
	RCL 8	34 08	
	RCL 0	34 00	
	+	61	
	RCL 0	34 00	
	+	61	
	f COS	31 63	
	RCL 8	34 08	
	RCL 7	34 07	
180	-	51	$(\alpha_1 - \alpha_o)$
	RCL 5	34 05	
	X	71	
	5	05	
	7	07	
	.	83	
	3	03	
	÷	81	
	g e^x	32 52	
	X	71	
190	CHS	42	
	STO 9	33 09	
	RCL 0	34 00	
	RCL 0	34 00	
	+	61	
	RCL 7	34 07	
	+	61	
	f COS	31 63	cos $(\alpha_o + 2\beta)$
	RCL 9	34 09	
	+	61	
200	2	02	
	X	71	
	h π	35 73	
	X	71	
	RCL 1	34 01	
	X	71	
	RCL 4	34 04	
	X	71	
	RCL 6	34 06	
	X	71	
210	h ABS	35 64	P
	h ENG	35 23	
	f -x-	31 84	
	f FIX	31 23	
	h RTN	35 22	
220			

LABELS

A	B	C	D	E
a	b	c	d	e
0	1	2	3	4
5	6	7	8	9

FLAGS

0
1
2
3

SET STATUS

FLAGS	ON	OFF
0	☐	☐
1	☐	☐
2	☐	☐
3	☐	☐

TRIG	
DEG	☐
GRAD	☐
RAD	☐

DISP	
FIX	☐
SCI	☐
ENG	☐
n	____

Program Description

Program Title Design of Preform and Calculation of Load in Nosing of Shells

Name Dr. G. D. Lahoti, Research Scientist **Date** 05/02/77

Address Battelle's Columbus Laboratories, 505 King Avenue

City Columbus State Ohio Zip Code 43201

Program Description, Equations, Variables, etc.

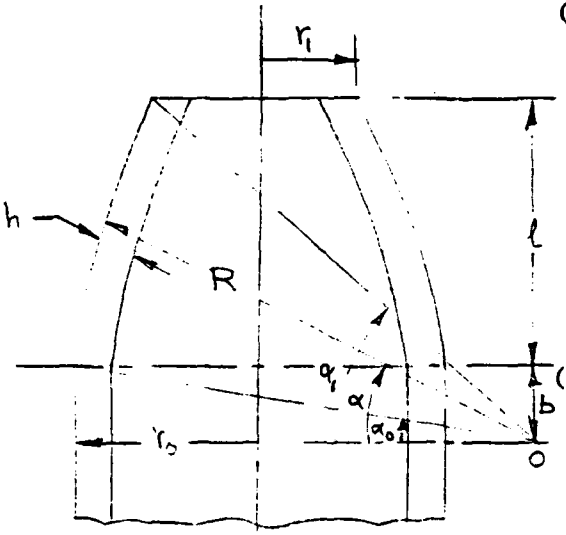

Fig A-3

(1) When $e_{max} = 0$, no elongation

$$h_o = \frac{hr}{r_o \cos(\alpha - \alpha_o)}$$

where $r = r_o - R(\cos\alpha_o - \cos\alpha)$

$$\alpha_o = \sin^{-1}(b/R)$$

$$\alpha = \sin^{-1}\left(\frac{b+x}{R}\right)$$

(2) When $e_{max} \neq 0$, with elongation

$$h_o = \frac{hr}{r_o \cos(\alpha - \alpha_o)}\left(1 + \frac{de}{dx}\right)$$

where $e = e_{max}\left(\frac{x}{\ell}\right)^n$

If e_{max} is known, $n = \frac{\ell}{e_{max}}\left(1 - \frac{1}{2}\cdot\frac{r_1 - r_o}{r_o}\right)\cos(\alpha - \alpha_o) - 1$

or, $h_o = \frac{hr}{r_o\cos(\alpha - \alpha_o)}\left(1 + \frac{ne_{max}}{\ell^n}x^{n-1}\right)$

(3) The nosing Load P is given as

$$P = 2\pi Rh\bar{\sigma}\left\{\cos(\alpha_o + 2\beta) - e^{\mu(\alpha_1 - \alpha_o)}\cos(\alpha_1 + 2\beta)\right\}$$

where $\beta = \tan^{-1}\mu$

Operating Limits and Warnings (1) When length of the nosed portion is given in a full number and a fraction, the preform calculations are carried out up to the full number only, and the thickness at the tip should be determined by extrapolation. (2) When $e_{max} \neq 0$, the initial thickness at the tip of the nose cannot be calculated. When ($\ell = e_{max}$) is a full number, the calculated value of h_o at the tip of the nose should be ignored. Correct value can be obtained by extrapolation.

APPENDIX B

TEMPERATURE DISTRIBUTION IN INDUCTIVELY HEATED TUBULAR COMPONENTS

APPENDIX B

TEMPERATURE DISTRIBUTION IN INDUCTIVELY HEATED TUBULAR COMPONENTS

Heat Generation Due to Induction Heating

Magnetic Field Intensity

In induction heating, the field intensity created by the alternating current induces the heating current in the charge. Therefore, the distribution of field intensity gives a direct indication of the distribution of heat and temperature gradient in the charge.

Neglecting the minor variations due to end effects, flux variations and flux leakages, the magnetic flux intensity surrounding the charge satisfies Maxwell's equation(1-7)*.

$$\frac{d^2H}{dr^2} + \frac{1}{r}\frac{dH}{dr} - \frac{iH\omega\mu 4\pi}{\rho} = 0 \quad , \tag{B-1}$$

where H = magnetic field intensity surrounding the workpiece, oersteds
r = radius of test element, Figure B-1, cm ($b \leq r \leq a$)
a = outer radius of the charge, cm
b = inner radius of the charge, cm
ω = angular velocity of the alternating current, radians/sec
ρ = resistivity of the material charged, ohm-cm
μ = permeability of the material charged, gauss/oersted

The solution of Equation (B-1) gives the value of H at any point inside the charge. Its general solution is

$$H = A\, I_o(kr\sqrt{i}\,) + B\, K_o(kr\sqrt{i}\,) \quad , \tag{B-2}$$

---

* Numbers in parentheses designate the references at the end of the appendix.

where $k^2 = \frac{4\pi\omega\mu}{\rho} = \frac{8\pi^2 f\mu}{\rho}$

I_o, K_o = Bessel's functions of first and second kind and of order zero

A,B = constants to be evaluated from boundary conditions.

At the outer surface, where r = a, flux intensity is maximum and is equal to H_o. Therefore,

$$H_o = A\, I_o(a) + B\, K_o(a) \quad . \tag{B-3}$$

For simplicity in writing, $I_o(kr\sqrt{i}\,)$ and similar expressions are abbreviated as $I_o(r)$, etc., in Equation (B-3) and subsequent equations. At the inner surface, where r = b, no electro-motive force (emf) is induced.

$$E_{r=b} = I_r \rho\Big|_{r=b} = -\frac{\rho}{4\pi} \left.\frac{\partial H}{\partial r}\right|_{r=b} = 0 \quad , \tag{B-4}$$

where I_r = current density along the test element at a radius r.
From Equations (B-2), and (B-4).

$$\left.\frac{\partial H}{\partial r}\right|_{r=b} = k\sqrt{i}\, \left[A\, I_o'(b) + B\, K_o'(b)\right] = 0 \quad . \tag{B-5}$$

Solving Equations (B-3) and (B-5) simultaneously yields:

$$\begin{aligned} A &= -H_o\, K_o'(b)/[K_o(a)\, I_o'(b) - I_o(a)\, K_o'(b)] \\ B &= H_o\, I_o'(b)/[K_o(a)\, I_o'(b) - I_o(a)\, K_o'(b)] \end{aligned} \tag{B-6}$$

Power Loss in Heating

The heat generated in the test element at a radius r, thickness ∂r and length $\partial \ell$, Figure B-1, can be calculated by considering the total current in the element. The total current in the element is given by:

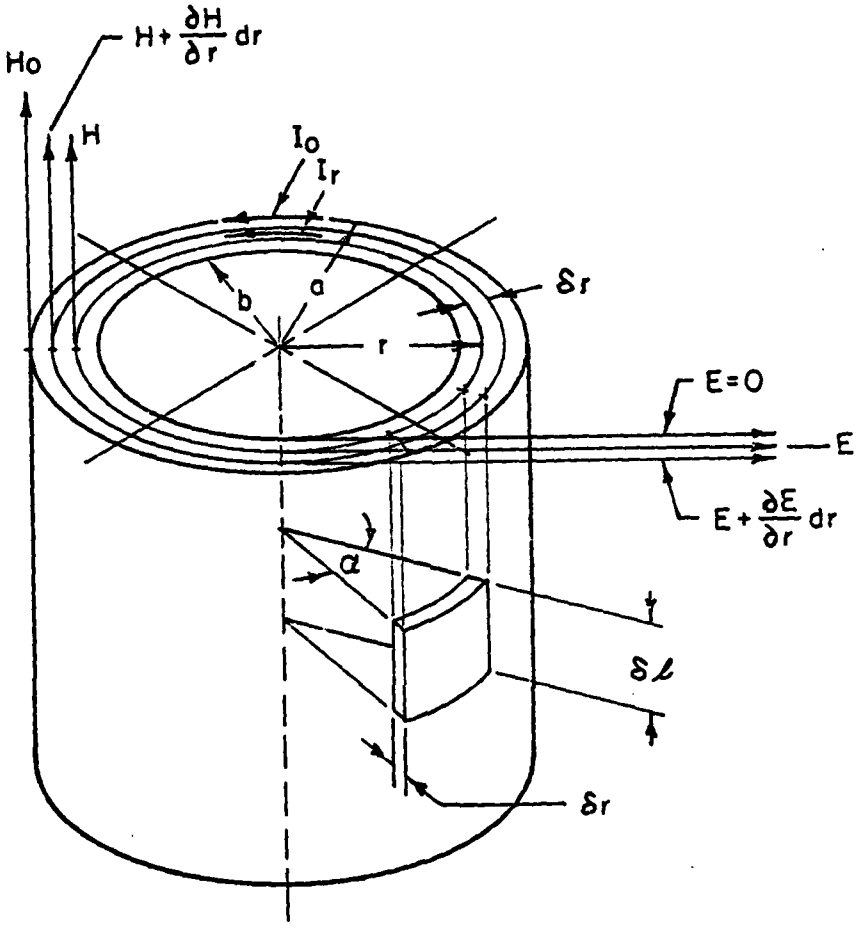

Fig B-1 Magnetic and Electric Field Intensities in a Hollow Cylinder

$$I_t = I_r \, \delta r \, \delta \ell$$

$$= - \frac{1}{4\pi} \frac{\partial H}{\partial r} \, \delta r \, \delta \ell$$

$$= - \frac{1}{4\pi} k\sqrt{i} \, [A \, I_o'(r) + B \, K_o'(r)] \, \delta r \, \delta \ell \quad . \qquad \text{(B-7)}$$

The resistance of the test element is

$$R = \frac{\rho \, \alpha \, r}{\delta r \, \delta \ell} \quad , \qquad \text{(B-8)}$$

where α = angle subtended by the element at the center.

The power loss or the heat generation rate in the element is given by:

$$P = I_t^2 R \text{ ergs/sec}$$

$$= \frac{k^2}{16\pi^2} \rho \, \alpha \, r \, [|A \, I_o'(r) + B \, K_o'(r)|^2] \, \delta r \, \delta \ell \, . \qquad \text{(B-9)}$$

Substituting (B-6) in (B-9)

$$P = \frac{H_o^2 \, k^2 \, \rho \, \alpha \, r}{16\pi^2} \left[\left| \frac{I_o'(r) - \phi \, K_o'(r)}{I_o(a) - \phi \, K_o(a)} \right|^2 \right] \delta r \, \delta \ell \text{ ergs/sec} \quad , \qquad \text{(B-10)}$$

where $\phi = I_o'(b)/K_o'(b)$

$I_o(r) = I_o(kr\sqrt{i}) = \text{ber } kr + i \text{ bei } kr$

$K_o(r) = K_o(kr\sqrt{i}) = \text{ker } kr + i \text{ kei } kr$

$I_o'(r) = I_o'(kr\sqrt{i}) = (\text{ber' } kr + i \text{ bei' } kr)/\sqrt{i}$

$K_o'(r) = K_o'(kr\sqrt{i}) = (\text{ker' } kr + i \text{ kei' } kr)/\sqrt{i}$

$H_o = 0.4\pi \, N_c \, I_c \, \sqrt{2} \, / \ell_w$

I_c = rms current in the induction coil, amp

N_c = number of turns in the coil

ℓ_w = length of the coil, cm

Denoting $Q = \left| \frac{I_o'(r) - \phi K_o'(r)}{I_o(a) - \phi K_o(a)} \right|^2$ and substituting the values for H_o and k in Equation (B-10) yields:

$$P = \left(\frac{4\pi N_c I_c}{\ell_w} \right)^2 \mu f \alpha r Q \delta r \delta \ell \, 10^{-9} \text{ watts.} \qquad \text{(B-10a)}$$

If the charge is heated for a duration of δt seconds, energy expended in heating the element is $P\delta t$ watt seconds, or joules.

Temperature Rise

Thus, the temperature rise, $d\theta$, in the element during the time δt is obtained as:

$$d\theta = \frac{P\delta t \, 10^6}{Cd r \alpha \delta r \delta \ell} \, C \quad , \qquad \text{(B-11)}$$

where C = heat capacity of the material charged, joule/kg-K
d = density of the material charged, kg/m^3.

Substituting (B-10a) into (B-11)

$$d\theta = \left(\frac{4\pi N_c I_c}{\ell_w} \right)^2 \frac{\mu f}{Cd} Q \delta t \, 10^{-3} C \quad . \qquad \text{(B-11a)}$$

As one can readily observe, $d\theta$ is a function of r only. That is, temperature gradients are in the radial direction only.

Heat Transfer by Conduction, Convection and Radiation

In order to predict the local temperatures, it is necessary to consider the heat equalization due to heat transfer. Because of the complexity of the phenomenon, it is appropriate to use the finite difference method for solving the heat transfer equations. Thus, it will be possible to take into account the heat loss due to conduction to the unheated portion of the tube, and due to convection and radiation to the environment.

Generalized Difference Equations for Heat Transfer

For the purpose of heat transfer analysis by the finite difference method, a portion of the vertical cross section of the tube, shown in Figure B-2, is assumed to be divided into a number of trapezoidal elements. The outside surface of the tube assumed to be straight, and it may or may not be tapered. The inner surface may be either straight or curved defined by a set of X, Y coordinates of points on the curve. When the inner surface is curved, intermediate points needed for grid system are obtained by polynomial interpolation.

Given these geometric entities, the length of the tube being heated, the thickness at the nosing end, Hl in Figure B-2, the thickness at the reference location, HO, the taper angle, ϕ, and the number of divisions in the radial and axial directions, a grid system of trapezoidal elements is generated. The curved portion of the inner surface of the tube in each element is approximated to with a straight line, as shown in Figure B-2.

With reference to Figure B-3, during a time interval Δt, heat transfer due to conduction takes place between the central element "0", and the adjacent elements "ℓ" (left), "u" (up), "r" (right), and "d" (down). The temperature change in the volume element "0" after conduction during a time interval, Δt, is given as the heat balance as follows:

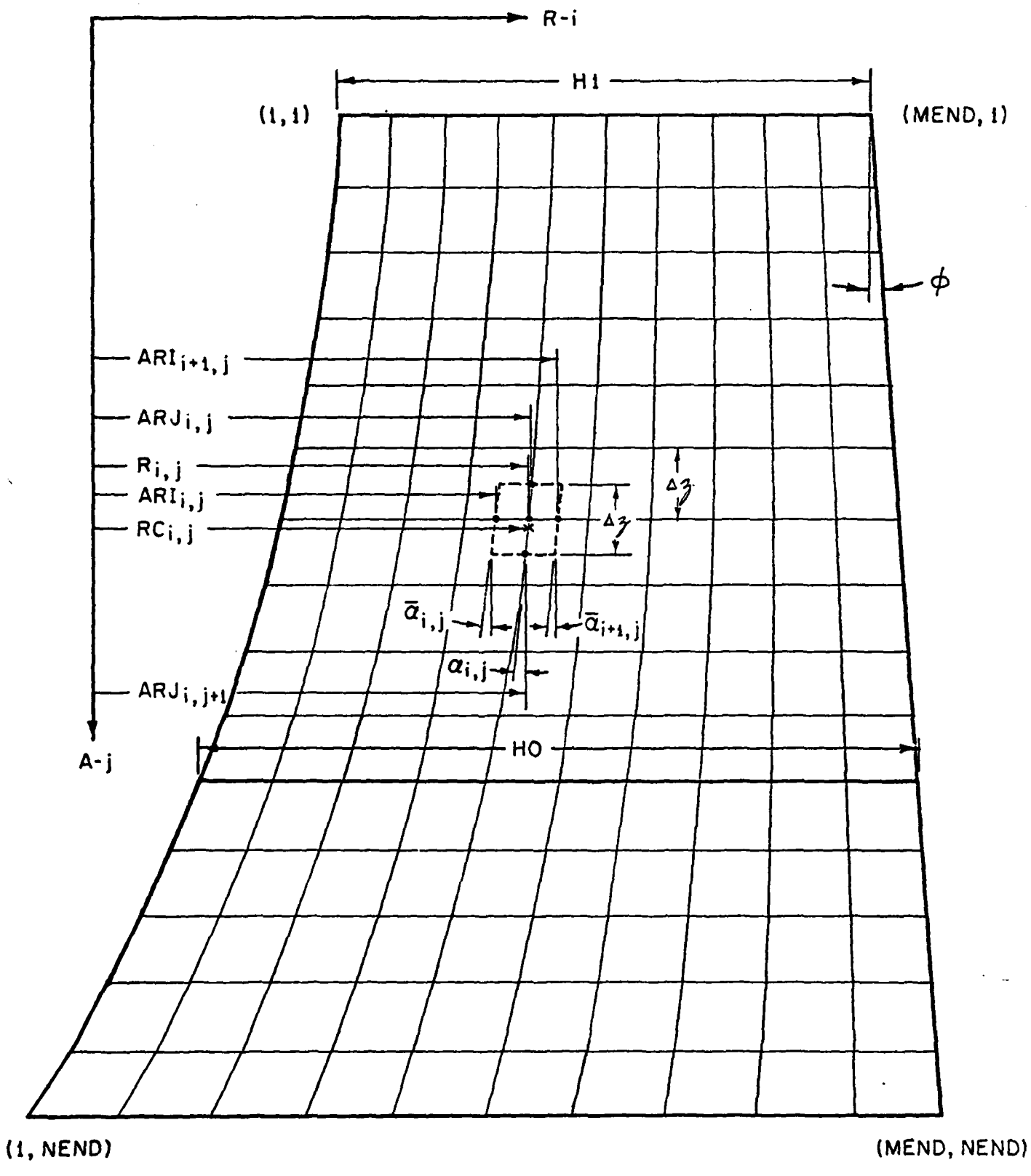

Fig 5-2 Trapezoidal Elements in the Grid System for Heat Transfer Analysis

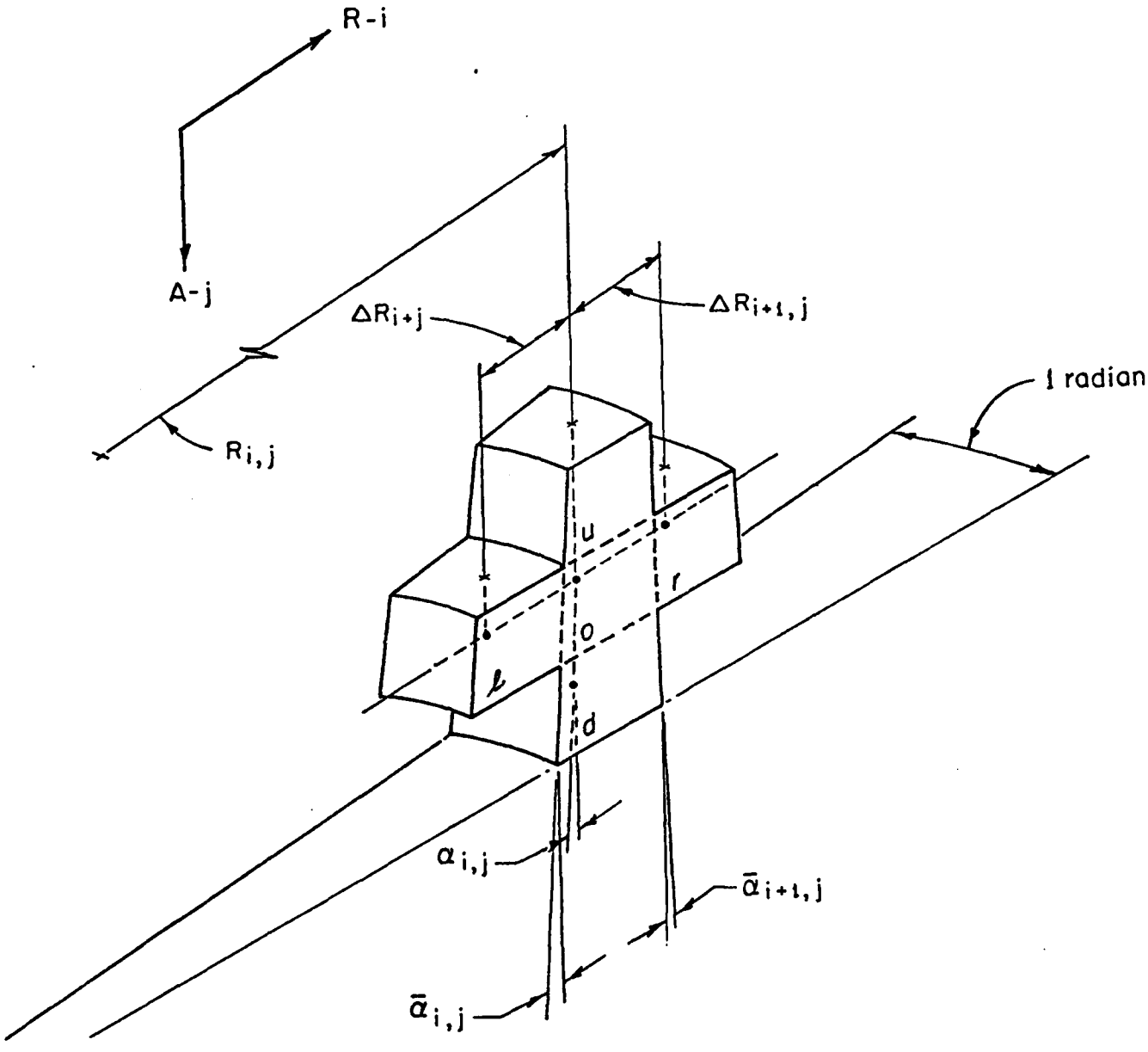

Fig B-3 Representation of Cylindrical Grid System for Deriving the Difference Equations of Heat Conduction

$$k_{\ell} \frac{\Delta}{\Delta R_{i,j}} ARI_{i,j} \frac{\Delta z}{\cos\bar{\alpha}_{i,j}} (\theta_{i-1,j} - \theta_{i,j})$$

$$+ k_r \frac{\Delta t}{\Delta R_{i+1,j}} ARI_{i+1,j} \frac{\Delta z}{\cos\bar{\alpha}_{i+1,j}} (\theta_{i+1,j} - \theta_{i,j})$$

$$+ \frac{\Delta t}{\Delta z} \cos\alpha_{i,j} \quad k_u ARJ_{i,j} T_{i,j} (\theta_{i,j-1} - \theta_{i,j})$$

$$+ k_d ARJ_{i,j+1} T_{i,j+1} (\theta_{i,j+1} - \theta_{i,j})$$

$$= \overline{\Delta R}_{i,j} \Delta z RC_{i,j} \rho c (\theta'_{i,j} - \theta_{i,j}) , \qquad \text{(B-12)}$$

where, in addition to the dimensions given Figures B-2 and B-3,

$\theta_{i,j}, \theta'_{i,j}$ = temperatures of the element (i,j) before and after time interval Δt, respectively

k_u, k_d, k_{ℓ}, k_r = thermal conductivities between the central element "0" and the surrounding elements "u", "d", "ℓ", "r", respectively

$RC_{i,j}$ = centroid of the central element "0"

Δt = time interval during which heat transfer takes place

ρ, C = Specific gravity and specific heat of the material in the element (i,j)

$T_{i,j} = (\Delta R_{i,j} + \Delta R_{i+1,j} + \Delta R_{i,j-1} + \Delta R_{i+1,j-1})/4$

$\overline{\Delta R}_{i,j} = (\Delta R_{i,j} + \Delta R_{i+1,j})/2$

Simplifying Equation (B-12) , the temperature $\theta'_{i,j}$ of the element "0" after time Δt is given by:

$$\theta_{i,j} = \frac{1}{K} \left\{ \theta_{i,j} \left[K - k_\ell \frac{\Delta t}{\Delta R_{i,j}} \frac{ARI_{i,j}}{\cos\bar{\alpha}_{i,j}} - k_r \frac{\Delta t}{\Delta R_{i+1,j}} \frac{ARI_{i+1,j}}{\cos\bar{\alpha}_{i+1,j}} \right.\right.$$

$$\left. - \frac{\Delta t}{\Delta z^2} \cos\alpha_{i,j} \left(k_u \, ARJ_{i,j} \, T_{i,j} + k_d \, ARJ_{i,j+1} \, T_{i,j+1} \right) \right]$$

$$+ k_\ell \frac{\Delta t}{\Delta R_{i,j}} \frac{ARI_{i,j}}{\cos\bar{\alpha}_{i,j}} \theta_{i-1,j}$$

$$+ k_r \frac{\Delta t}{\Delta R_{i+1,j}} \frac{ARI_{i+1,j}}{\cos\bar{\alpha}_{i+1,j}} \theta_{i+1,j}$$

$$+ \frac{\Delta t}{\Delta z^2} \cos\alpha_{i,j} \left[k_u \, ARJ_{i,j} \, T_{i,j} \, \theta_{i,j-1} \right.$$

$$\left. \left. + k_d \, ARJ_{i,j+1} \, T_{i,j+1} \, \theta_{i,j+1} \right] \right\} , \qquad \text{(B-13)}$$

where $K = \overline{\Delta R}_{i,j} \, RC_{i,j} \, \rho C.$

Stability Criterion

The coefficient of $\theta_{i,j}$ cannot be negative. This case would be physically absurd, since it would mean that the warmer the center element "0" is before Δt, the colder it would be after Δt. Hence,

$$\frac{1}{\Delta t} \geq \frac{1}{K} \left[\frac{k_\ell}{\Delta R_{i,j}} \frac{ARI_{i,j}}{\cos\bar{\alpha}_{i,j}} + \frac{k_r}{\Delta R_{i+1,j}} \frac{ARI_{i+1,j}}{\cos\bar{\alpha}_{i+1,j}} \right.$$

$$\left. + \frac{\cos\alpha_{i,j}}{\Delta z^2} \left(k_u \, ARJ_{i,j} \, T_{i,j} + k_d \, ARJ_{i,j+1} \, T_{i,j+1} \right) \right] . \qquad \text{(B-14)}$$

The above inequality determines the maximum allowable value of Δt for given thermal conductivities and the element sizes. This is called the stability criterion or the convergence condition, and must be satisfied in order to eliminate rapid and uncontrollable computing errors.

Estimation of Element Properties at Various Boundaries

Depending upon the location of a volume element, the boundary conditions and the thermal and physical properties of that element would vary. For example, an element which is in contact with air would also be subject to convective and radiative heat transfer.

Elements in the Interior of Tube: Referring to Equation (B-13), we have:

$$k_\ell = k_r = k_u = k_d = k_b,\ K = \Delta R_{i,j}\ RC_{i,j}\ \rho_b C_b \quad ,$$

where k_b, ρ_b, c_b = thermal conductivity, specific gravity, and specific heat of the tube material, respectively.

Elements on the Front End of the Tube: The appropriate difference equation for heat balance in the element "0", shown by the broken lines in Figure B-4a, is the following:

$$\frac{k_\ell}{2}\frac{\Delta t}{\Delta R_{i,j}}\ ARI_{i,j}\ \frac{\Delta z}{\cos\bar{\alpha}_{i,j}}\ (\theta_{i-1,j} - \theta_{i,j})$$

$$+\ \frac{kr}{2}\frac{\Delta t}{\Delta R_{i+1,j}}\ ARI_{i+1,j}\ \frac{\Delta z}{\cos\bar{\alpha}_{i+1,j}}\ (\theta_{i+1,j} - \theta_{i,j})$$

$$+\ \frac{\Delta t}{\Delta z}\cos\alpha_{i,j}\quad k_d\ ARJ_{i,j+1}\ T_{i,j+1}\ (\theta_{i,j+1} - \theta_{i,j})$$

$$+\ (h_f + h_r)\ R_{i,j}\ \overline{\Delta R}_{i,j}\ \Delta t\ (\theta_o - \theta_{i,j})$$

$$=\ \overline{\Delta R}_{i,j}\ RC_{i,j}\ \frac{\Delta z}{2}\ \rho C\ (\theta'_{i,j} - \theta_{i,j}) \quad , \qquad \text{(B-15)}$$

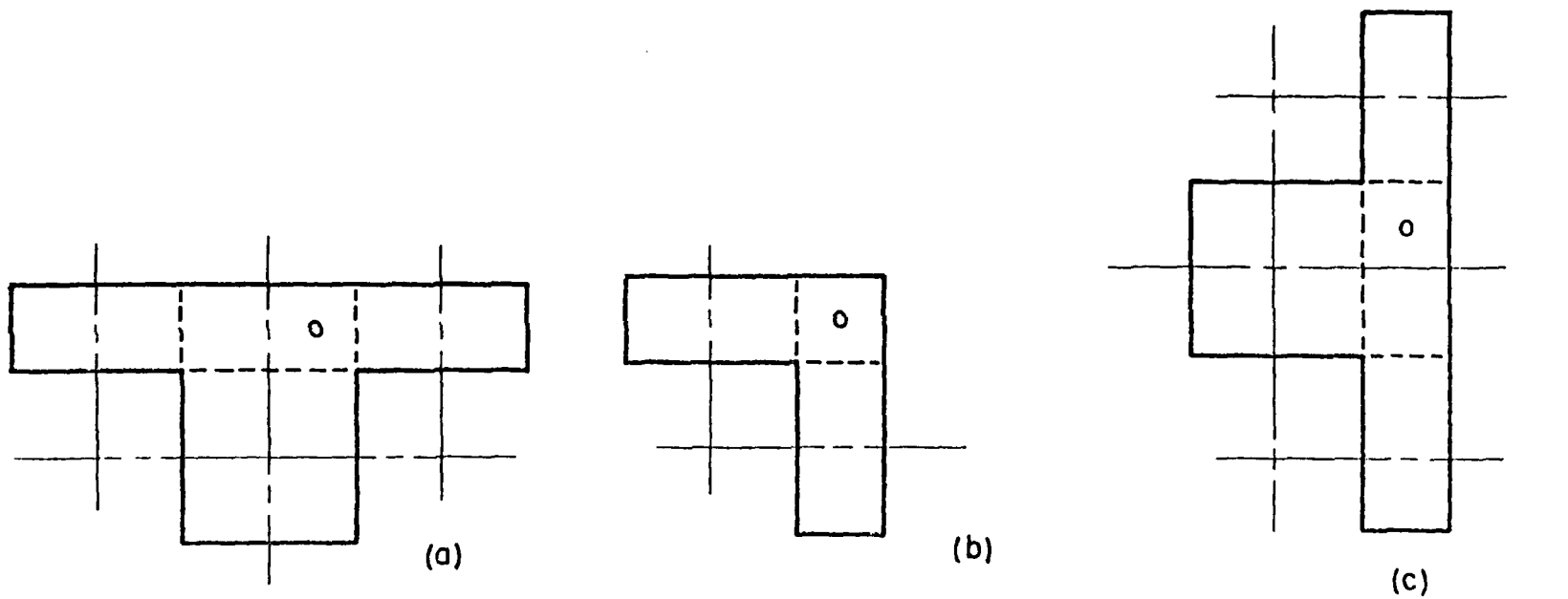

Fig B-4 Various Volume Elements Considered for Estimating the Heat Transfer Coefficients

where, in addition to the quantities defined earlier,

h_f = film heat transfer coefficient at the flat end surface of the tube

h_r = coefficient of radiation

θ_o = the ambient temperature,

and h_r, coefficient of radiation, is given by:

$$h_r = \varepsilon \sigma (T_o^2 + T_{i,j}^2) (T_o + T_{i,j}) , \qquad \text{(B-16)}$$

where ε = emissivity of the surface

σ = Stefan-Boltzmann's natural constant

$T_o, T_{i,j}$ = absolute temperatures of atmosphere and of the element, respectively.

Thus, comparison of Equation (B-15) with Equation (B-12)

$$k_\ell = k_r = k_b/2$$

$$k_d = k_b$$

$$k_u = \left[(h_f + h_r) R_{i,j} \overline{\Delta R}_{i,j} \frac{\Delta z}{\cos\bar{\alpha}_{i,j}} \right] \Big/ (ARJ_{i,j} T_{i,j})$$

$$K = \Delta R_{i,j} RC_{i,j} \rho_b C_b/2$$

$\theta_{i,j-1} = \theta_o$ = atmospheric temperature.

Elements at the Corners of the Tube. For an element at the outer corner shown by broken lines in Figure B-4b, the heat balance yields the following substitutions in Equation (B-12):

$$k_\ell = k_d = k_b/2$$

$$k_r = \frac{(h_c + h_r)}{2} R_{i,j} \frac{\cos\bar{\alpha}_{i+1,j}}{\cos\alpha_{i,j}} \frac{\Delta R_{i+1,j}}{ARI_{i+1,j}}$$

$$k_u = \left[\frac{(h_f + h_r)}{2} R_{i,j} \Delta R_{i,j} \frac{\Delta z}{\cos\alpha_{i,j}}\right] \Big/ \left[(ARJ_{i,j} T_{i,j})\right]$$

$$K = \overline{\Delta R}_{i,j} RC_{i,j} \rho_b C_b/4$$

$$\theta_{i+1,j} = \theta_{i,j-1} = \theta_o \quad ,$$

where h_c = film heat transfer coefficient at the free cylindrical surface of the tube.

Similar expressions for the inner corner of the tube will be:

$$k_r = k_d = k_b/2$$

$$k_\ell = \frac{(h_c + h_r)}{2} R_{i,j} \frac{\cos\alpha_{i,j}}{\cos\alpha_{i,j}} \frac{\Delta R_{i,j}}{ARI_{i,j}}$$

$$k_u = \left[\frac{(h_f + h_r)}{2} R_{i,j} \Delta R_{i,j} \frac{\Delta z}{\cos\alpha_{i,j}}\right] / (ARJ_{i,j} T_{i,j})$$

$$K = \overline{\Delta R}_{i,j} RC_{i,j} \rho_b C_b/4$$

$$\theta_{i-1,j} = \theta_{i,j-1} = \theta_o \quad .$$

Elements on the Inner and Outer Cylindrical Surfaces of the Tube. For an element at the outer cylindrical surface, shown by broken lines in Figure B-4c, the following substitutions are provided by the heat balance:

$$k_\ell = k_b$$

$$k_r = (h_c + h_r)\, R_{i,j}\, \frac{\Delta R_{i+1,j}}{ARI_{i+1,j}}\, \frac{\cos\bar{\alpha}_{i+1,j}}{\cos\alpha_{i,j}}$$

$$k_u = k_d = k_b/2$$

$$K = \overline{\Delta R}_{i,j}\; RC_{i,j}\; \rho_b C_b/2$$

$$\theta_{i+1,j} = \theta_o$$

Similar expressions for the elements on the inner cylindrical surface will be:

$$k_\ell = (h_c + h_r)\, R_{i,j}\, \frac{\Delta R_{i,j}}{ARI_{i,j}}\, \frac{\cos\bar{\alpha}_{i,j}}{\cos\alpha_{i,j}}$$

$$k_r = k_b$$

$$k_u = k_d = k_b/2$$

$$K = \overline{\Delta R}_{i,j}\; RC_{i,j}\; \rho_b C_b/2$$

$$\theta_{i-1,j} = \theta_o$$

REFERENCES

(1) Simpson, P. G., "Induction Heating", McGraw-Hill, 1960.

(2) Warren, A. G., "Mathematics Applied to Electrical Engineering", Chapman and Hall, 1958.

(3) Rodigin, N. M., "Induction Heating of Steel Articles with Normal-Frequency Currents", State Scientific Technical Publishing House of Literature on Ferrous and Nonferrous Metallurgy, Moscow, 1950 (in Russian).

(4) Pipes, L. A., "Applied Mathematics for Engineers and Physicists", McGraw-Hill, 1958.

(5) Reddick, H. W., and Miller, F. H., "Advanced Mathematics for Engineers", John Wiley, 1955.

(6) McLachlan, N. W., "Bessel Functions for Engineers", Oxford Press, 1955.

(7) Stansel, N. R., "Induction Heating", McGraw-Hill, 1949.

(8) Tudbury, C. A., "Basics of Induction Heating", Forging Industries Association, Cleveland, Ohio, 1960.

APPENDIX C

ANALYSIS OF METAL FLOW IN NOSING OF SHELLS

APPENDIX C

ANALYSIS OF METAL FLOW IN NOSING OF SHELLS

Introduction

In nosing of shells, the shape of the outer surface of the shell follows the die profile while the inner surface is not supported. Thus, during the nosing operation, the part of the shell within the die zone can move either radially inward, or in the direction of the tangent to the die profile, or in both the directions simultaneously. Under plastic state, metals flow in the direction of least resistance; therefore, the metal flow in cold nosing is affected by the frictional restraint at the die-workpiece interface and by the work-hardening characteristics of the material being deformed. In hot nosing, the metal flow depends upon the friction, the temperature of the workpiece and the speed of the die. In general, wall thickening increases with increasing friction, and in fact, under severe friction conditions, the shell may shrink in length instead of elongating.

In this Appendix, the metal flow in nosing of shells is analyzed using the Hill's general method of analysis[1]. This analysis is valid for straight-circular tubular preforms with uniform wall thickness, as in the case of nosing of 105 mm and smaller size shells. For larger shells, where the preform wall thickness is not uniform, this analysis can be applied only approximately.

Hill's General Method

The first step of this method consists of choosing a class of velocity fields from which the best approximation will eventually be selected. These velocity fields must satisfy all kinematic conditions. The associated stress (given by the material constitutive law) is either determined uniquely, or at least to within a hydrostatic pressure, if the material is incompressible. The associated stress

---

(1) R. Hill, "A General Method of Analyses for Metalworking Processes", Int. J. Mech. Phys. Solids, 11, 1963, p 305.

distribution in the deformation zone of a chosen velocity field will generally not satisfy all the statical requirements. A question that now arises is how to select, from the considered class of velocity fields, that one which most nearly satisfies the statical requirements.

Noting the converse of the virtual work-rate principle for a continuum, the final selection criterion is that "the statical conditions can be regarded as closely satisfied, overall, when

$$\int \sigma_{ij} \frac{\partial w_j}{\partial x_i} \, dV = \int \tau_j \, w_j \, dS_I - p \int n_j \, w_j \, dS_F + \int [(n_i \, \tau_i) \, n_j + mk\ell_j] \, w_j \, dS_C \qquad \text{(C-1)}$$

for a sufficiently wide subclass of virtual orthogonalizing motions w_j". The surface S of the deforming zone generally consists of three distinct parts, $S = S_C + S_F + S_I$, where S_C is the material-tool interface, S_F is unconstrained and S_I is the interface between the deformation and the rigid zones. In Equation(C-1), τ_j denotes the surface traction computed from the considered approximating field σ_{ij}. On surface S_F, there is ordinarily at most a uniform fluid pressure, p. The frictional constraint over surface S_C is represented by a constant frictional shear stress mk (where k is the shear yield strength of the deforming material and m is a constant, $0 \leq m \leq 1$), n_j is the local unit outward normal, and ℓ_j is a unit tangent vector opposed to the direction of the relative velocity of slip in the approximating field. Although the method is applicable, in principle, to all types of friction, the representation of constant frictional stress is used here.

The orthogonalizing family of velocities w_j to be selected must be sufficiently wide and should be just extensive enough to select a single approximating velocity field from the particular class constructed to satisfy the kinematic conditions. If the class of velocity fields were defined by equations involving an unknown function of just one position variable, then the orthogonalizing family must also involve an arbitrary function of one variable.

Once the family of velocity fields is chosen, the calculus of variations technique is applied to Equation(C-1), treating w_j as a variation. Then we obtain a system of equilibrium equations and boundary conditions, suited to the particular

approximating class and uniquely determining its best member.

Analysis

As shown in Figure C-1, consider a shell of outside radius r_o and uniform wall thickness h_o being nosed by a die of ogive radius R, moving at a speed U. A coordinate system (α,θ,t), where α is the meridional direction, θ is the circumferential direction and t is the thickness direction, is selected. It is assumed that α,θ and t are the principal directions also. The inner profile of the nosed portion is described by a function $h(\alpha)$, which indicates the wall thickness in the t direction at a given α. If r is the outside radius at a given α, a class of approximating velocity fields having the following components is selected:

$$\left.\begin{aligned} v_\alpha &= \frac{1}{rh} \\ v_\theta &= 0 \\ v_t &= \frac{h'}{rh^2}\, t \end{aligned}\right\} \qquad \text{(C-2)}$$

where $r = R\cos\alpha - a$, and the prime denotes a derivative with respect to α. These velocities satisfy the condition of incompressibility given by

$$\frac{\partial v_\alpha}{\partial \alpha} + \frac{v_\alpha}{r} \cdot \frac{\partial r}{\partial \alpha} + \frac{v_\alpha}{h} \cdot \frac{\partial h}{\partial \alpha} = 0 \ . \qquad \text{(C-3}$$

The velocity field given by Equation (C-2) also satisfies the velocity boundary conditions. At the tool-workpiece interface, we have

$$v_t\Big|_{t=0} = 0 \ . \qquad \text{(C-4)}$$

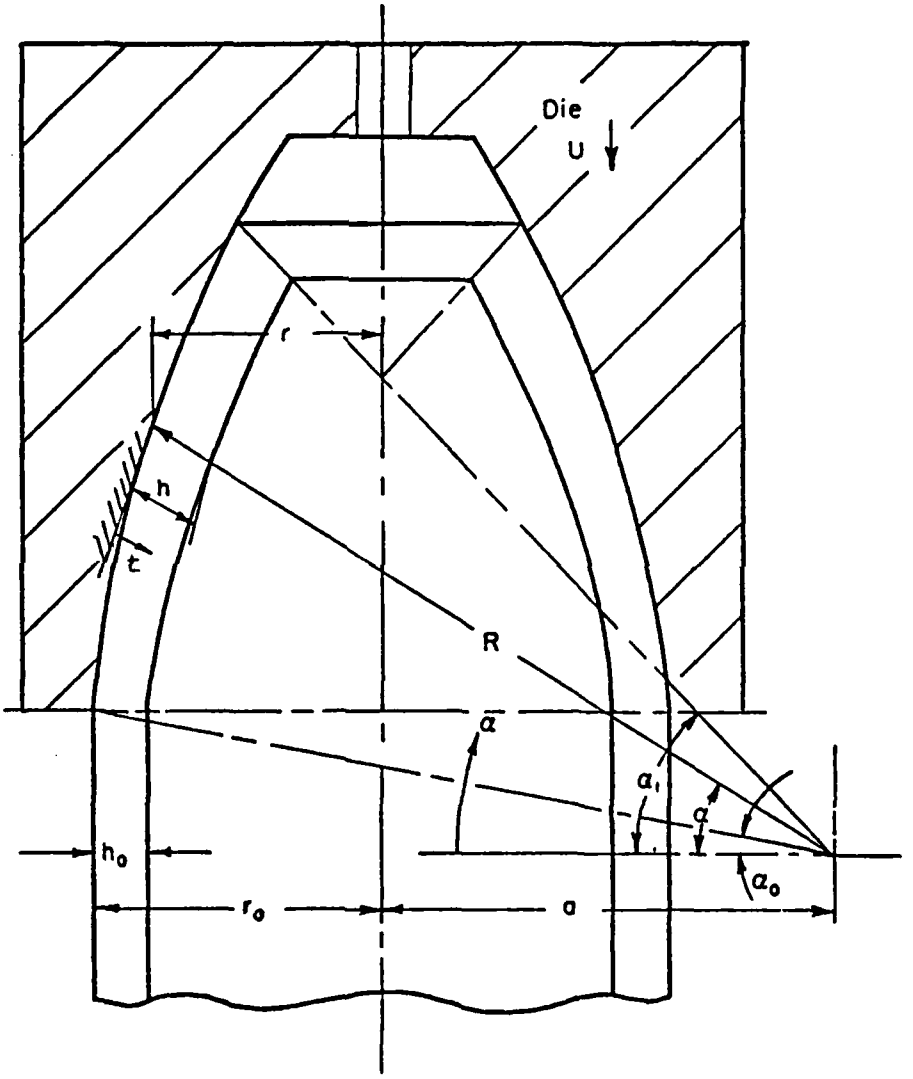

Fig C-1 Configuration of Shell During Nosing

At the free inner surface of the nosed portion

$$\left.\frac{v_t}{v_\alpha}\right|_{t=h} = h' \quad . \tag{C-5}$$

Thus, the velocity field given by Equation(C-2) is kinematically admissible.

In order to determine the unknown thickness function $h(\alpha)$ in Equation(C-2), we select the following virtual orthogonalizing velocity field:

$$\left.\begin{aligned} w_\alpha &= \frac{\phi(\alpha)}{r} \\ w_\theta &= 0 \\ w_t &= -\frac{\phi'(\alpha)}{r}\, t \quad , \end{aligned}\right\} \tag{C-6}$$

where $\phi(\alpha)$ is an arbitrary function of α and has at least a continuous first derivative. The prime denotes a derivative as usual. Rewriting the selection criterion given by Equation(C-1) in terms of the (α,θ,t) coordinate system, we have

$$\int \left\{ S_\alpha \left(\frac{1}{R}\, \frac{\partial w_\alpha}{\partial \alpha} \right) + S_\theta \left(\frac{1}{R} \cdot \frac{w_\alpha}{r} \cdot r' \right) + S_t \left(\frac{1}{R} \cdot \frac{\partial w_t}{\partial t} \right) \right\} dV$$

$$= \int \left[\sigma_\alpha w_\alpha \right]_{\alpha=\alpha_o}^{\alpha=\alpha_1} dS_I + \int mk \left[w_\alpha \right]_{t=0} dS_C \quad , \tag{C-7}$$

where S_α, S_θ, S_t are deviatoric stress components, σ_α is the meridianal stress, V is the volume of the deformation zone, S_I is the area of cross section at the base of the nose and S_C is the area of contact between the shell and the die.

Substituting Equation(C-6) into Equation (C-7), we get

$$\frac{1}{R}\int\left\{S_\alpha\left(\frac{\phi'}{r}-\frac{\phi r'}{r^2}\right)+S_\theta\left(\frac{\phi r'}{r^2}\right)+S_t\left(-\frac{\phi'}{r}\right)\right\}dV$$

$$=T_1\frac{\phi(\alpha_1)}{r_1}-T_o\frac{\phi(\alpha_o)}{r_o}-mk\int_{\alpha_o}^{\alpha_1}\frac{\phi(\alpha)}{r}\,dS_C\ ,$$

where T_1 and T_o are the forces acting on the cross section at $\alpha=\alpha_1$ and $\alpha=\alpha_o$, respectively. Obviously, T_1 is identically equal to zero and T_o is proportional to force exerted by the dies. In the above equation, $dV=(R-t)\,r\,d\theta\,dt\,d\alpha$, and $dS_C=2\pi r\,Rd\alpha$. Upon substituting and integrating with respect to θ, we get

$$\frac{2\pi}{R}\int_{\alpha_o}^{\alpha_1}F(\alpha)\,\phi'(\alpha)\,d\alpha+\frac{2\pi}{R}\int_{\alpha_o}^{\alpha_1}G(\alpha)\,\phi(\alpha)\,d\alpha=T_1\frac{\phi(\alpha_1)}{r_1}$$

$$-T_o\frac{\phi(\alpha_o)}{r_o}-2\pi\,mk\cdot R\int_{\alpha_o}^{\alpha_1}\phi(\alpha)\,d\alpha\ ,$$

where $$F(\alpha)=\int_o^h(S_\alpha-S_t)(R-t)\,dt$$

$$G(\alpha)=\int_o^h(-S_\alpha+S_\theta)\frac{r'}{r}(R-t)\,dt\ .$$

Integrating the first term on the left-hand side of the above equation and rearranging yields

$$\frac{2\pi}{R}\int_{\alpha_o}^{\alpha_1}\left\{-\frac{d}{d\alpha}F(\alpha)+G(\alpha)+mk\,R^2\right\}\phi(\alpha)\,d\alpha$$

$$+\frac{2\pi}{R}\left[F(\alpha)\,\phi(\alpha)\right]_{\alpha=\alpha_o}^{\alpha=\alpha_1}=T_1\frac{\phi(\alpha_1)}{r_1}-T_o\frac{\phi(\alpha_o)}{r_o}\ .\qquad\text{(C-8)}$$

Since $\phi(\alpha)$ is totally arbitrary, the Equation(C-8) is satisfied when

$$\frac{d}{d\alpha} F(\alpha) - G(\alpha) = mk R^2 \qquad \text{(C-9)}$$

together with

$$T_o = \frac{2\pi}{R} r_o F(\alpha_o)$$

$$T_1 = \frac{2\pi}{R} r_1 F(\alpha_1) \quad . \qquad \text{(C-10)}$$

Since $T_1 = 0$, $F(\alpha_1) = 0$. Equation(C-9) is a second-order ordinary differential equation in $h(\alpha)$ and can be solved using the following two boundary conditions:

$$h(\alpha_o) = h_o$$

and

$$F(\alpha_1) = 0 \quad . \qquad \text{(C-11)}$$

Once the solution is available, the first of Equations(C-10) gives the required nosing load $T_o \cdot \cos\alpha_o$.

The components of the deviatoric stress S_α, S_θ, and S_t are obtained from the Levy-Mises flow rule and the yield criterion. The yield criterion can be written approximately in the form of

$$S_\theta = -\frac{2}{3}\bar{\sigma} \quad , \qquad \text{(C-12)}$$

where $\bar{\sigma}$ is the material flow stress. If $\dot{\varepsilon}_\alpha$, $\dot{\varepsilon}_\theta$ and $\dot{\varepsilon}_t$ are the strain-rate components, from the flow rule

$$S_\alpha = S_\theta \cdot \frac{\dot{\varepsilon}_\alpha}{\dot{\varepsilon}_\theta} = \frac{2}{3}\bar{\sigma} \left(1 + \frac{h'}{h} \cdot \frac{r}{r'}\right)$$

$$S_t = S_\theta \cdot \frac{\dot{\varepsilon}_t}{\dot{\varepsilon}_\theta} = -\frac{2}{3}\bar{\sigma} \left(\frac{h'}{h} \cdot \frac{r}{r'}\right) \quad . \qquad \text{C-13)}$$

Substituting Equations (C-12) and (C-13) in expressions for $F(\alpha)$ and $G(\alpha)$, we obtain:

$$F(\alpha) = \frac{2}{3}\bar{\sigma}\, h \left(1 + 2\,\frac{h'}{h}\cdot\frac{r}{r'}\right)\left(R - \frac{h}{2}\right)$$

$$G(\alpha) = -\frac{2}{3}\bar{\sigma}\, h\,\frac{r'}{r}\left(1 + 2\,\frac{h'}{h}\cdot\frac{r}{r'}\right)\left(R - \frac{h}{2}\right) \qquad \text{(C-14)}$$

Finally, substituting for $F(\alpha)$ and $G(\alpha)$ in Equation (C-9), the differential equation for the thickness function $h(\alpha)$ is given as follows:

$$(2R - h)\,\frac{r}{r'}\cdot\frac{d^2h}{d\alpha^2} + \left(5R - 3h - \frac{rr''}{(r')^2}\right)\frac{dh}{d\alpha} - \frac{r}{r'}\left(\frac{dh}{d\alpha}\right)^2$$

$$+ \left(R - \frac{h}{2}\right)\frac{r'}{r}\,h - \frac{\sqrt{3}}{2}\,mR^2 = 0 \quad , \qquad \text{(C-15)}$$

where
$$r = R\cos\alpha - a$$
$$r' = -R\sin\alpha \qquad \text{(C-16)}$$
$$r'' = -R\cos\alpha$$

The boundary conditions are:

$$h(\alpha_o) = h_o$$
$$h'(\alpha_1) = -\left[\frac{hr'}{2r}\right]_{\alpha=\alpha_1}$$
$$(\text{from } F(\alpha_1) = 0)$$

Equation (C-15) is a second order ordinary differential equation defining the wall thickness, h, of the shell along the meridional direction during nosing operation. With the boundary conditions (C-16), it can be easily solved using a numberical technique. However, since the boundary conditions are available at each end of the interval, some type of iterative method is required for numerical integration of Equation (C-15). For this purpose, initially two guesses of $h'(\alpha_o)$ are made and the Equation (C-15) is solved by a fifth order Runge-Kutta Method.

Normally, these solutions will not satisfy the second of the boundary conditions(C-16). Therefore, a third guess value of $h'(\alpha_o)$ is determined using the first two solutions by linear extrapolation such that the projected error in $h'(\alpha_1)$ is zero, and the entire integration procedure is repeated. This last step is repeated with last two solutions until the error in $h'(\alpha_1)$ is within specified error bounds.

Further, the Equation(C-15) is singular when $\alpha_o = 0$, since $r'(\alpha = \alpha_o = 0) = 0$. In this particular case, a solution can be obtained by taking α_o as a small positive quantity instead of zero. The error caused by this approximation is relatively small.

APPENDIX D

ANALYSIS OF STRESSES IN NOSING OF SHELLS

APPENDIX D

ANALYSIS OF STRESSES IN NOSING OF SHELLS

A schematic diagram of nosing of shells is shown in Figure D-1. The length of the nonuniform walled preform is divided into a number of segments. If the number of segments is sufficiently large, the variation in thickness along the length of a segment can be ignored, and the average thickness of the segment can be taken as its uniform thickness. Then Onat and Prager's analysis can be applied to each element. Once the element is inside the die, its new average thickness is calculated from volume constancy, if elongation due to nosing is given.

Let us consider the analysis of stresses for Element 1. The analyses for subsequent elements will be the same, except for boundary conditions which will be described later. Assuming that the shell does not elongate during nosing, the rate of deformation in the meridianal direction, $\dot{\varepsilon}_m$, vanishes:

$$\dot{\varepsilon}_m = 0 \quad . \tag{D-1}$$

Therefore, from incompressibility condition, the rates of extension, $\dot{\varepsilon}_c$ and $\dot{\varepsilon}_n$ in the circumferential and the normal directions, respectively, must have equal absolute values, but opposite signs, the sign of $\dot{\varepsilon}_c$ corresponding to that of σ_c, the circumferential stress. Thus,

$$\dot{\varepsilon}_c = - \dot{\varepsilon}_n < 0 \quad . \tag{D-2}$$

Further, considering an elemental section at radius $r = R \cos\alpha - a$ (see Figure D-1) and the thickness h, we have:

$$\dot{\varepsilon}_c = - \frac{\dot{r}}{r} , \quad \dot{\varepsilon}_n = \frac{\dot{h}}{h} \quad , \tag{D-3}$$

where $\dot{r}$ and $\dot{h}$ are the instantaneous rates of change in r and h as this element is pushed toward the apex of the die. From Equations (D-2) and (D-3), it is clear that the product rh maintains a constant value during the nosing process. Thus,

$$rh = r_o h_o \quad , \tag{D-4}$$

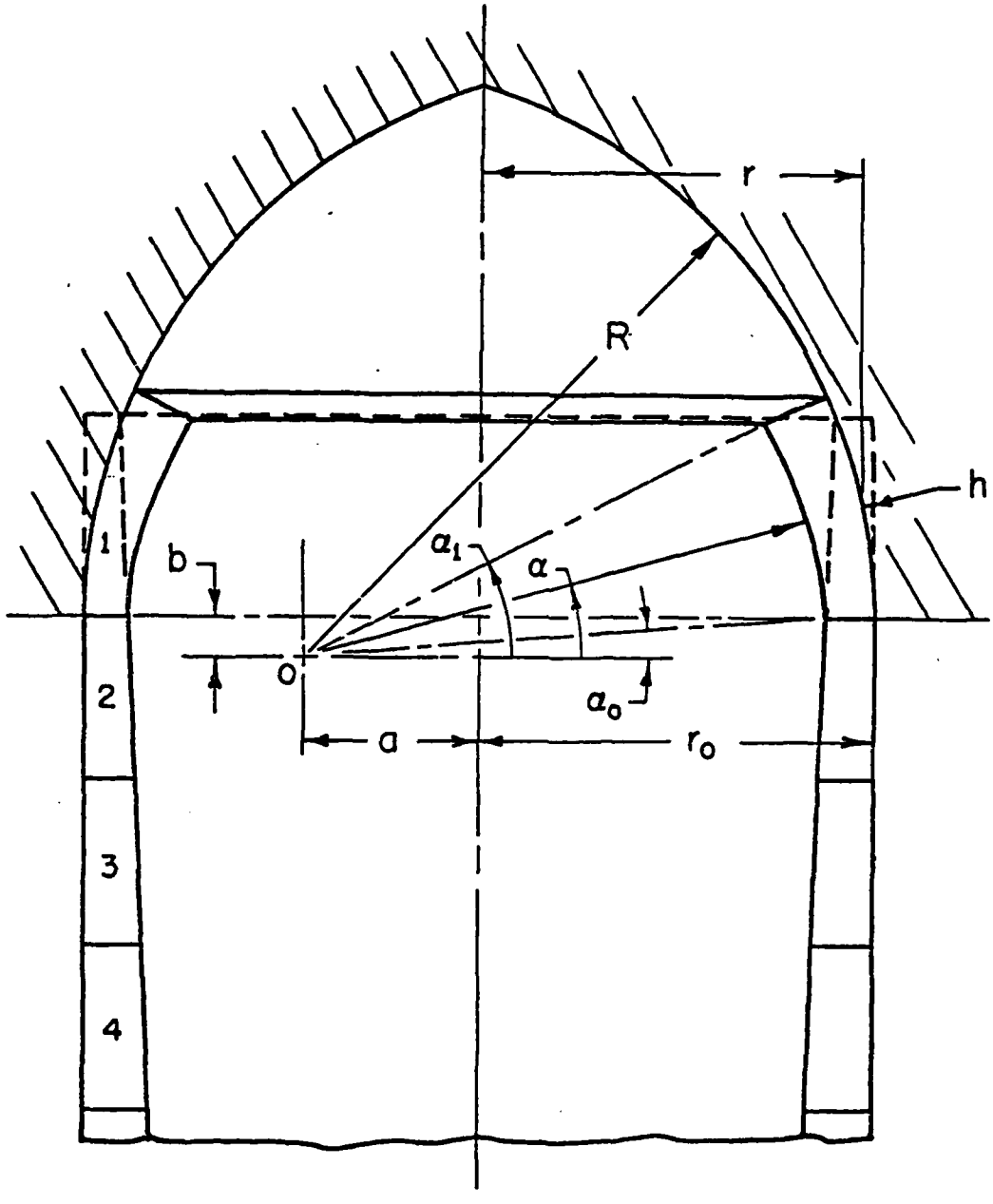

Fig D-1 Schematic Diagram of Nosing of Shells

where r_o and h_o are the initial radius and initial thickness of the element. Therefore, the variation in the wall thickness of the nose is given by:

$$h = \frac{r_o h_o}{R \cos\alpha - a} \quad . \tag{D-5}$$

The surface traction exerted by the die on the nose is the normal pressure p and the friction shear stress $f = \mu p$, where μ is the coefficient of friction. The meridianal and the circumferential stresses produced by these surface tractions in the thin-walled nose far exceed p and f in absolute value. The state of stress in the nose wall can, therefore, be treated as plane with the circumferential stress σ_c and the meridianal stress σ_m as the principal stresses. Since these principal stresses will be compressive and since σ_c can be expected to exceed σ_m in absolute value, according to Tresca's yield criterion, we have:

$$\sigma_c = -\bar{\sigma} \quad . \tag{D-6}$$

The equilibrium of forces in the meridianal and the circumferential directions give:

$$\frac{d}{d\alpha}(rh\,\sigma_m) + h\sigma_c \sin\alpha - r\mu p = 0 \quad ,$$

and $$rh\,\sigma_m + h\sigma_c \cos\alpha + rp = 0 \quad . \tag{D-7}$$

Resolving Equation (D-7) to eliminate p, yields:

$$\frac{d}{d\alpha}(rh\,\sigma_m) + \mu rh\,\sigma_m + Rh\,\sigma_c\,(\sin\alpha + \mu\cos\alpha) = 0 \quad . \tag{D-8}$$

The substitution of h from Equation (D-5) and σ_c from Equation (D-6) in Equation (D-8) gives:

$$\frac{d\sigma_m}{d\alpha} + \mu\sigma_m = \bar{\sigma}\,\frac{\sin\alpha + \mu\cos\alpha}{\cos\alpha - a/R} \tag{D-9}$$

Integrating for σ_m, we get:

$$\sigma_m = e^{-\int \mu \, d\alpha} \left\{ \int f(\alpha) \, e^{\int \mu \, d\alpha} \, d\alpha + C \right\} \tag{D-10}$$

where $$f(\alpha) = \bar{\sigma} \frac{\sin\alpha + \mu \cos\alpha}{\cos\alpha - a/R} \quad .$$

Since at $\alpha = \alpha_1$, $\sigma_m = \sigma'$, the specified value of the meridianal stress (which is zero for element 1), we have:

$$\sigma_m = e^{\mu(d_1 - \alpha)} \left\{ \sigma^1 - \int_{\alpha}^{\alpha_1} f(\alpha) \, e^{\mu(\alpha - \alpha_1)} \, d\alpha \right\} \tag{D-11}$$

Once σ_m is calculated for element 1 from the known boundary condition, σ_m for element 2 and subsequent elements can be calculated.

Strains in Shell Nose

If ε_m, ε_c and ε_n are the strains in the meridianal, the circumferential and the normal directions at a point where outside radius is r and wall thickness is h, then:

$$\varepsilon_m = ds/dx \quad ,$$

$$\varepsilon_n = - \frac{h_o - h}{h} \quad , \tag{D-12}$$

$$\varepsilon_c = - \frac{r_o - r}{r_o} \quad ,$$

where ds and dx are the final and initial length of a segment in the meridianal direction. Since volume remains unchanged during plastic deformation, we have:

$$\frac{r}{r_o} \cdot \frac{h}{h_o} \cdot \frac{ds}{dx} = 1 \quad ,$$

or $$(\varepsilon_m + 1)(\varepsilon_c + 1)(\varepsilon_n + 1) = 1 \quad . \tag{D-13}$$

Thus, if ε_c and ε_n are known from Equation (D-12), ε_m can be determined from Equation (D-13). If ε_m, ε_c and ε_n are taken as the principal strains, the effective strain is then given by:

$$\bar{\varepsilon} = \frac{2}{3}\sqrt{\frac{1}{2}\{(\varepsilon_m - \varepsilon_c)^2 + (\varepsilon_c - \varepsilon_n)^2 + (\varepsilon_n - \varepsilon_m)^2\}} \quad . \tag{D-14}$$

Strain Rates in Shell Nose

If h and r are the wall thickness and the outside radius at a point in the shell nose, the strain rates in the meridianal ($\dot{\varepsilon}_m$), the circumferential ($\dot{\varepsilon}_c$) and the normal direction ($\dot{\varepsilon}_n$) can be calculated from the velocity field given in Appendix C as follows:

$$\dot{\varepsilon}_m = -\frac{1}{R}\left\{\frac{r'}{r^2 h} + \frac{h'}{rh^2}\right\} \quad ,$$

$$\dot{\varepsilon}_c = \frac{1}{R}\left\{\frac{r'}{r^2 h}\right\} \quad , \tag{D-15}$$

$$\dot{\varepsilon}_n = \frac{1}{R}\left\{\frac{h'}{rh^2}\right\} \quad ,$$

where h' and r' are derivatives of h and r with respect to α. Since

$$h = \frac{h_o r_o}{R\cos\alpha - a} \quad , \text{ and } r = R\cos\alpha - a,$$

$$h' = -\frac{R\, h_o r_o \sin\alpha}{(R\cos\alpha - a)^2} \quad ,$$

$$r' = -R\sin\alpha \quad .$$

The effective strain rate is then given by:

$$\dot{\bar{\varepsilon}} = \frac{2}{3}\sqrt{\frac{1}{2}\{(\dot{\varepsilon}_m - \dot{\varepsilon}_c)^2 + (\dot{\varepsilon}_c - \dot{\varepsilon}_n)^2 + (\dot{\varepsilon}_n - \dot{\varepsilon}_m)^2\}} \quad . \tag{D-16}$$

Temperatures in Shell Nose

During nosing, heat is generated in the shell due to plastic deformation and friction at the tool-workpiece interfaces. Simultaneously, heat is transported with the moving material and heat transfer takes place. Some of the generated heat remains in the product, some of it is conducted to the die, and some may even increase the temperature of the material moving into the die. Thus, the general problem to be examined is that of time-dependent heat flow in an incompressible moving medium with heat generation in the medium.

In the present approximate analysis, it is assumed that heat is generated uniformly in the shell wall due to plastic deformation and friction, and a steady state of temperatures is reached after an initial period of transients. Since the temperature gradients in the meridianal direction are not as large as in the radial direction, heat transfer in the radial direction alone is considered. The temperature increase due to heat generated due to plastic deformation is given by:

$$\Delta T = \bar{\sigma}\,\bar{\varepsilon}\,/C\rho \quad , \tag{D-17}$$

where C and ρ are specific heat and density of shell material. Since friction factor is very small in shell nosing, the energy due to friction at the tool-workpiece interface can be neglected. The temperature decrease due to heat conduction to the die can be estimated as:

$$\Delta T' = -\frac{2K\,(T' - T_o)}{\log\,(r_d/r)\cdot V\rho C}\quad \Delta t \quad , \tag{D-18}$$

where K = Thermal conductivity of die material

$T' = T + \Delta T$, T = initial temperature

T_o = Ambient temperature

r_d = Die outside radius

Δt = Time interval

V = Volume of the element.

Thus, temperature, T_f, of an element inside the die after time Δt is given by:

$$T_f = T' - \Delta T' \quad . \tag{D-19}$$

This procedure is repeated for each element at time intervals of Δt.

APPENDIX E

DESCRIPTION OF THE COMPUTER PROGRAM NOSING

APPENDIX E

DESCRIPTION OF THE COMPUTER PROGRAM NOSING

The computer program NOSING is an integrated form of three separate computer programs--INHEAT, NOSFLW, and NOSTRS--developed to determine the optimum process variables in hot and cold nosing of shells. In this integrated form, NOSING can predict

(a) As-nosed and preform shape
(b) The temperature profile in the preform due to induction heating prior to nosing
(c) The metal flow during nosing
(d) The load-stroke relationship during nosing, considering the flow stress of the shell material as a function of strain, strain rate, and temperature
(e) The possibility of local buckling or Euler's buckling during nosing.

Thus, with the use of NOSING, generating data to plot performance curves is relatively simple, and the process optimization for a given set of input conditions can be easily established with a minimum number of computer runs.

All routines in NOSING have been coded as subroutines or function routines. Hence, they can be used in a simple one-line structure or in a superposed overlay structure as depicted in Figure E-1. In its present overlay structure, NOSING requires 41000_8 memory locations. With one-line structure, this requirement will increase to 53000_8 memory locations.

The computer program NOSING can be run both in batch and in interactive mode. When run in interactive mode, the input data is tested for every foreseeable error and the user is given an opportunity to modify the data, if necessary. In the batch run, whenever the input lacks any vital data, the program stops after printing appropriate error messages.

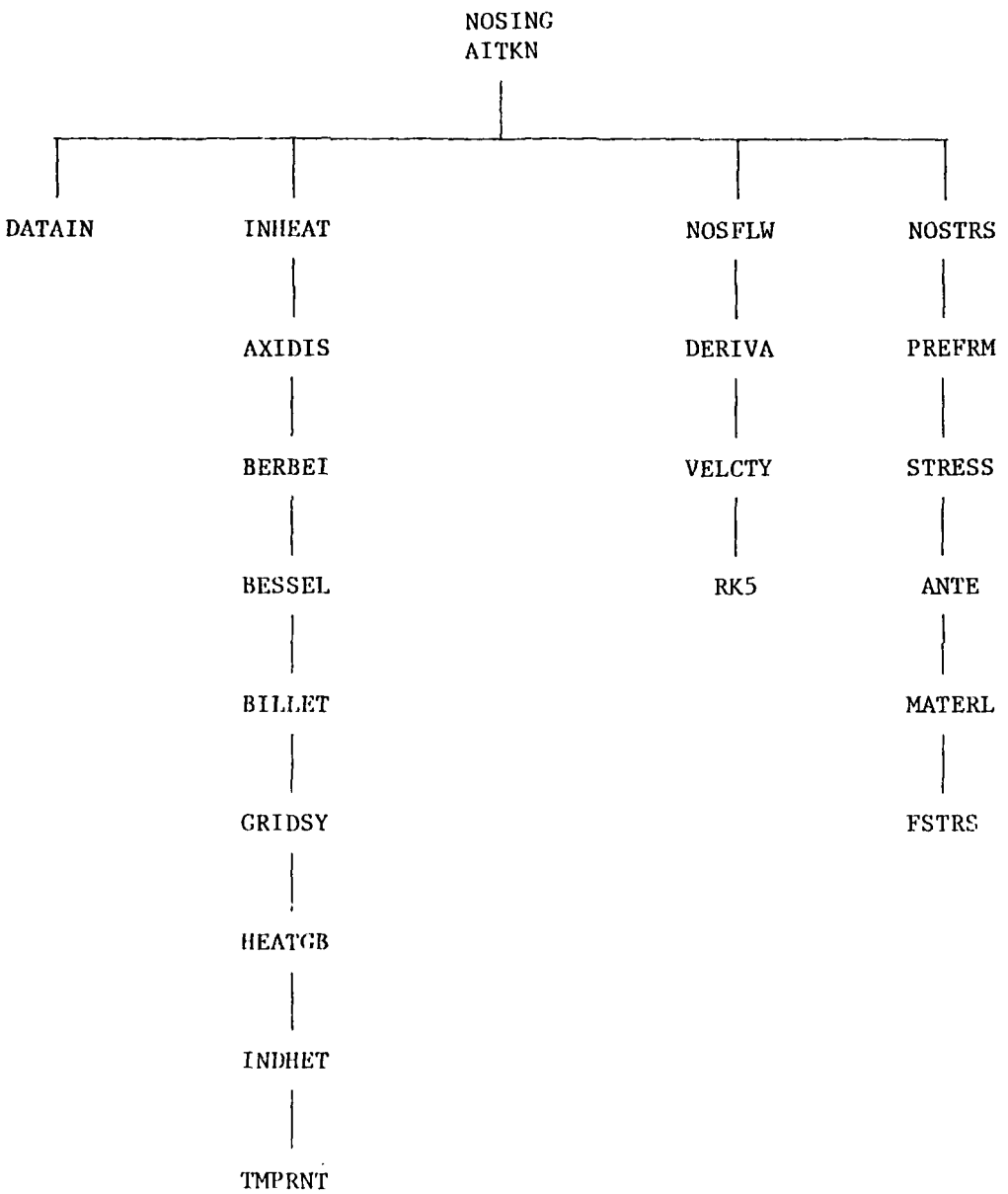

Fig E-1 Overlay Structure of the Computer Programs Nosing

This Appendix describes the functions of the various subprograms in NOSING. After a brief description of the input procedure with suitable examples, sample outputs from NOSING are presented to illustrate the output capability of NOSING. In the following section, each subroutine is described in alphabetical order by its purpose, calling sequence, description of the variables transferred as formal parameters, variables transferred through common blocks, brief description of the routine and the names of the calling, and the called subroutines.

In Table E-1, on page E-31, all the variables transferred through the COMMON blocks are described in alphabetical order. Table E-2, on page E-35, summarizes the list of intermediate results written on a separate file facilitating program debugging, if necessary.

Input to the Program NOSING

All input variables necessary for process optimization are read via the NAMELIST called IDATA. Supplying data by namelists has one major advantage. In namelist inputs, only those variables that need changing are assigned values. For this reason, those variables which have a fixed value most of the time are assigned default values* by the system.

Input to the program NOSING can be either in SI units or in the conventional (inch-lb-C) units. Output from NOSING will be in the units used for input variables. However, all computations are performed internally in SI units.

The variables included in the namelist IDATA are listed below. Following the description of each variable, units, wherever applicable, are given in square brackets. The default value of the variables, if any, is given in parenthesis.

---

* Stored value for a variable. If the user does not assign a value, the stored value will be automatically assigned to that variable.

AL	Axial length of the nosed portion [mm; inch]
AM	Friction shear factor at the die-workpiece interface (0.1)
AMBTEM	Ambient temperature [C] (20.)
AMU	Coefficient of friction (0.1)
BATCH	Logical variable. To be set to FALSE to run the program interactively (TRUE)
BILTEM	Billet temperature [C] (AMBTEM)
B1	Axial distance of the center of arc R1 from nose base [mm; inch]
B2	Axial distance of the center of arc R2 from nose base [mm; inch]
COTIME	Cooling time. Time required to transfer the billet from the induction heating table to the nosing press [seconds]
DI	Inside diameter of the rough turned shell at the nose base [mm; inch] (if DO and HO are given, DI = DO - 2 x HO)
DIEOD	Outside diameter of the nosing die [mm; inch]
DO	Outside diameter of the rough turned shell [mm; inch] (if DI and HO are given, DO = DI + 2 x HO)
EFFICN	Efficiency of the induction coil [percent] (50.)
ELNG	Estimated elongation during nosing. Will be estimated by metal flow analysis unless the user assigns a value. Present metal flow analysis is not valid for preforms with nonuniform wall thickness. Hence, assign a value to ELNG if the preform has nonuniform wall thickness. [mm; inch]
FREQ	Frequency of the induction heating current [cycles/sec]
GESS1	First guess of the slope of inner profile at the nose base
GESS2	Second guess of the slope of inner profile at the nose base
HETIME	Duration of induction heating [seconds]
HO	Wall thickness of the preform at the nose base, or wall thickness of the preform with uniform wall [mm; inch] (if DO and DI are given, HO = (DO - DI)/2)

IC	RMS current in the induction coil. Real variable, not integer. [Ampere]
IPRINT	Printing option. Refer Table E-2. (-1)
ITER	Maximum number of iterations to be performed during metal flow analysis. (25)
LC	Length of the induction coil. Real variable, not integer. [mm; inch] (AL - ELNG)
NC	Number of turns in the induction coil. Real variable, not integer.
NDA	Number of axial segments for stress analysis and temperature estimation. (20)
NDOASN	Maximum number of iterations to be performed during temperature estimation. Useful during program debugging.
NDR	Number of radial segments for temperature estimation. (6)
NSIZE	Shell size in millimeters.
R1	Radius of curvature of the outside nose profile. [mm; inch]
R2	Radius of curvature of the inside nose profile. [mm; inch]
SIUNIT	Logical variable. To be set to FALSE when the input data are in conventional (inch-lb-C) units. (TRUE)
TEMP	Variable dimensioned 25. Temperatures in the preform. To be supplied only when an estimation by finite-difference temperature analysis is not desired. If supplied, there should be NDA + 1 values, beginning from the base to the tip of the nose.
UNIPFM	Logical variable. To be set to FALSE when the preform has nonuniform wall thickness. When UNIPFM is FALSE, metal flow analysis will not be performed. (TRUE)
VELD	Axial velocity of nosing die. [mm/sec; inch/sec]

Input by Namelists

When entering data by namelists, the first column is always left blank. Following a $ sign in the second column, the namelist name, IDATA, is entered without any embedded blanks. Following at least one blank space after the name of the namelist, various parameters are entered and are equated to their values with commas between each parameter. The order in which parameters appear within a namelist input is immaterial. The namelist data listing is terminated by another $ sign. If the input exceeds one line length, the line is terminated after a comma by entering a line feed using the line-feed (LF) key and not the carriage-return key. Every continuation line is also started with a blank space in the first column. The data listing is finally terminated by a $ sign. In the batch run, every continuation card should have the first column blank. Since any error in spelling the variable name is likely to cause abnormal termination of the program execution, it is advisable to have a list of the variable names included in the namelist while trying to run the NOSING program interactively.

The examples given below show alternative ways of putting the data by namelists.

Example 1

```
b$IDATA  DO = 6.2, DI = 4.9, AL = 11., LC = 10.5, SIUNIT = F,
b TEMP = 375., 425., 525., 575., 600., 650., NDA = 5$
```

(b denotes blank space)

Example 2

```
b$IDATA  DO = 6.2, HO = 0.65, LC = 10.5, R1 = 65.5, IPRINT = 5,
bTEMP(1) = 375., TEMP(2) = 425., TEMP(3) = 525., TEMP(4) = 575.,
b TEMP(5) = 600., 650., NDA = 5$
```

As seen from Example 1, the right side TRUE or FALSE for the logical variable may be abbreviated to T and F respectively.

Error Recovery During the Data Input

Any error in the data input, such as (1) failure to enter the $ sign at the end of the data list, (b) misspelled variable name, and (c) embedded

blanks in the name of the variable will normally return the program control to the computer operating system, thereby causing an abnormal termination of the job. However, a special software package called "Error Recovery Package" is included in the NOSING system, which recovers the error and returns the control to a point specified by the package. Thus, whenever an error occurs while inputting the data by namelist, the message ENTER IDATA VARIABLES LIST will be printed. In interactive run, the user can retype the list correctly. In the batch run, after the data ends, a card with the word STOP in the first four column, should be included to short the program in case of errors in the input.

Output from the Program NOSING

Most outputs of NOSING are written directly on the OUTPUT file. However, when the variable IPRINT is assigned a positive number, several intermediate results are listed as described in Table E-2. To avoid lengthy output during interactive run, these intermediate results are written on a separate file called TAPE3. This special file TAPE 3 will be automatically disposed to the line printer when the program execution is normally terminated. But when abnormal termination of program execution occurs for any reason, the user should dispose TAPE3 to line printer to obtain the intermediate results. During the interactive run, type DISPOSE, TAPE3, PR=C or ROUTE, TAPE3, DC=PR, TID=C when the system is in COMMAND mode. In the batch run, add either DISPOSE, TAPE3, PR=C. or ROUTE, TAPE3, DC=PR, TID=C. control card after an EXIT. card in the control cards stream.

The first output from the program NOSING is the input data as read-in, as seen in Figure E-2. Other sample outputs as printed by NOSING are shown in Figures E-3, E-4, and E-5. Figure E-3 shows the results after metal flow analysis. Figure E-4 is a partial temperature distribution after induction heating prior to nosing. Figure E-5 shows the as-nosed profile, the preform geometry, and the stress and load distributions.

THE FOLLOWING RESULTS ARE FOR NOSING OF 155 MM SHELLS

THE PREFORM HAS NON-UNIFORM WALLS PRIOR TO NOSING

INPUT TO THE PROGRAM NOSING

OUTSIDE DIAMETER OF THE ROUGH-TURNED SHELL,INCH	=	6.200
INSIDE DIAMETER OF THE ROUGH-TURNED SHELL,INCH	=	4.900
WALL THICKNESS AT THE NOSE BASE,INCH	=	.650
RADIUS OF CURVATURE R1 OF OUTSIDE NOSE PROFILE,IN	=	65.500
AXIAL DISTANCE OF CENTER OF R1 FROM NOSE BASE,IN.	=	-5.250
AXIAL LENGTH OF THE NOSED PORTION AFTER NOSING,IN	=	11.000
AXIAL VELOCITY OF THE NOSING DIE,INCH/SEC	=	1.000
OUTSIDE DIAMETER OF THE NOSING DIE,INCH	=	12.000
FRICTION SHEAR FACTOR AT DIE-WORKPIECE INTERFACE	=	.010
COEFFICIENT OF FRICTION	=	.050
NUMBER OF AXIAL SEGMENTS FOR STRESS ANALYSIS AND TEMPERATURE ESTIMATION	=	10
ESTIMATED ELONGATION DUE TO NOSING INCH	=	.500
LENGTH OF THE INDUCTION COIL INCH	=	0.000
RMS CURRENT IN THE INDUCTION COIL AMP	=	400.000
NUMBER OF TURNS IN THE COIL	=	14.
SUPPLY FREQUENCY CYCLES/SECOND	=	10000.
BILLET TEMPERATURE PRIOR TO HEATING C	=	20.0
AMBIENT TEMPERATURE C	=	20.0
HEATING TIME SECONDS	=	20.000
COOLING TIME SECONDS	=	5.000
COIL EFFICIENCY PERCENT	=	50.0
NUMBER OF RADIAL DIVISIONS FOR TEMP. ESTIMATION	=	4

Fig E-2 Sample Input Data as Printed by NOSING

THE FOLLOWING RESULTS ARE FOR NOSING OF 105 MM SHELLS

THE PREFORM HAS UNIFORM WALLS OF THICKNESS HO

INPUT TO THE PROGRAM NOSING

OUTSIDE DIAMETER OF THE ROUGH-TURNED SHELL,MM	=	108.000
INSIDE DIAMETER OF THE ROUGH-TURNED SHELL,MM	=	84.000
WALL THICKNESS AT THE NOSE BASE,MM	=	12.000
RADIUS OF CURVATURE R1 OF OUTSIDE NOSE PROFILE,MM	=	650.000
AXIAL DISTANCE OF CENTER OF R1 FROM NOSE BASE,MM	=	-25.000
AXIAL LENGTH OF THE NOSED PORTION AFTER NOSING,MM	=	150.000
AXIAL VELOCITY OF THE NOSING DIE,MM/SEC	=	25.000
OUTSIDE DIAMETER OF THE NOSING DIE,MM	=	250.000
FRICTION SHEAR FACTOR AT DIE-WORKPIECE INTERFACE	=	.010
COEFFICIENT OF FRICTION	=	.050
NUMBER OF AXIAL SEGMENTS FOR STRESS ANALYSIS AND TEMPERATURE ESTIMATION	=	10

GUESS FOR SLOPE AT NOSE BASE(H≠) = 20.000

GUESS FOR SLOPE AT NOSE BASE(H≠) = 21.000

Fig E-3 Sample Output After Metal Flow Analysis

RESULTS FROM THE CONVERGED SOLUTION

ALFA	WALL THICKNESS	OUTER SURFACE AXIAL DISTANCE	OUTER SURFACE RADIUS	INNER SURFACE AXIAL DISTANCE	INNER SURFACE RADIUS
DEG	MM	MM	MM	MM	MM
2.204	12.000	0.000	54.000	0.000	42.009
3.546	12.494	15.199	53.237	14.426	40.767
4.887	13.007	30.375	52.118	29.267	39.158
6.229	13.547	45.521	50.644	44.051	37.177
7.570	14.124	60.629	48.816	58.768	34.815
8.911	14.748	75.689	46.635	73.405	32.065
10.253	15.433	90.694	44.102	87.948	28.915
11.594	16.196	105.636	41.218	102.381	25.353
12.936	17.060	120.507	37.985	116.688	21.358
14.277	18.059	135.297	34.405	130.844	16.904
15.618	19.240	150.000	30.480	144.820	11.951

ESTIMATED UNIT PRESSURE (P/(A*SIGMA)) = .405E+00

ELONGATION OF SHELL DUE TO NOSING, PERCENT= 4.0111

MAXIMUM THICKENING OF SHELL WALL, PERCENT= 60.3299

VELOCITY, STRAIN, AND STRAIN RATE DISTRIBUTION

ALFA	AXIAL DISTANCE	OUTER RADIUS	MERIDIANAL VELOCITY	NORMAL VELOCITY	STRAIN	STRAIN RATE
DEG	MM	MM	MM/S	MM/S	MM/MM	1/S
2.204	0.000	54.000	25.000	519.401	0.000	.052
3.546	15.199	53.237	24.356	522.377	.041	.054
4.887	30.375	52.118	23.898	536.259	.082	.059
6.229	45.521	50.644	23.612	561.762	.125	.068
7.570	60.629	48.816	23.496	600.612	.171	.080
8.911	75.689	46.635	23.554	655.868	.222	.095
10.253	90.694	44.102	23.802	732.532	.279	.114
11.594	105.636	41.218	24.267	838.704	.343	.140
12.936	120.507	37.985	24.998	987.764	.417	.173
14.277	135.297	34.405	26.073	1202.768	.501	.219
15.618	150.000	30.480	27.625	1525.908	.600	.287

Fig E-3 (Continued)

VALUE OF DELT AS CALCULATED BY HEAT63 = .11403
NUMBER ITERATIONS REQUIRED = 176

TEMPERATURE DISTRIBUTION AFTER INDUCTION HEATING AND PRIOR TO COOLING

	1	2	3	4	5
1	688.87	699.74	715.35	734.16	742.09
2	679.30	691.90	710.35	732.80	745.76
3	660.34	674.87	697.31	725.70	746.18
4	639.63	656.06	682.37	717.91	746.91
5	620.29	636.50	669.28	710.46	747.66
6	604.50	622.96	656.42	703.20	748.28
7	590.67	607.93	644.03	696.09	748.77
8	574.90	594.17	631.96	689.41	749.18
9	560.23	580.55	621.22	683.56	749.57
10	545.30	567.02	610.38	677.68	749.77
11	502.25	524.90	576.10	653.49	745.39
12	130.23	132.24	135.33	138.30	139.30
13	35.18	35.36	35.53	35.62	35.57
14	21.50	21.52	21.53	21.53	21.52
15	20.12	20.12	20.12	20.12	20.12
16	20.01	20.01	20.01	20.01	20.01

DELT = .11403 NUMBER OF ITERATIONS REQUIRED FOR COOLING = 44

TEMPERATURE DISTRIBUTION PRIOR TO NOSING:

	1	2	3	4	5
1	675.02	691.15	683.23	681.32	675.24
2	690.36	687.79	690.88	689.16	682.25
3	670.06	678.99	683.74	683.23	676.05
4	656.31	666.95	674.69	676.50	669.50
5	641.81	654.34	665.57	670.44	664.02
6	627.64	642.01	656.85	665.14	659.54
7	614.60	630.50	648.58	660.28	655.63
8	603.77	620.23	640.59	655.59	652.03
9	595.31	610.39	633.10	651.28	648.89
10	587.15	599.71	624.22	645.67	644.73
11	536.36	553.30	581.62	609.07	611.19
12	158.79	160.62	162.57	163.76	163.22
13	43.63	43.86	44.00	44.03	43.89
14	22.93	22.96	22.97	22.97	22.95
15	20.29	20.29	20.29	20.29	20.29
16	20.02	20.02	20.02	20.02	20.02

Fig E-4 Partial Sample Output for Temperature Distribution in the Preform Corresponding to Input in Figure E-2

AS-NOSED PROFILE OF THE SHELL

AXIAL DISTANCE INCH	INNER RADIUS INCH	AXIAL DISTANCE INCH	OUTER RADIUS INCH
10.839	.631	11.000	1.263
9.750	.900	9.900	1.535
8.661	1.149	8.800	1.786
7.571	1.379	7.700	2.018
6.482	1.589	6.600	2.230
5.393	1.779	5.500	2.423
4.304	1.951	4.400	2.596
3.215	2.104	3.300	2.750
2.126	2.238	2.200	2.886
1.037	2.353	1.100	3.002
0.000	2.450	0.000	3.100

PREFORM FOR 155 MM SHELL

SEGMENT NO.	AXIAL DISTANCE INCH	WALL THICKNESS INCH	TEMP-RATURE C
1	10.500	.288	900.000
2	9.450	.333	875.000
3	8.400	.378	775.000
4	7.350	.426	700.000
5	6.300	.470	675.000
6	5.250	.510	650.000
7	4.200	.546	600.000
8	3.150	.577	575.000
9	2.100	.605	525.000
10	1.050	.630	450.000
11	0.000	.650	375.000

Fig E-5 Sample Output After Stress and Load Calculations for Input in Figure E-2

SUMMARY OF RESULTS

OSING OF THIS SHELL IS POSSIBLE IN 1 HIT

SEG. NO.	SIGM(I),KSI	SIGT(I),KSI	SIGC(I),KSI	WALL THICKNESS,INCH	TEMPERATURE,C
1	0.	-.2492E+02	-.4596E+02	.7068E+00	.8129E+03
2	-.1081E+02	-.1700E+02	-.4612E+02	.6731E+00	.7936E+03
3	-.1934E+02	-.1481E+02	-.4605E+02	.6568E+00	.7213E+03
4	-.2746E+02	-.1570E+02	-.5369E+02	.6546E+00	.6650E+03
5	-.3497E+02	-.1610E+02	-.5948E+02	.6534E+00	.6449E+03
6	-.4135E+02	-.1515E+02	-.5960E+02	.6523E+00	.6257E+03
7	-.4670E+02	-.1412E+02	-.5838E+02	.6515E+00	.5869E+03
8	-.5328E+02	-.1916E+02	-.8344E+02	.6508E+00	.5656E+03
9	-.5953E+02	-.2035E+02	-.9190E+02	.6504E+00	.5209E+03
10	-.6570E+02	-.2251E+02	-.1048E+03	.6501E+00	.4477E+03
11	-.7030E+02	-.1966E+02	-.9072E+02	.6500E+00	.3750E+03

Fig E-5 (Continued)

SEG. NO.	DIE DISPL.,IN	NOSING FORCE,LB
1	.1050E+01	-.6118E+04
2	.2100E+01	-.1767E+05
3	.3150E+01	-.4218E+05
4	.4200E+01	-.8429E+05
5	.5250E+01	-.1437E+06
6	.6300E+01	-.2210E+06
7	.7350E+01	-.3205E+06
8	.8400E+01	-.4430E+06
9	.9450E+01	-.6024E+06
10	.1050E+02	-.7968E+05

Fig E-5 (Continued)

Details of the Computer Program NOSING

The basic functions of the main program and the various subprograms of the computer program NOSING are briefly described below.

Main Program NOSING

This main program, NOSING, serves essentially as a coordinating routine. It initializes various input parameters, connects the input/output files for interactive use, initializes the error recovery package, calls various subprograms for preform design and stress analysis and finally disposes TAPE3 to the line printer.

Function ANTE

Purpose: Calculates the integral of the meridianal stress

Function Reference: AINTGR = ANTE (A1, A2)
A1, A2 = Lower and upper limits of integral

Variables Transferred Through Common*: ALFO1, AMU, DO

Description: * Calculates the integral using the Simpson's rule

Called by: STRESS

Function AXIDIS

Purpose: From the given set of coordinate data for points defining the distribution curve, this function routine computes the multiplication factor to estimate the actual amount of heat generated at a given point along the axis of the shell.

Function Reference: FACTOR = AXIDIS(J,DELZ)
J = Axial coordinate of the element under study
DELZ = Axial distance between any two successive elements along the axis.

---

* All variables transferred through the COMMON blocks are described in Table E-1.

Variables Transferred
Through COMMON: NN, XX, ZZ

Description: * Any intermediate value of XX at the desired ZZ value is obtained by polynomial interpolation using the library routine AITKN.

Calling Routines: AITKN

Called By: INDHET

Subroutine BERBEI

Purpose: For a given value of X, computes the Bessel's functions ber(X), bei(X), ber'(X), bei'(X), ker(X), kei(X), ker'(X), and kei'(X)

Calling Sequence: CALL BERBEI(X,BERI,INDEX)

X = Coefficient of the Bessel's function

BERI = An array of eight elements carrying back the ber, bei, ber', bei', ker, kei, ker', and kei' values

INDEX = When INDEX is set to zero, ber', bei', ker', and kei' are not computed

Description: * All Bessel functions are computed by polynomial approximations using the equations given in the Handbook of Mathematical Functions, U.S. Department of Commerce

* Two sets of equations are used; one for values of eight or less and the other for values greater than eight.

Called By: BESSEL

Function BESSEL

Purpose: Calculates the value of Q in Equation (B-10a) given in Appendix B, where

$$Q = \left| \frac{I_o'(r) - \phi K_o'(r)}{I_o(a) - \phi K_o(a)} \right|^2$$

$$\phi = I_o'(b)/K_o'(b)$$

$$I_o(r) = I_o(kr\sqrt{i}) = \text{ber } kr + i \text{ bei } kr$$

$$K_o(r) = K_o(kr\sqrt{i}) = \text{ker } kr + i \text{ kei } kr$$

$$I_o'(r) = I_o'(kr\sqrt{i}) = (\text{ber}' kr + i \text{ bei}' kr)/\sqrt{i}$$

$$K_o'(r) = k_o'(kr\sqrt{i}) = (\text{ker}' kr + i \text{ kei}' kr)/\sqrt{i}$$

a = Outer radius of the tube

b = Inner radius of the tube

r = Radius of the element under study

$k^2 = (8\pi^2 f\mu)/\rho$

f = Frequency of the induction voltage

μ, ρ = Permeability and thermal conductivity of the material charged.

Function Reference: Q = BESSEL(X,A,B,XK)

X = Radius of the element, r

A = Outer radius of the tube, a

B = Inner radius of the tube, b

XK = k

a,b,r, and k are already defined.

Calling Routines: BERBEI

Called By: INDHET

Subroutine BILLET

Purpose: Computer the thermal, electrical, and magnetic properties of AISI 1045 steel at a given temperature

Calling Sequence: CALL BILLET(TEMP,ATMTEM)

TEMP = Temperature of the element under study

ATMTEM = Atmospheric temperature

Variables Transferred Through COMMON: AKB, CRB, DENSTY, HCB, HFB, IC, NC, LC, PERMEB, RHO

Description: * All material property data used in this subroutine, with the exception of permeability, were obtained from the ASME Handbook on "Metals Properties", McGraw Hill, 1954. Thermal conductivity, heat capacity, and electrical resistivity for AISI 1045 steel were not readily available. Hence, these properties for AISI 1040 steel are used here as close approximations.

* Thermal conductivity and electrical resistivity at a given temperature are estimated by linear interpolation from the stored set of discrete data.

* Permeability of magnetic materials vary considerably with changes in the temperature, the magnetic flux density, and the size of the billet. Adequate data to meet all the needs of the present program are not available from any known source of information. A rough approximation given by the formula $\mu = \frac{32400}{H_o} + 1$ is used, where H_o is the maximum flux density.

Permeability remains constant at the saturated value for temperatures up to 600 C. Beyond the Curie temperature, which is 768 C for 1045 steel, permeability becomes unity. The transition between 600 and 768 C is very sharp and is approximated to a square function in this program.

Calling Routines: AITKN

Called By: HEATGB, HEATRN, INDHET

Subroutine DATAIN

Purpose: Reads the process variables and prints the supplied data. Prints appropriate warning messages if the input is not complete. During interactive run, enables the user to re-assign values, if necessary.

Calling Sequence: CALL DATAIN

Variables Transferred Through COMMON: AL, AM, AMBTEM, AMU, BATCH, BILTEM, B1, B2, COTIME, DI, DIEOD, DO, EFFICN, ELNG, FREQ, GESS1, GESS2, HETIME, HO, IC, IPRINT, ITER, LC, NC, NDA, NDOASN, NDR, NSIZE, R1, R2, SIUNIT, TEMP, UNIPFM, VELO

Called By: NOSING

Subroutine DERIVA

Purpose: This subroutine supplies the second order ordinary differential equation for variation in wall thickness during nosing in the form of first and second derivatives. This subroutine is given in the EXTERNAL mode.

Calling Sequence: CALL DERIVA (X,F,D)

X, independent variable

F(1), dependent variable

F(2), derivative of F(1), with respect to X

D(1), derivative of F(1), with respect to X (output)

D(2), derivative of D(1), with respect to X (output)

Called By: RK5

Function FSTRS

Purpose: Calculates the required parametric values for the interpolation routine AITKN

Function Reference: A = FSTRS(MSTRN,MTEMP,T,ASTR,AC,AM,TEMP,STR,STRRAT)

MSTRN: Size of the strain array of the flow stress data (input)

MTEMP: Size of the temperature array of the flow stress data (input)

T: Temperatures at which discrete flow stress data are available in the program (input)

ASTR: Strain values at which discrete flow stress data are available in the program (input)

AC: Constant C in the equation

$$\text{Flow stress} = C\ (\text{strain rate})^{m}\ \text{(input)} \qquad \text{(E-1)}$$

AM: Exponent M in Equation (E-1) (input)

TEMP: Stock temperature (input)

STR: Strain in the stock (input)

STRRAT: Strain rate in the stock (input)

Description: * Calculate the intermediate parametric values for use by the library interpolation routine AITKN.

* Call AITKN twice to estimate the values of C and m in Equation (E-1).

* Estimate the flow stress substituting the values of C and m in Equation (E-1).

Routines Called: AITKN

Called By: MATERL

Subroutine GRIDSY

Purpose: Generates a grid system for heat transfer calculations. Also computes a number of parametric values used in heat transfer calculations.

Calling Sequence: CALL GRIDSY

(No formal parameters)

Variables Transferred Through COMMON: AL2, ARI, ARJ, CTETA, CTETAB, DELZ, DI, DO, DRI, IPRINT, MEND, NDA, NDR, NEND, OUTP, PHI, R, RC, RSLT, SC1, T, TSCR

Description: * Using the supplied data for AL2, PHI, DO, and DI (Refer to Figure E-6), $R_{i,j}$'s are computed.

* From the values of $R_{i,j}$, $ARI_{i,j}$, $ARJ_{i,j}$, $\Delta R_{i,j}$, $\alpha_{i,j}$, $\bar{\alpha}_{i,j}$, $T_{i,j}$, and $RC_{i,j}$ are computed.

$RC_{i,j}$ is the centroid of the element (i,j) as shown in Figure E-6.

$\Delta R_{i,j}$ is the distance between the center points of the elements (i,j) and (i-1,j); i.e., $\Delta R_{i,j} = R_{i,j} - R_{i-1,j}$.

$T_{i,j} = (\Delta R_{i,j} + \Delta R_{i+1,j} + \Delta R_{i+1,j-1})/4$.

* When IPRINT $\geq$ 5, values of R are listed on the results file RSLT or TAPE3

When IPRINT $\geq$ 7, values of the centroids, RC, are listed on the file RSLT.

When IPRINT $\geq$ 8, values of ARI, ARJ, and ΔR are listed on the file RSLT.

Note: The listed values of ARJ are the products of ARJ and T; i.e., $ARJ_{i,j}$(listed) = $ARJ_{i,j}$(computed) x $T_{i,j}$.

When IPRINT $\geq$ 9, cos $\alpha_{i,j}$ and cos $\bar{\alpha}_{i,j}$ are listed on the file RSLT.

Calling Routines: AITKN

Called By: INHEAT

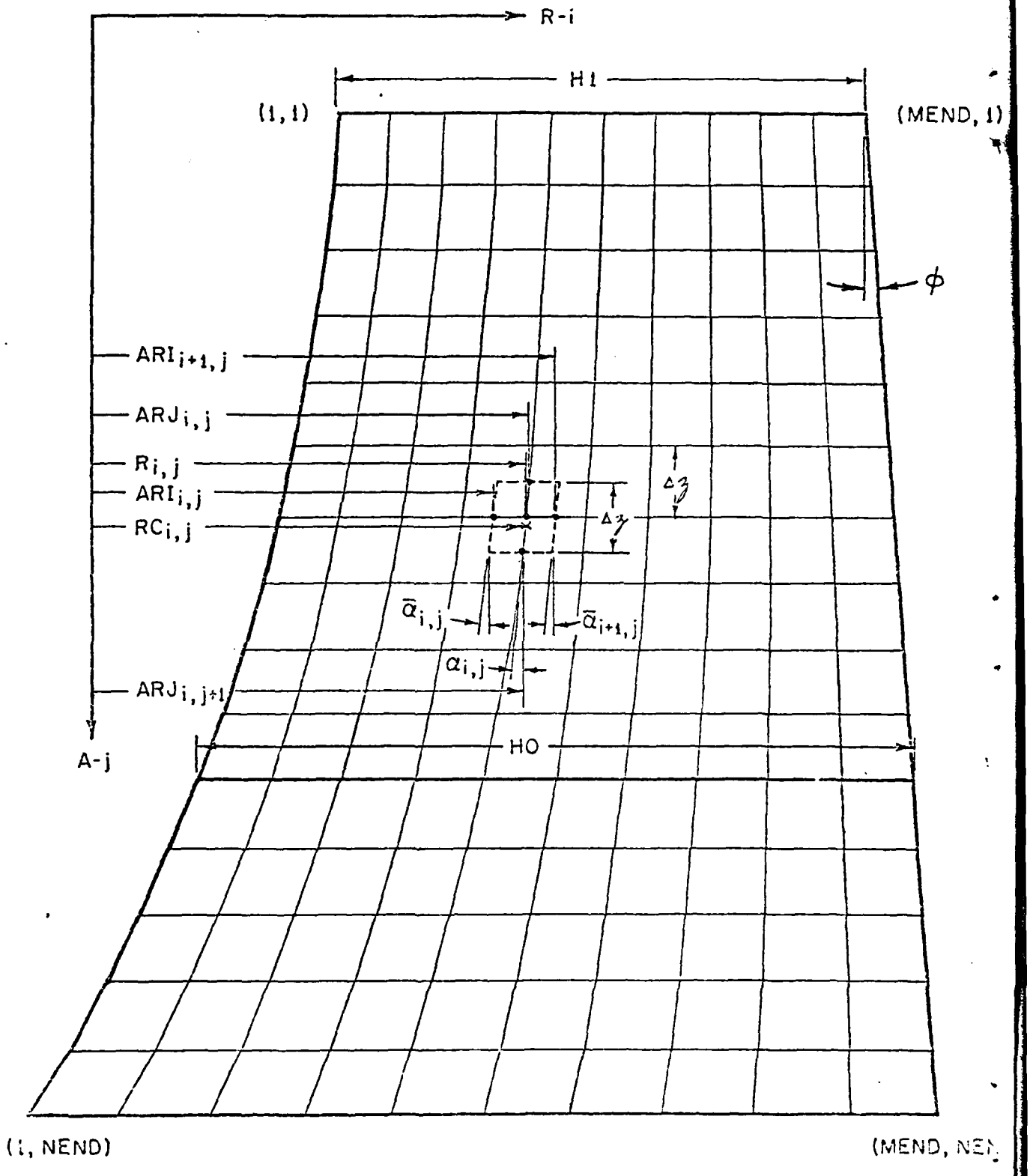

Fig E-6 Trapezoidal Elements in the Grid System for Heat Transfer Analysis

The temperature distribution is written on the RSLT file, after every cycle if IPRINT is set to 9, and is written after every 10 cycle if IPRINT is set to any value between 3 and 9.

Calling Routines: BILLET, HEATRN, INDHET, TMPRNT

Called By: INHEAT

Subroutine HEATRN

Purpose: Computes the change in temperature distribution due to heat transfer. The same routine is used to estimate the temperature changes due to heat equalization during induction heating and due to heat balancing during cooling.

Calling Sequence: CALL HEATRN

(No formal parameters)

Variables Transferred Through COMMON: AKB, AMBTEM, ARI, ARJ, BILTEM, CRB, CTETA, CTETAB, DELT, DELZ, DRI, HCB, HFB, INCODE, IPRINT, MEND, NEND, R, RC, RSLT, T, TSCR

Description:

* As described in Appendix B, equivalent k_u, k_d, k_ℓ, k_r, $\theta_{i-1,j}$, $\theta_{i+1,j}$, $\theta_{i,j-1}$, $\theta_{i,j+1}$, and K are calculated for elements at different locations.

* The temperature change in any particular element after heat transfer is estimated by substituting the equivalent k's, θ's, and K in Equation B-12 of Appendix B.

* If IPRINT = 7 or IPRINT $\geq$ 9, values of I, J, k_u, k_d, k_ℓ, k_r, K, cos $\alpha_{i,j}$, $\theta_{i,j}$, $\theta'_{i,j}$ and three more local variables are listed on the RSLT file.

In case of unexpected results, values of these variables will be helpful to figure out the cause of malfunction.

* Temperature values are transferred back to the "T" arrays from the scratch "TSCR" arrays.

Subroutine HEATGB

Purpose: This monitor routine computes the minimum time interval, Δt, in order to satisfy the stability criterion, Equation B-14 in Appendix B. By issuing calls to HEATRN and INDHET, this routine estimates the heat generation and equalization during induction heating and during heat balancing while the billet is transferred from the induction heating equipment to the press.

Calling Sequence: CALL HEATGB
(No formal parameters)

Variables Transferred Through COMMON: AKM, AMBTEM, ARI, ARJ, BILTEM, COTIME, CRB, CTETA, CTETAB, DELT, DELZ, DRI, HCB, HETIME, HFB, INCODE, IPRINT, LC, MEND, NDOASN, NEND, OUTP, R, RC, RSLT, T

Description:

* Temperatures in all grid points are initialized by assigning the value of the supplied billet temperature.

* The minimum time interval, Δt, is estimated by satisfying the stability criterion at the most adverse forging condition.

* From the prescribed "heating time" and the "cooling time", and the computed minimum time interval, Δt, numbers of iterations required to cover the heating period and the cooling period are calculated.

* The temperature distribution during induction heating is estimated by repeated calls to INDHET and HEATRN.

The temperature distribution is written on the RSLT file after every cycle if IPRINT is set to 9, and is written after every 10 cycles if IPRINT is set to any value between 3 and 9.

The temperature distribution at the end of the induction heating period is listed on the output file.

* The change in temperature distribution due to cooling during the transfer of the billet from the heating equipment to the press is calculated by repeating the calls to HEATRN.

Calling Routines: BILLET

Called By: HEATCB

Subroutine INDHET

Purpose: Calculates the amount of heat generated in induction heating

Calling Sequence: CALL INDHET

(No formal parameters)

Variables Transferred Through COMMON: CRB, DELT, DELZ, FREQ, IC, IPRINT, LC, MEND, NC, NEND, PERMEB, R, T

Description: * Amount of heat generated in each element is calculated using Equation B-11a in Appendix B.

* If IPRINT $\geq$ 8, values of W, permeability, Q, CRB, $\Delta\theta$, and k are listed in the RSLT file, where

$$W = \left(\frac{4\pi N_c I_c}{L_c}\right)^2 f \Delta t \, 10^{-3}$$

CRB = C d

$\Delta\theta$ = Change in temperature

N_c = Number of turns in the coil

I_c = Current in the coil, Amp

L_c = Length of the coil, mm

f = Frequency of the induction voltage, cps

Δt = Minimum time interval for heat transfer calculations

C = Thermal conductivity of the material charged

d = density of the material charged

$k^2 = (8\pi^2 \mu f/\rho)$

Calling Routine: AXIDIS, BESSEL, BILLET

Called By: HEATGB

Subroutine INHEAT

Purpose: Coordinates the functions of all routines used for temperature estimation

Calling Sequence: CALL INHEAT

(No formal parameters)

Variables Transferred Through COMMON: AL2, DI, DO, HO, LC, MEND, NDA, OUTP, Q1, RSLT, SC1, T

Calling Routines: GRIDSY, HEATGB

Called By: NOSING

Subroutine MATERL

Purpose: Calculates the flow stress for AISI 1045 steel at different temperatures, strains, and strain rates from the stored discrete flow stress data. Also supplies the specific heat, thermal conductivity, young's modulus, poison's ratio, and density of AISI 1045 steel.

Calling Sequence: CALL MATERL (STRAIN, STRRAT, TEM, FSTRES)

STRAIN = Local strain in the material

STRRAT = Local strain rate in the material

TEM = Local temperature of the material

FSTRES = Estimated flow stress (output)

Variables Transferred Through COMMON: ANU, DENSTY, E, SPHEAT, THCON

Description: * If the temperature is less than 500 C, flow stress is calculated using the formula:

$$\bar{\sigma} = K(\bar{\varepsilon})^n \qquad \text{(E-2)}$$

where $\bar{\sigma}$ = average flow stress

ε = average strain

K,n = constants

* If the temperature is more than 500 C, flow stress is calculated using the formula:

$$\bar{\sigma} = C(\dot{\bar{\varepsilon}})^m \qquad \text{(E-3)}$$

where $\bar{\sigma}$ = average flow stress

$\dot{\bar{\varepsilon}}$ = average strain rate

C,m = constants.

For this purpose, true values of C and m are obtained from the stored discrete data by interpolation. Function FSTRS performs the interpolation using the library routine AITKN.

Calling Routines: FSTRS

Called By: STRESS

Subroutine NOSFLW

Purpose: In addition to coordinating the functions of all other routines in the metal flow analysis section, this routine solves the differential equation for thickness function.

Calling Sequence: CALL NOSFLW

(No formal parameters)

Variables Transferred Through COMMON: A, AL, ALFA, ALFO, ALF1, AM, B1, B2, DI, DO, GESS1, GESS2, H, HO, HP, IPRINT, ITER, NDA, RR, R1, SIUNIT, ZZ

Description: The second order ordinary differential equation is solved numerically by the 5th order Runge Kutta method. Since one boundary condition is available at each end of the interval, an iterative method is employed. That is, the solution is started at the beginning of the interval by assuming a value of the second boundary condition. If this solution satisfies the boundary condition at the end of the interval, then the assumed value at the beginning is the actual value, and the calculated solution is the required solution. Otherwise, the second boundary condition at the beginning is adjusted by linear interpolation until the boundary condition at the end of the interval is satisfied by the last calculated solution.

Calling Routine: RK5, VELCTY

Called By: NOSING

Subroutine NOSTRS

Purpose: Defines the as-nosed profile from the supplied data and prints the geometry, calls PREFRM to define the preform geometry and STRESS to estimate loads and stresses during nosing.

Calling Sequence: CALL NOSTRS

(No formal parameters)

Variables Transferred

Through COMMON: AL, ALFA, ALFD1, ALFD2, AL2, B1, B2, NDA, RRI, RRD, R1, R2, TEMP, X, XI, Z

Calling Routines: PREFRM, STRESS

Called By: NOSING

Subroutine PREFRM

Purpose: Defines the preform geometry from the known finish shape

Calling Sequence: CALL PREFRM

(No formal parameters)

Variables Transferred

Through Common: AL, ALFA, ALFO1, AL2, B1, DL, DO, ELNG, H, HO, HP, NDA, NSIZE, R, R1, SC1, SIUNIT, TEMP, UNIPFM, Z

Description: * Nosing preform is designed using simple strain considerations given by Nadai. The estimated elongation due to nosing is distributed along the length by a power law. Preform thickness is then calculated from volume constancy requirements.

Called By: NOSTRS

Subroutine RK5

Purpose: This routine solves a system of first order ordinary differential equations with given initial values, by a fifth-order Runge-Kutta method. It has an automatic

control of step size in order to minimize the number of steps necessary ot obtain a prescribed accuracy. The routine performs at least seven evaluations of the derivative for each step.

Calling Sequence: CALL RK5 (X,Y,B,EPS,N,FI,FP)

X = a variable corresponding to independent variable

B = the size of interval

EPS = prescribed relative error. Recommended value, $10^{-8} \leq EPS \leq 10^{-4}$

N = number of equations to be integrated

FI = a real variable. Set FI $\leq$ 0 when entering the routine the first time

FP = the name of the routine supplied by the user to evaluate the derivatives. DERIVA in this case.

Y = an array of dependent variable, the solution array (output)

Note: This routine is valid for N $\leq$ 25.

Called By: NOSFLW

Subroutine STRESS

Purpose: Calculates the stress and the load during nosing operation.

Calling Sequence: CALL STRESS

(No formal parameters)

Variables Transferred Through COMMON: ALFA, ALOAD, AMBTEM, AMU, ANU, DENSTY, DIEOD, DL, DO, E, EPS, EPSRT, H, HO, HP, IPRINT, NDA, PI, R, RRI, RRD, R1, SIGC, SIGM, SIGT, SIUNIT, SPHEAT, TEMP, THCON, VELO

Description: * The stress analysis used here was given by Nadai and modified by Onat and Prager. Basically, the nosing process is simulated in a finite number of discrete steps. The stresses at each step are calculated in each segment, beginning from the free tip of the nose. At each step, strains, strain rate, and temperatures are also calculated in each segment and the flow stress of a segment is taken as a function of the strain, strain rate, and temperature.

Also, the local buckling or Euler's buckling is checked at each step. In the end, a load-displacement table is generated.

Routines Called: ANTE, MATERL

Called By: NOSTRS

Subroutine TMPRNT

Purpose: Lists the temperature distribution with an appropriate caption on a prescribed file.

Calling Sequence: CALL TMPRNT(K,PROCODE,FILNAM)

K = Number of iterations completed

PRCODE = A code number to identify the caption to be printed

FILNAM = File number on which the results are to be printed

Variables Transferred

Through COMMON: MEND, NEND, T

Description: * The temperature distribution at the end of iteration "K" is listed on the file "FILNAM" with a caption designated by "PRCODE".

Called By: HEATGB

Subroutine VELCTY

Purpose: This subroutine calculates the velocity field in the deformation zone

Calling Sequence: CALL VELCTY

(No formal parameters)

Variables Transferred

Through COMMON: ALFA, DO, H, HO, HP, NDA, PI, RR, R1, SIUNIT, VELD, ZZ

Description: * Based on the assumed velocity field, the meridianal, the circumferential, and the normal components of velocity, strain rate, and strain are calculated for an assumed thickness profile of the nosed position.

Called By: NOSFLW

DESCRIPTION OF THE VARIABLES INCLUDED IN THE COMMON BLOCKS

There are ten labeled common blocks in NOSING. In the description given below, variables included in all these ten blocks are pooled together and listed in alphabetical order. The number code given in parenthesis following each variable name refers to the common block in which the particular variable appears. Explanation of the number code is given below. Default value of each variable, if any, is given in brackets below the variable name. Units, wherever applicable, are also given after the description of each variable.

Code	Common Block Name
1	NOSNG
2	PRFORM
3	MTLFLW
4	INDUCH
5	SCRACH
6	FLOW
7	PFSTR
8	HEAT
9	BILPRO
10	HETDIS

Table E-1 Description of Variables in Common Blocks

A(6)	Radial distance of ogive center from shell axis. (mm; inch)
AL(1)	Axial length of the nosed portion. (mm; inch)
AKB(9)	Thermal conductivity of the shell material. (watt/m-K)
ALFA(6)(7)	Angular location of a segment. (radian)
ALFO(3)	Angular location of nose base. (radian)
ALFO1(7)	Angular location of nose base at outside diameter. (radian)
ALFO2(7)	Angular location of nose base at inside diameter. (radian)
ALF1(3)	Angular location at the tip of the nose. (radian)
ALOAD(7)	Nosing load at various die penetrations. (N, Lb)
AL2(7) [AL - ELNG]	Axial length of the nosed portion in the preform. (mm; inch)
AM(1) [0.01]	Friction shear factor at the die-workpiece interface.
AMBTEM(1) [20]	Ambient temperature. (C)
ANU(2)	Poisson's ratio of the shell material.
ARI(8)	Average radius in I-direction. Refer to Figure E-6.
ARJ(8)	Average radius in J-direction. Refer to Figure E-6.
BATCH(1) [TRUE]	Logical variable. Set to false while running the program in the interactive mode.
BILTEM(1) [AMBTEM]	Initial billet temperature. (C)
B1(1)	Axial distance of the center of arc R1 from the nose base. (mm; inch)
B2(1)	Axial distance of the center of arc R2 from the nose base. (mm; inch)
COTIME(4)	Time required to transfer the heated billet to the nosing press. (seconds)
CRB(9)	Product of heat capacity and density of the shell material. (Joule/m^3.K)

Table E-1 (Continued)

CTETA(8)	Cosine of angle α. Angle α is shown in Figure E-6.
CTETAB(8)	Cosine of angle $\bar{\alpha}$. Angle $\bar{\alpha}$ is shown in Figure E-6.
DELT(8)	Maximum time interval, Δt, for heat transfer calculations.
DELZ(8)	Axial distance between two successive elements. Refer to Figure E-6.
DENSTY(9)	Density of the shell material. (Kg/m^3)
DI(1) [DO - 2 x HO]	Inside diameter of the rough turned shell at the nose base. (mm; inch)
DIEOD(2)	Outside diameter of the nosing die. (mm; inch)
DL(7)	Incremental displacement. (mm; inch)
DO(1) [DI = 2 x HO]	Outside diameter of the shell. (mm; inch)
DRI(8)	ΔR shown in Figure B-3 of Appendix B.
E(2)	Young's modules of the shell material.
EFFICN(4) [50]	Efficiency of the induction coil. (percent)
ELNG(2)	Elongation of tube during nosing. (mm; inch)
EPS(7)	Effective strain.
EPSTR(7)	Effective strain rate. (1/sec)
FLOW(7)	Flow stress. (N/mm^2, psi)
FREQ(4)	Frequency of the induction voltage. (cycles/second)
GESS1(3)	First guess of the slope of inner profile at the nose base.
GESS2(3)	Second guess of the slope of inner profile at the nose base.
H(6)(7)	Instantaneous wall thickness during nosing. (mm, inch)
HCB(9)	Film heat transfer coefficient at the cylindrical surface of the tube. ($watt/m^2.K$)
HETIME(4)	Heating time. (seconds)
HFB(9)	Film heat transfer coefficient at the flat end of the tube. ($watt/m^2.K$)
HO(1) [(DO - DI)/2]	Wall thickness of the preform at the nose base, or wall thickness of the preform with uniform thickness wall. (mm; inch)
HP(6)(7)	Wall thickness of the preform. (mm; inch)
IC(4)	Current in the induction coil. (Amperes)

Table E-1 (Continued)

IPRINT(1)	A code used to print a number of intermediate results. Values listed under the direction of this code are summarized in Table E-2. When the end results are not satisfactory, the intermediate results will be very helpful to figure out the cause of program malfunction.
ITER(1) [25]	Maximum number of interactions to be performed during metal flow analysis.
LC(4)	Length of the induction coil (mm).
MEND(8)	Maximum coordinate value of an element in the radial direction. Refer to Figure E-6.
NC(4)	Number of turns in the induction coil.
NDA(1) [20]	Number of axial segments for stress analysis and temperature estimation.
NDOASN(1)	A variable used to limit the number of iterations performed in heat transfer calculations. When NDOASN is assigned a value, the calculated number of iterations is ignored and the heat transfer calculations are repeated NDOASN times. Helpful while debugging.
NDR(1) [6]	Number of radial segments for temperature calculations
NEND(8)	Maximum coordinate value of an element in the axial direction. Refer to Figure E-6.
NN(10)	Size of the arrays XX and ZZ.
NSIZE(1)	Shell size in millimeters.
OUTP(8)	Name of the output file.
PERMEB(9)	Permeability of the shell material. (Gauss/cersted)
PHI(8)	Angle ϕ shown in Figure E-6.
PI(1) [3.141592654]	Value of π used in area, volume, and angle calculations.
Q1,Q2,Q3,Q4(5)	Scratch variables. Used to transmit values between routines in different segments.
R(7)(8)	During preform calculations, radius of as-nosed shape at various axial locations. During heat transfer calculations, radial distance of the center of the element. Refer to Figure E-6.
RC(8)	Centroid of the element.
RHO(9)	Thermal resistivity of the shell material (ohm-cm).

Table E-1 (Continued)

RR(6)	Outside radius in the nosed portion. (mm; inch)
RRI(7)	Inside radius in the nosed portion.(mm; inch)
RRO(7)	Outside radius in the nosed portion. (mm; inch)
RSLT(8)	Name of a temporary file, TAPE3, on which intermediate results are listed when IPRINT is set to a value between 0 and 9.
R1(1)	Radius of curvature of the outside nose profile.(mm; inch)
R2(1)	Radius of curvature of the inside nose profile. (mm; inch)
SIGC(7)	Circumferential stress (N/mm^2; psi)
SIGM(7)	Meridianal stress (N/mm^2; psi)
SIGT(7)	Normal pressure (N/mm^2; psi)
SIUNIT(1) [TRUE]	Logical variable. Set to FALSE when the input data are lb-inch-C units.
SPHEAT(2)	Specific heat of the shell material. (J/Kg)
T(8)	Temperature array. In the subprogram GRIDSY, T is used as a scratch array
TEMP(2)	An array of temperature distribution in the preform prior to nosing.
THCON(2)	Thermal conductivity of the shell material.(W/m.K)
TSCR(8)	A scratch array to store intermediate temperature values.
UNIPFM(1) [TRUE]	Logical variable. Set to FALSE when the preform has non-uniform wall thickness.
VELD(1)	Axial velocity of the nosing die. (mm/sec; inch/sec)
X(7)	Axial location on outside surface of nosed portion.(mm; inch)
XI(7)	Axial location on inside surface of nosed portion. (mm; inch)
XX(10)	X coordinates of the points defining the heat distribution along the axis of the tube.
Z(7)	Axial location of a segment.(mm; inch) In heat transfer calculations, Z coordinates of the points defining the heat distribution along the axis of the tube. (mm; inch)
ZZ(6)(10)	In metal flow analysis, ZZ are the location of axial segments.(mm; inch)

List of Variables Written on the File TAPE3 for Different Settings of IPRINT

IPRINT is a variable included in the namelist IDATA. When IPRINT is set to a value between 0 and 9, during program execution, several intermediate results are written on a separate file named TAPE3. At the end of the program execution, the file is automatically disposed to the line printer. These intermediate results may be helpful to find possible errors if there are any. The list of variables written on TAPE 3 for different settings of IPRINT are summarized in this table. When IPRINT is set to a value, say 5, all the variables corresponding to 5, in the table shown below, as well as those corresponding to 5, will be written on TAPE 3.

Table E-2

IPRINT Setting	Variables Listed
2	* DELT and number of iterations required to estimate temperature distributions at the end of induction heating and after cooling from HEATGB.
3	* Temperature distributions (i.e., $\theta_{i,j}$ for i = 1 to MEND and j = 1 to NEND) after each ten iterations during induction heating and during cooling from HEATGB.
5	* Radius of each grid (i.e., $R_{i,j}$ for i = 1 to MEND and j = 1 to NEND) from GRIDSY.
2	* ALFA, ZZ, RR, H, AND H' after each iteration from NOSFLW.
7	* Centroid of each grid (i.e., $RC_{i,j}$ for i = 1 to MEND and j = 1 to NEND) from GRIDSY.
	* i,j,k_u,k_l,k_r,k_d,K,$\cos\alpha_{i,j}$,$\cos\bar{\alpha}_{i,j}$,$\theta_{i,j}$,$\theta'_{i,j}$ and three other variables for i = 1 to MEND and j = 1 to NEND from HEATRN.
8	* $ARI_{i,j}$,$\Delta R_{i,j}$,$ARJ_{i,j}$ for i = 1 to MEND and j = 1 to NEND from GRIDSY. Note: Values listed under $ARJ_{i,j}$ are actually the product of $ARJ_{i,j}$ and $T_{i,j}$.

Table E-2 (Continued)

IPRINT Setting	Variables Listed
	* W,μ (permeability), Q, C, Δθ, and K for each value of I and J from INDHET where $$W = \left(\frac{4\pi N_c I_c}{L_c}\right)^2 f \, \delta t \, 10^{-3} \quad .$$
	* C = Thermal capacity x density $$k^2 = \frac{8\pi^2 \mu f}{\rho}$$
9	* $\cos\alpha_{i,j}$, $\cos\bar{\alpha}_{i,j}$ for i = 1 to MEND and j = 1 to NEND from GRIDSY.
	* $\theta_{i,j}$ for i = 1 to MEND and j = 1 to NEND after each iteration during induction heating and during cooling from HEATGB
	* $i,j,k_u,k_d,k_l,k_r,K,\cos\alpha_{i,j},j,\cos\bar{\alpha}_{i,j},j,\theta_{i,j}$ and three other variables for i = 1 to MEND and j = 1 to NEND from HEATRN.

DISTRIBUTION

	Copies
A. Department of Defense	
Director of Defense Research and Engineering Office Attn: Mr. S. Persh Washington, DC 20301	1
Director Defense Advanced Research Projects Agency Attn: Dr. E. C. Van Reuth	1
Dr. C. Lehner	1
Dr. E. Blase 1400 Wilson Boulevard Arlington, VA 22209	1
Defense Documentation Center Attn: TIPDR Cameron Station Alexandria, VA 22314	12
B. Department of the Army	
Commander US Army Material Development Readiness Command Attn: DRCDMD	1
DRCDMR	1
DRCDMD-T	1
DRCD-L, Foreign Science & Tech Div	1
DRCDE-E, Edson Gardner	1
DRCDE-W	1
DRCMT, L. Croan	1
DRCMT, Col N Vinson	1
DRCDE-DE, E. Lippi 5001 Eisenhower Avenue Alexandria, VA 22333	1
Commander Aberdeen Proving Ground Attn: STEAP-TL, Technical Library	1
DRXSY	1
DRXSY-GA	1

	Copies
Director US Army Air Mobility Research & Development Lab Ames Research Center Attn: Mr. Paul Yaggy Moffet Field, CA 94035	1
Commander US Army Air Mobility R&D Labs Attn: SAVDL-ST Fort Eurstis, VA 23604	1
Commander US Army Material Development & Readiness Command Scientific and Technical Infor Team-Europe Attn. DRXST-STL APO, New York 09710	1
Commander Rock Island Arsenal Attn: DRXIB-MT Technical Information Div SARRI-ER	1 1 1
Commander US Army Harry Diamond Labs Attn: AMXDO-TIB 2800 Powder Mill Road Adelphia, MD 20783	1
Commander US Army Materials & Mechanics Research Center Attn: DRXMR-X, Dr. E. Wright DRXMR-PT Technical Information Div Watertown, MA 02172	1 1 1
Director US Army Maintenance Management Center Attn: DRXMD-A Lexington, KY 40507	1
Commander Watervliet Arsenal Attn: DRDAR-LCB-TL SARWV-PPI SARWV-QA SARWV-RD SARWV-RDR, Dr. T. Davidson Technical Information Div Watervliet, New York 12189	1 1 1 1 1 1

	Copies
Commander US Army Research Office P.O. Box 12211	
Attn: Dr. George Mayer, Director	1
Dr. E. Saibel	1
Research Triangle Park, NC 27709	
Commander US Army Natick Research & Development Command	
Attn: DRXRE, Dr. E. Sieling	1
Technical Information Div	1
Natick, MA 07160	
Commander US Army Foreign Science & Tech Center	
Attn: W. Marley	1
J. Bollendorf	1
7th Street, NE, Building 220 Charlottesville, VA 22901	
Commander Edgewood Arsenal	
Attn: SAREA-MT	
Aberdeen Proving Ground, MD 21010	
Commander US Army Mobility Equipment Research & Development Command	
Attn: STSFB-MWM, Mr. W. Baer	1
DRSME-RZT	1
Ft. Belvoir, VA 22060	
Commander Redstone Arsenal	
Attn: Technical Information Div	1
Huntsville, AL 35809	
Commander Ballistic Missile Defense Systems	
Attn: BNDSC-TS	1
DRDMI-R	1
DRCPM-LCE, B. Crosswhite	1
P.O. Box 1500 Huntsville, AL 35809	
Commander Rocky Mountain Arsenal	
Attn: Technical Information Div	1
Denver, CO 80240	

	Copies
Director US Army Production Equipment Agency Attn: DRXPE, J. Callaugher Rock Island, IL 61201	1
Director US Army Advanced Materials Concept Agency Attn: Technical Information Div 2461 Eisenhower Avenue Alexandria, VA 22314	1
Commander US Army Tank-Automotive R&D Command Attn: DRDTA-RKA, V. Pagano DRDTA-KP DRDTA-RE, C. Bradley DRDTA-Z, J. Panks Warren, MI 48090	1 1 1 1
Commander US Army Tank-Automotive Materiel Readiness Command Attn: DRSTA-E Warren, MI 48090	1
Commander US Army Aviation Systems Command Attn: DRSAV-ERE P.O. Box 209 St. Louis, MO 63166	1
Commander US Army Troop Support Command Attn: DRSTS-PLC 4300 Goodfellow Blvd St. Louis, MO 63120	1
Director USDARCOM Intern Training Center Attn: DRXMC-ITC-PPE Red River Army Depot Texarkana, TX 75501	1

	Copies
Commander	
US Army Armament R&D Command	
Attn: DRDAR-CG, MG B. Lewis	1
DRDAR-TD, Dr. R. Weigle	1
DRDAR-TDR, E. Eichelberger	1
DRDAR-SC, Dr. D. Gyorog	1
DRDAR-LC, Dr. J. Frasier	1
DRDAR-SCM, J. D. Corrie	3
Dr. E. Bloore	1
Project File	1
DRDAR-SCM-P, Mr. I. Betz	1
Dr. K. Iyer	3
DRDAR-SCM-P, Mr. F. Lee	10
DRDAR-LCU-M	1
DRDAR-LCU, Mr. Bushey	1
DRDAR-LC	1
DRDAR-PMM	1
DRDAR-PBM-GA, G. O'Brien	1
DRDAR-SC, Mr. W. Dittrich	1
Commander	
Rep, Alabama Army Ammunition Plant	1
Childersburg, AL 35044	
Commander	
Rep, Badger Army Ammunition Plant	1
Baraboo, WI 53919	
Commander	
Rep, Burlington Army Ammunition Plant	1
Burlington, NJ 08016	
Commander	
Rep, Cornhusker Army Ammunition Plant	1
Grand Island, NB 68801	
Commander	
Rep, Gateway Army Ammunition Plant	1
St. Louis, MO 63143	
Commander	
Rep, Hays Army Ammunition Plant	1
Pittsburgh, PA 15207	
Commander	
Holston Army Ammunition Plant	1
Kingsport, TN 37662	

	Copies
Commander Indiana Army Ammunition Plant Charlestown, IN 47111	1
Commander Iowa Army Ammunition Plant Burlington, IA 52600	1
Commander Rep, Joliet Army Ammunition Plant Joliet, IL 60436	1
Commander Kansas Army Ammunition Plant Parsons, KS 67357	1
Commander Lake City Army Ammunition Plant Independence, MO 64050	1
Commander Lone Star Army Ammunition Plant Texarkana, TX 75501	1
Commander Longhorn Army Ammunition Plant Marshall, TX 75671	1
Commander Louisiana Army Ammunition Plant Shreveport, LA 71102	1
Commander Milan Army Ammunition Plant Milan, TN 38358	1
Commander Newport Army Ammunition Plant Newport, IN 47966	1
Commander Radford Army Ammunition Plant Radford, VA 24141	1

	Copies
Commander Rep, Ravenna Army Ammunition Plant Ravenna, OH 42266	1
Commander Riverbank Army Ammunition Plant Riverbank, CA 95367	1
Commander Scranton Army Ammunition Plant Scranton, PA 18501	1
Commander Rep, St. Louis Army Ammunition Plant St. Louis, MO 63160	1
Commander Rep, Sunflower Army Ammunition Plant Lawrence, KS 66044	1
Commander Twin Cities Army Ammunition Plant New Brighton, MN 55112	1
Commander Volunteer Army Ammunition Plant Attn: SARVO-T Chattanooga, TN 37401	1
Commander Anniston Army Depot Attn: DRXAN-DM Anniston, AL 36201	1
Commander Corpus Christi Army Depot Attn: DRXAD-EFT Corpus Christi, TX 78419	1
Commander Fort Wingate Depot Activity Attn: DRXFW-M Gallup, NM 87301	1

	Copies
Commander Tobyhanna Army Depot Attn: DRXTO-ME-B Tobyhanna, PA 18466	1
Commander Tooele Army Depot Attn: DRXTE-SEN DRXTE-EMD Tooele, UT 84074	1 1
Commander Letterkenny Army Depot Attn: DRXLE-M DRXLE-MM Chambersburg, PA 17201	1 1
Commander Lexington-Blue Grass Army Depot Attn: DRXLX-SE-1 Lexington, KY 40507	1
Commander New Cumberland Army Depot Attn: DRXNC-SM New Cumberland, PA 17070	1
Commander Pueblo Army Depot Attn: DRXPU-ME DRXPU-SE Pueblo, CO 81001	1 1
Commander Red River Army Depot Attn: DRXRR-MM Texarkana, TX 75501	1
Commander Sacramento Army Depot Attn: DRXSA-MME-LB Sacramento, CA 95813	1

	Copies
Commander Seneca Army Depot Attn: DRXSE-SE Romulus, NY 14541	1
Commander Sharpe Army Depot Attn: DRXSH-SO DRXSH-M Lathrop, CA 95330	1 1
Commander Sierra Army Depot Attn: DRXSI-DQ Herlong, CA 96113	1

C. Department of the Navy

Chief Bureau of Ships Department of the Navy Attn: Code 343 Washington, DC	1
Chief Bureau of Aeronautics Department of the Navy Attn: Technical Information Div Washington, DC	1
Chief Bureau of Weapons Department of the Navy Attn: Technical Information Div Washington, DC 20025	1
Commander Naval Air Development Center Johnsville, Aero Materials Dept Attn: Mr. Forrest Williams Warminister, PA 18974	1
Commander Naval Air Systems Command Department of the Navy Attn: AIR 5203, Mr. R. Schmidt AIR 604 Washington, DC 20360	1 1

	Copies
Officer in Charge US Navy Material Industrial Research Office Attn: Code 227 Philadelphia, PA 19112	1
Commander Naval Ships Systems Command Department of the Navy Attn: Code 03423 Washington, DC 20023	1
Commander US Naval Weapons Laboratory Attn: Technical Information Div Dahlgren, VA 22448	1
Commander US Naval Engineering Experimental Station Attn: WCTRL-2, Materials Lab Annapolis, MD 21402	1
Commander US Naval Ordnance Laboratory Attn: Code WM Silver Spring, MD 20910	1

D. Department of the Air Force

Director Air Force Materials Laboratory Attn: AFML, Technical Library LTE LTM LTN Wright-Patterson AFB Dayton, OH 45433	 1 1 1 1
Director US Naval Research Laboratory Attn: Mr. W. S. Pellini, Code 6300, Metallurgy Div Mr. W. J. Ferguson Mr. J. Baker Dr. H. C. Posey Dr. F. Rosenthall Mr. C. Sanday Washington, DC 20375	 1 1 1 1 1 1

	Copies
Director Naval Ships Research & Development Center Attn: Mr. Abner R. Willmer Chief of Metals Research D. W. Taylor Code 042, Tech Lib Bethesda, MD 20084	 1 1 1
Director Air Force Armament Laboratory Attn: AFATL/DLOSL ADTC/DLJW Eglin AFB, FL 32542	 1 1
Director Air Force Weapons Laboratory Attn: Technical Information Div Kirtland AFB, NM 87118	 1
Director Air Force Materials Laboratory Wright-Patterson AFB Attn: AFML/LLD, Dr. T.M.F. Ronald AFML, Tech Library Dayton, OH 45433	 1 1
Commander Aeronautical System Div Wright-Patterson Air Force Base Attn: Technical Information Div Dayton, OH 45433	 1
Commander Air Research & Development Command Andrews Air Force Base Attn: RDRAA Washington, DC 20025	 1

E. Other Federal Agencies

Director National Academy of Science Attn: Materials Advisory Board 2101 Constitution Avenue, N.W. Washington, DC 20418	 1

	Copies
Director National Aeronautics & Space Administration Attn: Code RPM Federal Building #10 Washington, DC 20546	1
Director National Bureau of Standards Attn: Technical Information Div Washington, DC 20025	1

F. Private Organizations

Battelle Memorial Institute Attn: Metals & Ceramic Information Center Dr. T. Leontis 505 King Avenue Columbus, OH 43201	1 1
Materials Research Laboratory, Inc. Attn: Dr. E. J. Ripling 1 Science Road Glenwood, IL 60425	1